National Aeronautics and Space Administration
Headquarters
Washington, D. C.

(7a) July 1966
(7b) 132 p
(7c) Rept

Geophysical Corp. of America
(2) → (2) ~~GCA CORPORATION~~
~~GCA~~ TECHNOLOGY DIV~~ISION~~
Bedford, Mass~~achusetts~~ → (1)
GV-142710

(3) LABORATORY AND THEORETICAL INVESTIGATION
OF CHEMICAL RELEASE EXPERIMENT

Quarterly Progress Report No. 3

~~Covering the Period~~
9 Apr~~il 1966~~ - 8 July 1966

(8) Contract No. NASW-1341

TABLE OF CONTENTS

I. INTRODUCTION

A. GENERAL COMMENTS

This is the Third Quarterly Report covering the period from 9 April to 8 July 1966, under Contract NASW-1341, entitled "Laboratory and Theoretical Investigation of Chemical Release Experiments." This program has been operated at a slightly accelerated pace because of the availability of the key personnel. Consequently, the program is ahead of schedule in terms of its work accomplishments (which are reported below) and it is anticipated it will be finished approximately one month earlier than originally planned.

In accordance with discussions with Mr. H. Hipshar of NASA, Headquarters, the reports issuing from this program are being directly written up as communications for the scientific journals, rather than as GCA Scientific Reports on the program because of the large number of such reports. Papers already finished are included in the Appendix and number four to date with others expected shortly.

B. WORK SUMMARY

There is listed in paragraph C the papers submitted or in preparation under this contract. For those portions of the contract already completed a brief summary will be given in Section II of the pertinent paper. For those papers in preparation, a more extended discussion will be furnished in that section. A large portion of this quarter's work has simply been writing the papers.

As of this quarter, the following tasks of the contract have been completed:

(1) Examination of the chemiluminous reactions of trimethyl bismuth trimethyl phosphorous, dimethyl mercury and diethyl cadmium with atomic oxygen, atomic nitrogen and ozone.

(2) Measurement of relative intensities of the foregoing compounds and in one instance the absolute intensity of the chemiluminescence of ozone with TMA.

(3) The examination of the measurement of atmospheric temperature by the twilight fluorescence technique. Here analysis of previous measurements showed that the determination of relative vibrational transition probabilities were inconsistent. Consequently, new measurements were made. Further, the true potential energy curves for the A and X state of the AlO molecule were computed. The vibrational wave functions of the different vibrational levels, the Franck-Condon factors and the r-centroid were also computed.

(4) The deactivation of $O(^1D)$ by O_2 and the charge exchange cross section of C^+ with O_2 and N_2 has been measured.

(5) A study on the optical morphology of chemical release clouds as a function of scattering angle for clouds of intermediate opacity (τ = 1-10) has been completed.

(6) A study of the dynamic growth of particle clouds under conditions of various initial velocity distribution and drag laws has been completed.

In the remaining quarter of the contract, there remains to be completed:

(1) The fluorescence calculations and preliminary laboratory measurements of the vibrational transitions are to be checked in a simulator.

(2) A measurement of the rate of consumption of several organometallics with molecular oxygen.

It is also planned to publish the papers listed below as "in preparation."

Work has been held in abeyance on the differential spectrophotometry technique for determining the ratio of atomic oxygen and ozone by chemiluminescence with nitric oxide because of recent doubt case on the chemiluminescent reaction rate of atomic oxygen with nitric oxide by Golomb, et al, of the AFCRL group, and Spindler of the Canadian group. Some small effort will be put into the solution of this dilemma of reaction rates. There is an indication that the answer may be in the value of the quenching rates used in the work of Schiff.

C. LIST OF PUBLICATIONS (SCIENTIFIC JOURNAL ARTICLES SUBMITTED OR IN PREPARATION)

(1) "A Spectroscopic Study of the Chemiluminescent Reaction of Germanium Tetrahydride with Atomic Oxygen," A. Sharma and J. P. Padur, submitted to Proc. Phys. Soc.

(2) "The True Potential Energy Curves of $X^2\Sigma$ and $A^2\Sigma$ States of AℓO Molecule," A. Sharma, submitted to J. Quant. Mol. Spectrosc. Rad. Trans.

(3) "Franck-Condon Factors and R-Centroids of $A^2\Sigma - X^2\Sigma$ Band System of AℓO," A. Sharma, to be submitted to J. Quant. Mol. Spectrosc. Rad. Trans.

(4) "Relative Vibrational Transition Probability of $A^2\Sigma - X^2\Sigma$ Band System of AℓO," A. Sharma and P. Warneck, in preparation.

(5) "Studies of Ion-Neutral Reactions by a Photoionization-Mass Spectrometer Technique," P. Warneck, submitted to J. Chem. Phys.

(6) "The Chemiluminescent Reactions of Atomic Oxygen with COS and H_2S," A. Sharma, J. P. Padur and P. Warneck, submitted to J. Phys. Chem.

(7) "Atmospheric Ion Neutral Reactions," P. Warneck, in preparation.

(8) "The Morphology of Intermediate Optically Thick Vapor Atmosphere Clouds," J. Pressman and H. K. Brown, in preparation.

(9) "The Dispersion of Particulate Matter in the Upper Atmosphere for Different Initial Velocity Distributions and Drag Laws," J. Pressman and H. K. Brown, in preparation.

D. FISCAL SUMMARY (9 April through 8 July 1966)

Category	Hours	No. of People in Category
Principal Scientist	342	1
Staff Scientist	166	1
Senior Scientist	601	3
Junior Scientist	175	1
Senior Technician	166	5
Technical Typist/ Illustrator	70	5
Junior Technician	31	1

COST TO DATE

Labor	$24,800
Indirect Costs	0
Material & Supplies	3,800
Equipment	
Travel	0
Total to date (including overhead)	$67,900

E. TRAVEL SUMMARY

No trips taken this quarter.

II. DETAILS OF WORK PERFORMED

Below there is furnished succinct summaries of work already finished and more detailed discussions of work in progress.

A. DEACTIVATION OF $O(^1D)$ BY MOLECULAR OXYGEN AND NITROGEN

In the previous quarterly report, a series of experiments were described which attempted to identify the presence of ^1D oxygen atoms in a vessel by their emission of 6300Å radiation. This emission is strongly forbidden and is, therefore, difficult to detect, but an analysis of the experimental situation indicated that detection should be possible under optimum conditions. Since 6300Å radiation is the only property of $O(^1D)$ oxygen atoms which unequivocally indicates their presence, these experiments were considered essential. Nevertheless, no successful detection of 6300Å radiation could be achieved and it was concluded that the experimentally available production rate of $O(^1D)$ by photolysis of oxygen is insufficient.

The possibilities of using chemical tracers of $O(^1D)$ have been discussed in a previous quarterly report and the advantages of ozone production rates as indicator for presence of $O(^1D)$ has been pointed out. This method is best used in conjunction with the photolysis of oxygen using 1470Å Xenon resonance radiation because at this wavelength the primary process is

$$(1)\quad O_2 + h\nu \rightarrow O + O^*$$

Where O^* signifies excited O-atoms in the ^1D states. At sufficiently high pressures of oxygen the subsequent reactions are

(2) $O + 2\ O_2 \rightarrow O_3 + O_2$, fast

(3) $O^* + O_2 + M \rightarrow O_2 + M$, k_3

(4) $O^* + O_2 \rightarrow O_2 + O$, k_4

(5) $O^* + O_3 \rightarrow O_2 + O_2$, k_5

The determination of rate constants requires the quantitative measurement of the ozone quantum yield as a function of various experimental parameters. However, as is generally true with photochemical systems, only ratios of rate constants can be determined and absolute rate constants must be obtained by compairson with other available values. The method by which this can be accomplished has been discussed previously.

The experimental arrangement for the study of the above photolysis system has been described previously in a different context. Briefly, the production of ozone in a flow system is investigated as a function of pressure and temperature and as a function of foreign gas admixture. Figure 1 shows the results obtained for pure oxygen, a 1:1 mixture of nitrogen and oxygen, and 1:4 mixture of nitrous oxide and oxygen, all at room temperature. The decline of the ozone quantum yield with decreasing pressure for pure oxygen and the oxygen-nitrogen mixture indicates qualitatively that quenching of $O(^1D)$ by either gas cannot be very rapid, since otherwise the ozone quantum yield should be independent of pressure and would have a value of $g(O_3) \approx 2$. The decrease of the ozone quantum yield to values of about unity in the N_2O-O_2 mixture indicates a complete loss of $O(^1D)$ by reaction with N_2O, which is known to be rapid.

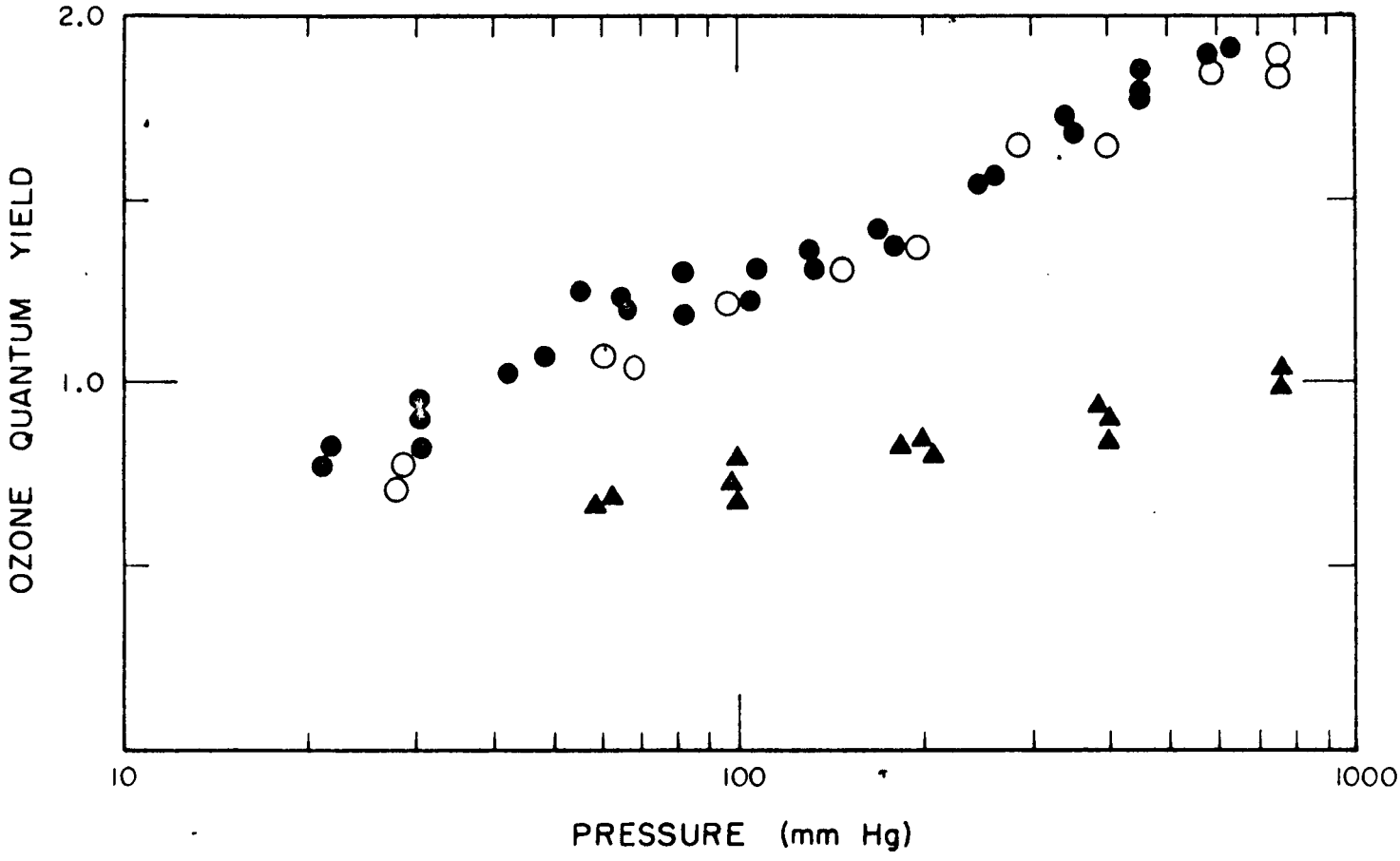

Figure 1

A detailed analysis of these data will not be given here. The results can be expressed in terms of k_4/k_5, k_6/k_5 and k_7/k_5 where k_6 and k_7 are the rate coefficients associated with the reactions.

$$(6)\ O^* + N_2 \rightarrow O + N_2$$

$$(7)\ O^* + N_2O \rightarrow N_2 + O_2$$

$$\rightarrow NO + NO$$

The partitioning ratio for the two types of reaction products in Reaction (7) are about 1:1. The resulting rate constant ratios are shown below

k_4/k_5	k_6/k_5	k_7/k_5
6.1×10^{-4}	2.7×10^{-4}	6.0×10^{-3}

It is evident that in all cases the reaction of $O(^1D)$ with ozone is much faster. A lower limit for k_5 has been given by Fitzsimmons and Bair from data concerning the flash photolysis of ozone. An upper limit to k_5 can be obtained from the temperature dependence of the ozone quantum yield in the present work which has been reported elsewhere. Thus, $k_5 \approx 7 \times 10^{-12}$ cc/molecule second. The absolute rate constant for the deactivation by oxygen is, accordingly, $k_4 \approx 4 \times 10^{-15}$ cc/molecule second. The other rate constants are $k_6 \approx 2 \times 10^{-15}$ cc/molecule second, $k_7 \approx 4 \times 10^{-14}$ cc/molecule second.

B. ION MOLECULE REACTIONS

This section deals with the determination of the rate constants associated with the reactions of atomic oxygen ions,

$$(8)\quad O^+ + O_2 \rightarrow O_2^+ + O$$

$$(9)\quad O^+ + N_2 \rightarrow NO^+ + N$$

which to a large extent controls the abundance of O^+ and NO^+ ions in the ionosphere. Under the present contract a novel experimental technique is used to determine the appropriate rate constants. This experimental method employs photoionization as the source of the primary ions, and thereby eliminates many of the difficulties associated with common electron impact ionization, for example, the generation of impurities at hot filaments, etc. A detailed description of the photoionization mass spectrometer technique has been given in the previous quarterly report. Briefly, it consists of ionizing a gas mixture in an ionization box, in a plane perpendicular to the ion exit aperature by repetitive pulses of ultraviolet light at wavelengths around 500Å. A vacuum ultraviolet monochromator is used to provide the required dispersion with 5Å resolution. In the ion source, the primary photo-ions are drifted to the ion exit aperature by means of a repeller field and during the drift they undergo the desired reactions. As soon as they leave the source, the ions are subjected to a strong focussing field at reduced pressure so that further reactions are suppressed. Accordingly, the primary ions react only during their residence time in the source. Making use of the pulsed nature of the light source, the residence time is determined by measuring the delay time observed between the formation of a particular ion and its arrival at the mass spectrometer detector. A graphical extrapolation procedure for delay times obtained with different repeller voltages is used to separate the

residence time in the source from the total flight time of the ions in the mass spectrometer for the employed conditions. The details of these techniques are described in a paper submitted to the Journal of Chemical Physics and entitled "Studies of Ion-Neutral Reactions by a Photoionization Mass Spectrometer Technique."

In the previous quarterly report a series of experiments were described which involved pure oxygen ionized at 585Å. From these data, the rate constant for Reaction (8) was obtained as $k_1 = 2.25 \times 10^{-11}$ cc/molecule second. In the present reporting period, additional experiments were performed with air, using ionizing light at two different wavelengths, either 584Å or 630Å, by selecting suitably strong lines emitted from the light source. Both wavelengths lie below the onset of O^+ formation at 658Å, so that the occurrence of Reactions (8) and (9) could be anticipated. Additional primary ions are O_2^+ and N_2^+. The former undergoes no noticeable reactions, but the latter reacts with O_2 by charge transfer:

$$(10)\quad N_2^+ + O_2 \rightarrow O_2^+ + N_2.$$

Altogether then there are three reactions occurring simultaneously making the analysis complicated. Fortunately Reaction (10) does not interfere with the loss of O^+ ions and the production of NO^+ ions according to Reactions (8) and (9), so that these can be treated separately. Moreover, in the actual experiments, the production of primary O^+ ions is only about 1/10 of O_2^+ ions, so that the generation of O_2^+ from Reaction (8) is negligible in comparison to that from Reaction (10). While this favors

the determination of the rate constant for Reaction (10), it also excludes the use of O_2^+ formation from Reaction (8) for the determination of k_1. However, k_1 and k_2 can be determined from the behavior of the O^+ and NO^+ ion currents alone. The appropriate rate equations are:

$$\frac{d(O^+)}{dt} = k_1(O^+)(O_2) + k_2(O^+)(N_2) = k_1(O^+)(O_2)(1 + \epsilon)$$

$$\frac{d(NO^+)}{dt} = k_2(O^+)(N_2) = k_1(O^+)(O_2)\ \epsilon$$

where $\epsilon = k_2(N_2)/k_1(O_2)$. Straight forward integration over the time period yields

$$(O^+) = (O^+)_o \exp\ [-\ k_1\ (1 + \epsilon)\ (O_2)\ t]$$

$$\frac{\Delta(O^+)}{(NO^+)} = \frac{1 + \epsilon}{\epsilon}$$

From these equations, the rate constants k_1 and k_2 can be obtained in the form

$$k_1 = \frac{1}{(1 + \epsilon)(O_2)t} \log \frac{(O^+)_o}{(O^+)}$$

$$k_2 = \frac{\epsilon\ k_1\ (O_2)}{(N_2)} = \frac{k_1}{4[\Delta(O^+)/\Delta(NO^+) - 1]}$$

As previously, the initial oxygen ion intensity, $(O^+)_o$, is derived from the sum of the ion intensities at the considered pressure weighted with the fraction of the O^+ ion intensity at low pressures. At pressures

below 100 microns where $\Delta(O^+)$ is not large enough to be useful for the determination of the rate constants, k_2 can still be obtained from the observed NO^+ ion intensity by using the approximation

$$k_2 = (NO^+)/(O^+)_o[N_2]t$$

Figure 2 shows the O^+ and NO^+ ion intensities resulting from these experiments, normalized with respect to the O^+ ion intensity slope at low pressures to take into account the difference in light intensities and ionization cross sections at the two wavelengths 585Å and 630Å. Also shown in Figure 2 by the solid line, is the initial O^+ ion intensity. The occurrence of Reactions (8) and (9) is evidenced by the loss of O^+ and the production of NO^+. Since, with the exception of the ionizing wavelength the experimental conditions were the same, the agreement of the two sets of data indicates that the reaction rates are independent of wavelength as indeed they are expected to be. A treatment of the experimental data shown in Figure 2, according to the above equations and the resulting averaged rate constants k_1 and k_2, are given in Tables 1 and 2. The averages obtained for k_1 are in good agreement with each other and also with the value reported in the last quarter. The average from these three values is $k_1 = 2.0 \times 10^{-11}$ cc/molecules sec. This value is in good agreement with that given recently by Sayers and collaborators, $k_1 = 1.6 \times 10^{-11}$ cc/molecule sec, but it is by a factor of two lower than the rate constant $k_1 = 4 \times 10^{-11}$ cc/molecule sec obtained by Fehsenfeld, et al. with the flowing afterglow device. However, even in this case, order of magnitude agreement is observed. It is significant that these values were obtained

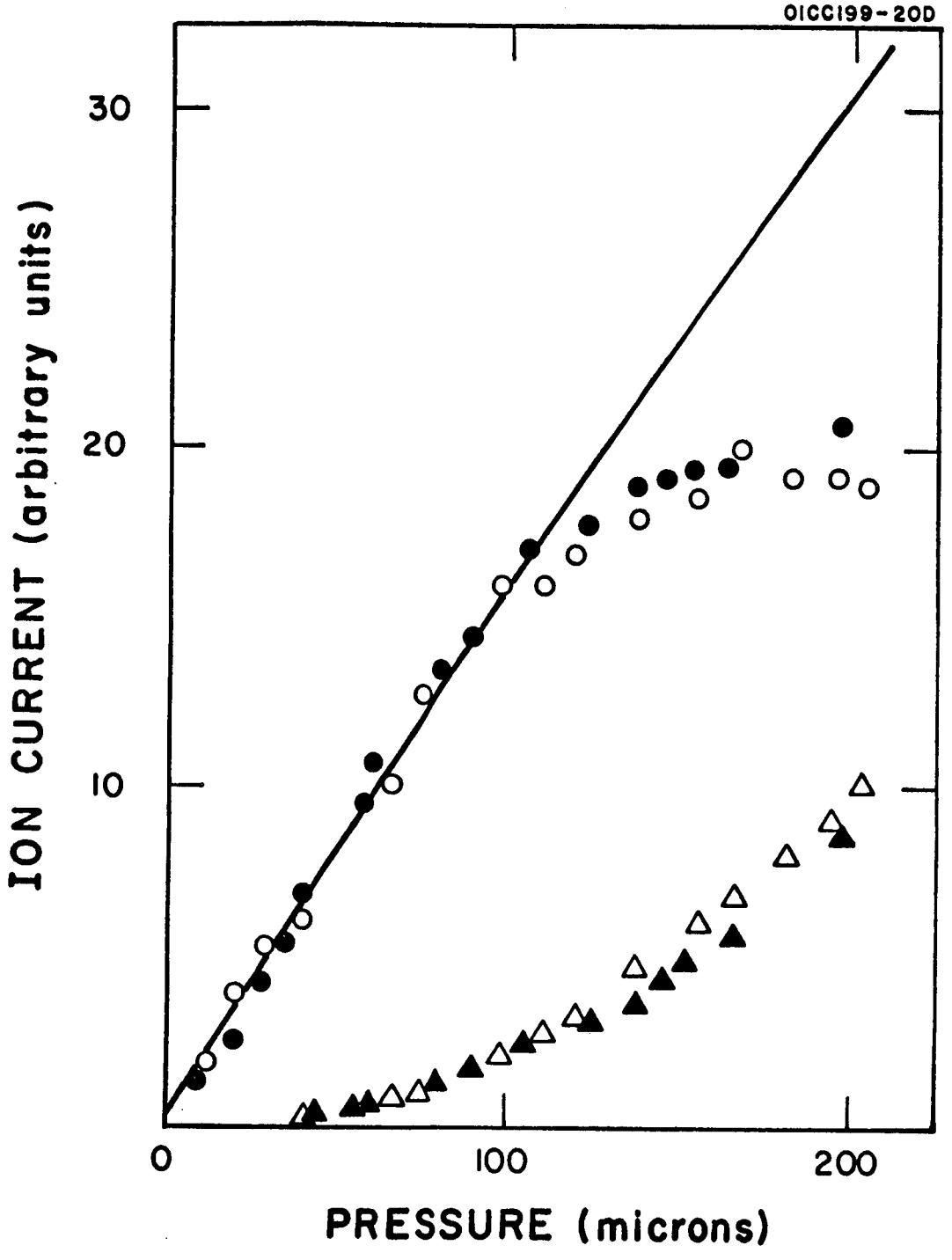
01CC199-20D
30
20
10
0
100
200
ION CURRENT (arbitrary units)
PRESSURE (microns)

Figure 2

TABLE 1

REACTIONS WITH OXYGEN AND NITROGEN OF O^+ IONS PRODUCED BY PHOTOIONIZATION OF AIR AT 585Å WAVELENGTH

P (microns)	(O^+) (Arbitrary Units)	(NO^+) (Arbitrary Units)	$(O^+)_o$ (Arbitrary Units)	ϵ	t (microsec)	$k_1 \times 10^{11}$ (cc/molecule sec)	$k_2 \times 10^{12}$ (cc/molecule sec)
44	27	0.7	34.4	---	3.7	---	4.75
59	48	1.6	44.8	---	4.2	---	5.45
61	39	1.5	44.8	---	4.2	---	4.82
80	55	3.0	55.8	---	4.9	---	5.20
90	63	3.7	63.2	---	5.2	---	4.70
105	70	4.8	68.3	---	5.4	---	4.45
138	72	6.6	83.0	1.33	5.4	1.32	4.30
145	69	7.8	83.7	1.00	5.8	1.74	4.45
152	76	8.4	96.0	1.00	5.9	1.98	4.90
165	75	9.9	99.0	0.76	6.2	2.20	4.20
198	72	10.8	104.0	0.90	6.7	2.20	5.15

Average $k_1 = 1.90 \times 10^{-11}$ cc/molecule sec, Av. $k_2 = 4.76 \times 10^{-12}$ cc/molecule sec

TABLE 2

REACTIONS WITH OXYGEN AND NITROGEN OF O^+ IONS PRODUCED BY PHOTOIONIZATION OF AIR AT 630Å WAVELENGTH

P (microns)	(O^+) (Arbitrary Units)	(NO^+) (Arbitrary Units)	$(O^+)_o$ (Arbitrary Units)	ϵ	t (microsec)	$k_1 \times 10^{11}$ (cc/molecule sec)	$k_2 \times 10^{12}$ (cc/molecule sec)
40	6.0	0.2	7.6	---	3.7	---	4.10
68	10.0	0.5	11.2	---	4.7	---	4.10
74	12.0	0.5	12.0	---	4.9	---	4.96
99	16.0	1.2	15.5	---	5.7	---	4.90
111	16.0	1.3	18.0	---	5.7	---	4.71
120	16.0	1.6	19.5	1.06	6.2	1.78	4.82
138	18.0	3.7	22.3	1.20	6.7	1.65	4.80
156	18.5	4.0	24.6	0.98	7.3	1.95	4.82
166	20.0	4.8	27.4	0.85	7.5	2.03	4.32
181	19.0	5.4	28.1	0.78	7.9	2.27	4.42
195	17.0	4.6	30.2	0.74	8.2	2.35	4.35
205	19.0	5.1	31.6	0.78	9.6	2.25	4.40

Average $k_1 = 2.04 \times 10^{-11}$ cc/molecule sec, Av. $k_2 = 4.53 \times 10^{-12}$ cc/molecule sec

by entirely different experimental methods because the agreement thus makes k_1 one of the best established thermal rate constants of atmospheric ion molecule reactions.

The average rate coefficient for the reaction of O^+ ions with nitrogen is $k_2 = 4.6 \times 10^{-12}$ cc/molecule sec. This value is in reasonable agreement with $k_2 = 3 \times 10^{-12}$ cc/molecule sec given by Fehsenfeld, et al. Langstroth and Hasted have employed the transient afterglow method and found $k_2 = 4.7 \times 10^{-12}$ cc/molecule sec, which would be in excellent agreement with the present value, were it not for the fact that they also reported $k_1 = 1.8 \times 10^{-12}$ cc/molecule sec. The last value is by an order of magnitude too low, thereby casting doubt on both of their determinations.

The present experiments also yield data on Reaction (10). The rate constants found for the experiments at 585Å and 630Å, respectively are $k_3 = 1.08 \times 10^{10}$ cc/molecule sec and $k_3 = 1.06 \times 10^{-10}$ cc/molecule sec, in good agreement with each other, with an earlier value obtained with light at wavelength near the onset of N_2^+ formation, and with the value of 1.0×10^{-10} cc/molecule sec, given by Ferguson and collaborators.

C. CHEMILUMINESCENCE IN THE REACTIONS OF ATOMIC OXYGEN WITH COS AND H_2S

The chemiluminescent intensity in the reactions O + COS and O + H_2S was studies in a flow system as a function of time and reactant concentrations. It has been shown previously that the emission from both reactions gives the same spectrum, so that the process leading to the chemiluminescence presumably is the same in both cases. In the present experiment, evidence was sought that the responsible reaction is

$$O + SO \rightarrow S\,O_2 + h\nu$$

This evidence has been obtained from the intensity time profile of the chemiluminescence and its reactant concentration dependence. Figure 3 shows that the intensity increases initially linearly with reaction time, and that the slope is a function of the reactant concentration. The initial slope was found to vary directly with the concentration of H_2S or COS and with the square of this oxygen atom concentration. The results can be interpreted in terms of Reactions (11) thru (13)

$$(11) \quad O + COS \rightarrow SO + CO$$

$$(12) \quad O + H_2S \rightarrow SO + H_2$$

$$(13) \quad O + SO \rightarrow SO_2 + h\nu$$

if it is taken into account that for sufficiently short reaction times the consumption of the initial reactant is still negligible. We therefore have for the reaction O + COS as an example:

$$\frac{\Delta(SO)}{\Delta t} = k_1\ (O)\ (COS)$$

$$\frac{\Delta\, I_1}{\Delta t} = k_3\ (O)\ \frac{\Delta(SO)}{\Delta t} = k_3\ k_1\ (O)^2\ (COS) \qquad (1)$$

The right-hand side of this equation represents the initial slope of the intensity time profile. Similarly for the $O + H_2S$ reaction

$$\frac{\Delta I_2}{\Delta t} = k_3\ k_2\ (O)^2\ (H_2S) \qquad (2)$$

Equations (1) and (2) predict a linear relationship with initial CSO or H_2S concentration and a quadratic one for the atomic oxygen concentration. This is in agreement with the relationship found in the present experiments.

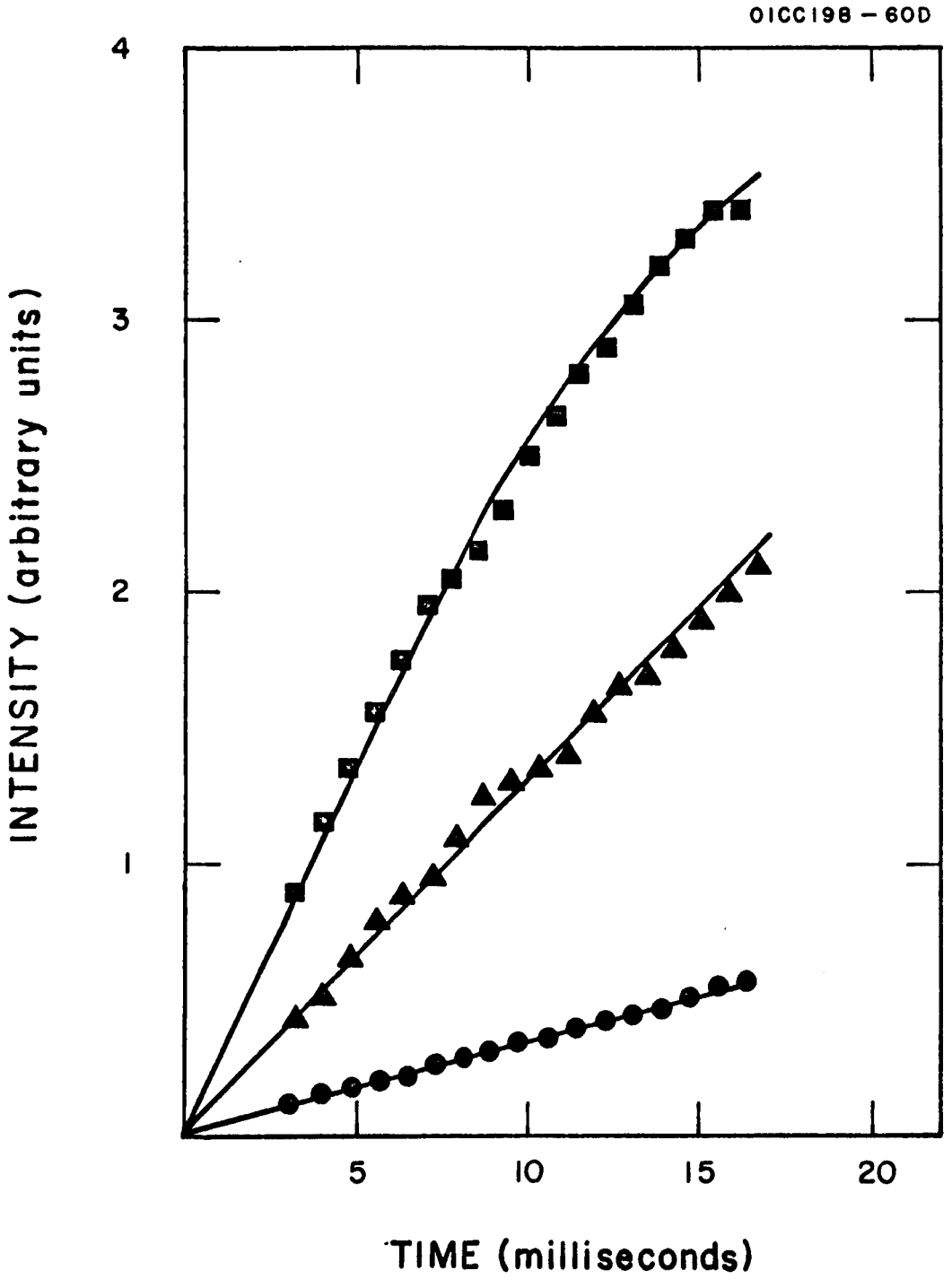
01CC198 – 60D
4
3
2
1
INTENSITY (arbitrary units)
5
10
15
20
TIME (milliseconds)

Figure 3

The absolute intensity in the O + H_2S reaction is brighter than that of the O + COS reaction and this fact is explained by a difference in the rate constants. From Equations (1) and (2) one obtains

$$\frac{\Delta I_2/\Delta t}{\Delta I_1/\Delta t} = \frac{k_2}{k_1} \frac{[H_2S]}{[COS]}$$

for equal oxygen atom concentrations. From the experiments, therefore, the ratios of these rate constants can be determined: $k_2/k_1 = 1.85$. Since k_1 had been measured previously in this laboratory as $k_1 = 0.91 \times 10^{-14}$ cc/molecule sec, we find $k_2 = 1.7 \times 10^{-14}$ cc/molecule sec.

It must be emphasized that this rate constant refers only to that portion of the O + H_2S reaction which leads to the formation of SO. The overall reaction path includes an additonal reaction and consequently is faster. The rate constant associated with Reaction (13)

$$(13) \quad O + SO \rightarrow SO_2 + h\nu$$

was also determined by comparing the light intensity from the O + COS reaction with that produced in the air-afterglow reaction

$$(14) \quad O + NO \rightarrow NO_2 + h\nu$$

The relative spectral distributions of both reactions were taken into account and an interference filter was used in the region around 4100Å where both spectra overlap. The introduction of NO to the system results in emission which is time independent, whereas the intensity produced in the COS reaction increases linearly with time. In the first cases, the intensity is given by $I_4 = k_4$ (O) (NO), in the second by Equation (1). A combination of these equations for constant oxygen atom concentration gives

$$k_3 = \frac{k_4 \, \Delta I_1/\Delta t}{k_1 (O)(COS) \; I_4}$$

or when the total intensities I_1 and I_4 are replaced by equivalent photomultiplier currents i_1 and i_4

$$k_3 = \frac{f_4 k_4 \; (NO) \; \Delta i_1/\Delta t}{f_3 k_1 \; (O) \; (COS) i_4} \qquad (3)$$

when f_4 and f_3 are the fractions of light intensity seen by the photomultiplier interference filter combination. Figure 4 shows the results. From the slope of the current-time profile for O + COS reaction, one obtains $\Delta i_1/\Delta t = 330 \times 10^{-7}$ A/sec, whereas $i_4 = 0.005 \times 10^{-7}$ A. The concentrations in molecules/cc are (COS) = 4.2×10^{14}, (NO) = 5×10^{14}, (O) = 1.65×10^{14}. With these data Equation (3) yields $k_3 = 5.7 \times 10^{-15}$ cc/molecule sec. This value is about eight times greater than that given by Rolfes, Reeves and Hartack, but the discrepancy is reduced by several experimental factors which will not be discussed in detail. However, it is significant that Reaction (13) is very effective and that it is about as rapid as Reactions (11) or (12), so that Reaction (13) determines to a large extent the course of the O + H_2S and O + COS reactions.

D. CHEMILUMINESCENT REACTION OF GERMANIUM WITH ATOMIC OXYGEN

The general results of the study of the chemiluminescent reaction of germanium tetrahydride and atomic oxygen has been previously reported. However, the results of our previous study has been now analyzed and has been presented in the paper. The abstract of the work is as follows:

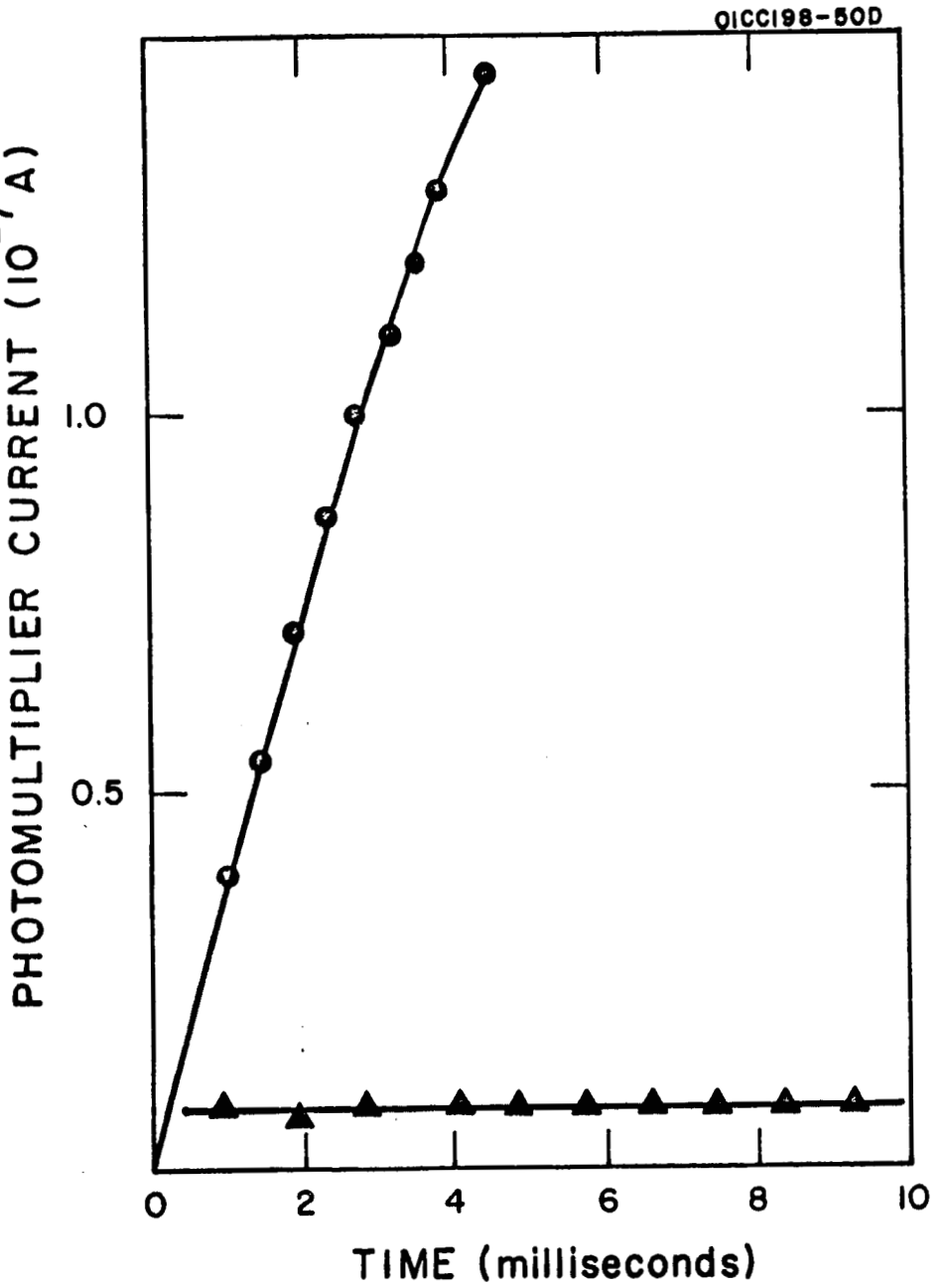
01CC198-50D
PHOTOMULTIPLIER CURRENT (10^{-7}A)
1.0
0.5
0
2
4
6
8
10
TIME (milliseconds)

Figure 4

"The spectrum of the glow produced during the gas phase reaction of germanium tetrahydride with atomic oxygen is studies in the region from 2450 to 5100Å. About 100 bands are measured between 2350 and 4000Å. Almost all bands on the short wavelength side of the spectrum belong to the D-X band system of GeO. Several new bands of the D-X system are observed together with a number of unidentified bands. The present study indicates the possibility of a new band system of GeO in the region 3000 and 5000Å."

E. TRUE POTENTIAL ENERGY CURVES OF AℓO

The relative intensity of the bands belonging to the $A^2\Sigma - X^2\Sigma$ system of AℓO observed during the rocket release of aluminum compounds in the upper atmosphere at twilight has been used to obtain information regarding upper atmospheric temperatures. The Franck-Condon factors for the above band system have been calculated after assuming that the $A^2\Sigma$ and $X^2\Sigma$ states of AℓO follows the Morse curve. The validity of the above assumption has been tested by a method given by Pekeris. It was found that the $X^2\Sigma$ state can be approximately represented by the Morse Potential, but the $A^2\Sigma$ state is expected to show a large deviation.

In view of the above finding, the true potential energy curve of the $A^2\Sigma$ and $X^2\Sigma$ states were calculated by the Rydberg-Klein-Rees method described by Zare. The results are given in Tables 3 and 4 and depicted in Figures 5 and 6 which show that the agreement between the true potential and Morse potential is reasonable for the $X^2\Sigma$ state — particularly for vibrational levels $v \leq 6$. However, the deviation of the true potential is appreciable for even lower vibrational levels.

TABLE 3

POTENTIAL ENERGY CURVE FOR $A^2\Sigma$ STATE OF AlO

(J = 0 Rotational State)

(v + 1/2)	U(r) cm^{-1}	r_+ Å	r_- Å
0	0	1.6668	
0.5	434.1	1.7325	1.6080
1.5	1295.3	1.7850	1.5685
2.5	2149.6	1.8235	1.5430
3.5	2996.6	1.8563	1.5233
4.5	3836.0	1.8860	1.5070
5.5	4668.1	1.9135	1.4929
6.5	5492.1	1.9394	1.4804
7.5	6309.1	1.9642	1.4693
8.5	7118.2	1.9880	1.4592
9.5	7921.0	2.0111	1.4499
10.5	8715.3	2.0337	1.4413
11.5	9505.3	2.0552	1.4337

TABLE 4

POTENTIAL ENERGY CURVE FOR $X^2\Sigma$ STATE OF AℓO

(J = 0 Rotational State)

(v + 1/2)	U(r) cm^{-1}	r_+ Å	r_- Å
0	0	1.6176	
0.5	487.9	1.6808	1.5633
1.5	1452.1	1.7309	1.5261
2.5	2401.4	1.7688	1.5026
3.5	3336.1	1.8014	1.4845
4.5	4257.8	1.8311	1.4696
5.5	5165.1	1.8589	1.4567
6.5	6058.1	1.8854	1.4452
7.5	6936.6	1.9110	1.4349
8.5	7801.1	1.9355	1.4257
9.5	8660.4	1.9593	1.4175
10.5	9487.3	1.9850	1.4084
11.5	10310.0	2.0065	1.4022

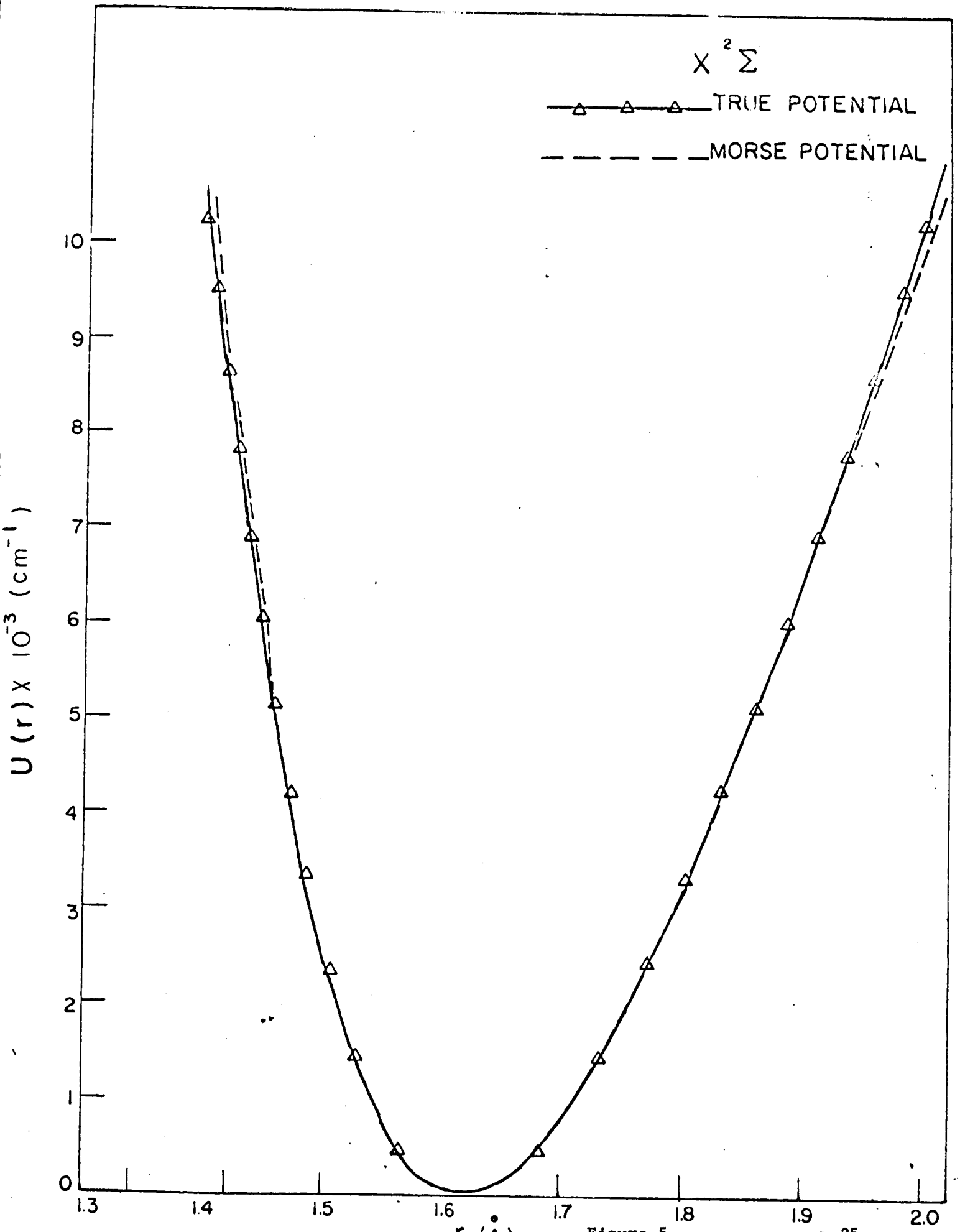
X ² Σ
TRUE POTENTIAL
MORSE POTENTIAL
U(r) X 10⁻³ (cm⁻¹)
0
1
2
3
4
5
6
7
8
9
10
1.3
1.4
1.5
1.6
1.7
1.8
1.9
2.0
r (Å)

Figure 5

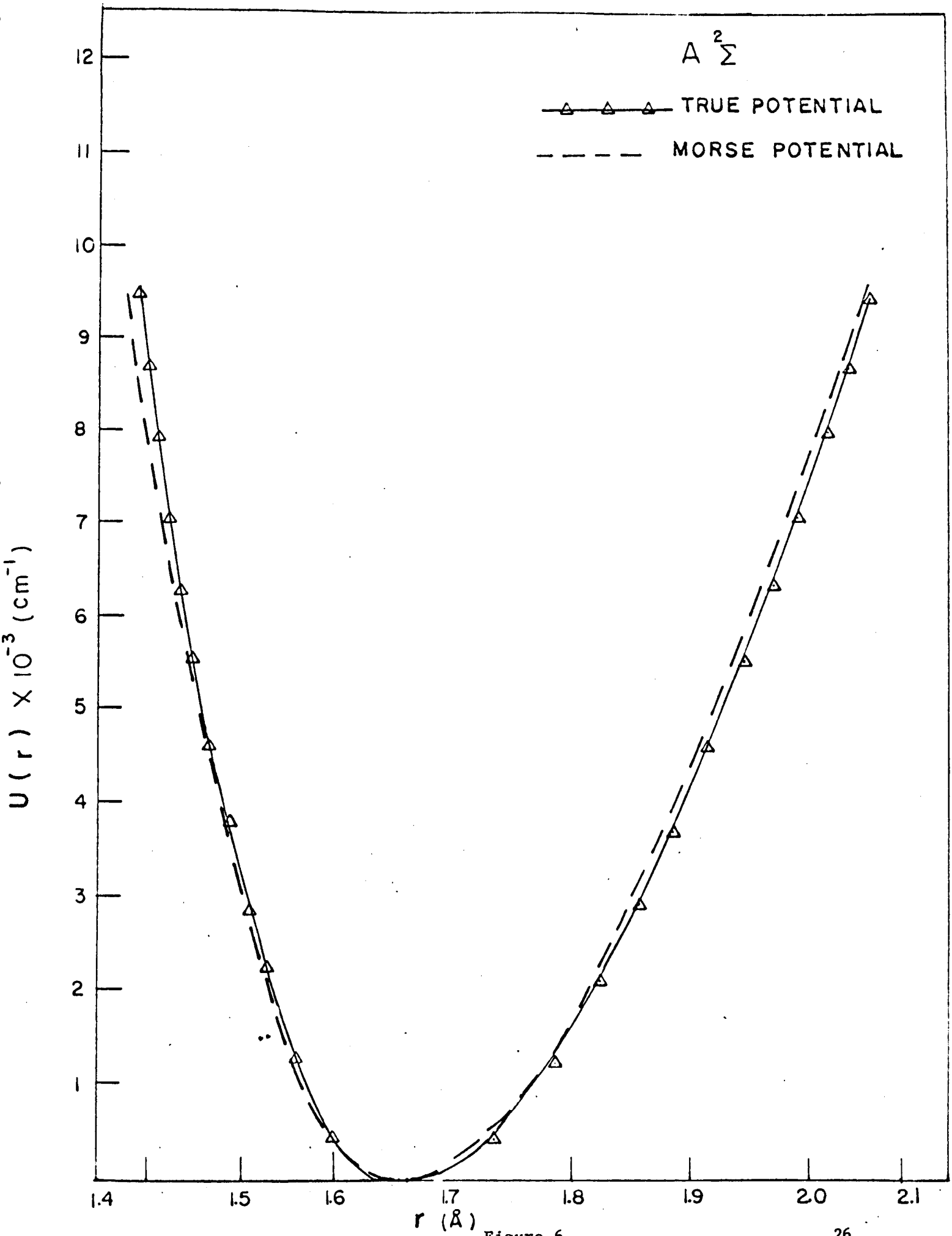
A $^2\Sigma$
TRUE POTENTIAL
MORSE POTENTIAL
U (r) X 10^{-3} (cm^{-1})
r (Å)
12
11
10
9
8
7
6
5
4
3
2
1
1.4
1.5
1.6
1.7
1.8
1.9
2.0
2.1

Figure 6

F. FRANCK-CONDON FACTORS OF $A^2\Sigma - X^2\Sigma$ SYSTEM OF AℓO

Since it has been found by previous workers that the Franck-Condon factors are quite sensitive to the shape of the potential, and also in view of the above results, the Franck-Condon factors and r-centroids for the $A^2\Sigma - X^2\Sigma$ system has been calculated from the RKR potentials. The repulsive and attractive part of the potentials beyond the range covered by the spectroscopic data were extrapolated by the following expressions:

$$V_{rep} = \frac{a}{r^{12}} + b$$

$$V_{att} = \frac{a'}{r^{b'}}$$

The constants a, b, a′ and b′ were computed from the last two turning points of the RKR potential. The vibrational wave functions required for the calculation of the Franck-Condon factors and r-centroids were obtained from the numerical solution of the Schrödinger equation:

$$\frac{d^2\psi(v)}{dr^2} + [E(v) - v(r)]\,\psi_v = 0$$

The computer program described by Zare was used on an IBM 7094 computer. This program essentially depends on the iterative method of Numerov and a second order iteration-variation procedure due to Löwdin. The wave functions were calculated between the limits of 1.1 and 3.0Å using steps of 0.001Å.

The accuracy of the calculated RKR potential was first tested by calculating the G(v) and B(v) values for vibrational levels from v = 6 to v = 9 and comparing them with the observed values. The computed and observed values of G(v) and B(v) are given in Tables 5 and 6. It has been concluded from the agreement between the computed and observed values of G(v) and B(v) that the calculated RKR potentials are accurate within the accuracy of the presently available spectroscopic data, although more refined spectroscopic data is desirable.

The integrals involved in the calculations of Franck-Condon factors and r-centroids were evaluated by Simpson's rule using steps of 0.001Å. The calculated Franck-Condon factors are given in Table 7 and are compared with the Franck-Condon factors calculated from the Morse potential by Nicholls. The maximum difference between the Franck-Condon factors calculated from the RKR potential and those calculated from Morse potential for the prominent bands is about 17 percent. However, the values of the Franck-Condon factors calculated from the two potentials for weak bands differs even in order of magnitude.

The calculated values of r-centroids are given in Table 8 which also contains the r-centroids calculated from Morse potential.

The relative intensities of emission of bands scaled to 10 in units of erg/sec and quantum/sec are given in Table 9. In the calculation of the relative intensity, the variation of electronic transition moment with the internuclear separation is not taken into account.

TABLE 5

COMPARISON OF THE OBSERVED AND CALCULATED G(v) AND B(v) VALUES FOR $X^2\Sigma$ STATE

v	G(v) Observed	G(v) Calculated	$G(v)_o - G(v)_c$	B(v) Observed	B(v) Calculated	$B(v)_o - B(v)_c$
0	487.9	487.7	0.2	0.63846	0.63796	0.00050
1	1452.1	1452.3	-0.2	0.63266	0.63286	0.00020
2	2401.4	2401.4	0.0	0.62686	0.62688	0.00002
3	3336.1	3336.4	-0.3	0.62106	0.62094	0.00012
4	4257.8	4257.8	0.0	0.61526	0.61525	0.00001
5	5165.1	5164.9	0.2	0.60946	0.60941	0.00005
6	6058.1	6058.1	0.0	0.60366	0.60356	0.00010
7	6936.6	6937.6	-1.0	0.59786	0.59774	0.00012
8	7801.1	7803.4	-2.3	0.59206	0.59200	0.00006
9	8660.4	8656.1	4.3	0.58626	0.58624	0.00002

TABLE 6

COMPARISON OF THE OBSERVED AND CALCULATED G(v) and B(v) VALUES FOR $A^2\Sigma$ STATE

v	G(v) Observed	G(v) Calculated	$G(v)_o - G(v)_c$	B(v) Observed	B(v) Calculated	$B(v)_o - B(v)_c$
0	434.1	434.2	-0.1	0.601845	0.601835	0.000010
1	1295.3	1295.8	-0.5	0.597375	0.597372	0.000003
2	2149.6	2149.8	-0.2	0.592905	0.592911	0.000006
3	2996.6	2997.0	-0.4	0.588435	0.588425	0.000010
4	3836.0	3836.5	-0.5	0.583965	0.583949	0.000016
5	4668.1	4668.4	-0.3	0.579495	0.579491	0.000004
6	5492.1	5492.9	-0.8	0.575025	0.575005	0.000020
7	6309.1	6309.8	-0.7	0.570555	0.570501	0.000054
8	7118.2	7119.3	-1.1	0566085	0.566018	0.000065
9	7921.0	7922.0	-1.0	0.561615	0.561528	0.000087

TABLE 7

FRANCK-CONDON FACTORS OF $A^2\Sigma - X^2\Sigma$ BAND SYSTEM OF AℓO MOLECULES

v′ \ v″	0	1	2	3	4	5	6	7	8	9
0	*7.297-1 †7.298-1	2.366-1 2.379-1	3.174-2 3.070-2	1.904-3 1.577-3	2.990-5 1.968-5	6.949-8 8.992-8	7.678-9 1.818-8	8.160-10 7.104-12	5.946-9	6.078-10
1	2.233-1 2.244-1	3.457-1 3.565-1	3.493-1 3.428-1	7.567-2 7.147-2	5.873-3 4.685-3	1.131-4 5.590-5	2.918-7 9.332-7	4.340-11 9.212-8	8.117-10	2.356-8
2	4.065-2 4.024-2	3.026-1 3.006-1	1.389-1 1.604-1	3.842-1 3.776-1	1.217-1 1.124-1	1.159-2 8.685-3	2.406-4 8.681-5	1.325-6 4.430-6	1.003-7	1.249-8
3	5.563-3 5.037-3	9.352-2 8.794-2	2.978-1 3.038-1	4.169-2 6.320-2	3.769-1 3.777-1	1.657-1 1.494-1	1.846-2 1.282-2	3.723-4 8.953-5	4.372-6	4.509-7
4	6.445-4 4.334-4	1.845-2 1.527-2	1.381-1 1.290-1	2.568-1 2.752-1	5.242-3 1.945-2	3.497-1 3.632-1	2.047-1 1.810-1	2.587-2 1.641-2	4.724-4	1.253-5
5	7.013-5 2.000-5	2.762-3 1.695-3	3.623-2 2.900-2	1.684-1 1.589-1	2.044-1 2.363-1	8.923-4 3.215-3	3.154-1 3.447-1	2.381-1 2.073-1	3.320-2	5.105-4
6	7.352-6 3.843-8	3.448-4 9.946-5	6.741-3 3.970-3	5.607-2 4.422-2	1.846-1 1.777-1	1.526-1 1.975-1	1.168-2 9.659-6	2.807-1 3.277-1	2.666-1	4.005-2
7	5.443-7 2.304-7	3.760-5 4.468-7	9.830-4 2.848-4	1.267-2 7.219-3	7.600-2 5.926-2	1.879-1 1.875-1	1.079-1 1.632-1	2.792-2 1.997-3	2.488-1	2.911-1
8	1.221-9	3.128-6	1.191-4	2.180-3	2.044-2	9.372-2	1.815-1	7.236-2	4.466-2	2.213-1
9	2.206-8	7.177-8	1.201-5	3.045-4	4.102-3	2.948-2	1.080-1	1.685-1	4.563-2	5.945-2

*$q_{v'v''}$ Calculated from RKR Potential †$q_{v'v''}$ Calculated from Morse Potential

TABLE 8

r-CENTROIDS (Å) OF $A^2\Sigma - X^2\Sigma$ SYSTEM OF AℓO

v′ \ v″	0	1	2	3	4	5	6	7	8	9
0	*1.647 †1.646	1.728 1.727	1.812 1.813	1.918 1.937	2.166 2.215	0.5621	1.227	1.795	1.663	1.402
1	1.575 1.574	1.658 1.657	1.738 1.739	1.825 1.826	1.938 1.957	2.184 2.295	0.5853	1.736	1.234	1.624
2	1.507 1.505	1.583 1.580	1.671 1.669	1.749 1.752	1.837 1.839	1.956 1.979	2.220 2.411	0.9608	2.333	1.351
3	1.436 1.429	1.516 1.511	1.590 1.586	1.693 1.685	1.761 1.765	1.849 1.852	1.974 2.003	2.277 2.606	1.233	2.222
4	1.364 1.326	1.448 1.436	1.524 1.517	1.598 1.591	1.758 1.713	1.773 1.779	1.862 1.866	1.992 2.030	2.352	1.441
5	1.300	1.376 1.336	1.457 1.443	1.531 1.522	1.605 1.596	1.451	1.786 1.794	1.874 1.881	2.011	2.452
6	1.243	1.299	1.386 1.346	1.465 1.449	1.537 1.527	1.611 1.600	1.616	1.800 1.809	1.887	2.031
7	1.119	1.220	1.306	1.396 1.354	1.473 1.454	1.543 1.531	1.618	1.642	1.815	1.900
8	7.186	1.110	1.428	1.705	1.956	2.181	2.401	2.664	2.686	3.370
9	3.126	0.7704	1.1142	1.460	1.739	1.982	2.202	2.420	2.698	2.713

*Calculated from RKR Potential

†Calculated from Morse Potential

TABLE 9

RELATIVE INTENSITY (SCALED TO TEN) OF THE A$^2\Sigma$ - X$^2\Sigma$ BAND SYSTEM

v′ \ v″	0	1	2	3	4	5	6	7	8	9
0	*10.00 †10.00	2.81 2.67	0.325 0.295	0.017 0.014	0.000 0.000	0.000 0.000	0.000 0.000	0.000 0.000	0.000 0.000	0.000 0.000
1	7.41 7.76	10.00 10.00	8.76 8.36	1.64 1.49	0.109 0.094	0.002 0.001	0.000 0.000	0.000 0.000	0.000 0.000	0.000 0.000
2	1.53 1.60	10.00 10.00	4.01 3.83	9.63 8.78	2.64 2.29	0.216 0.179	0.004 0.003	0.000 0.000	0.000 0.000	0.000 0.000
3	0.242 0.264	3.58 3.74	10.00 10.00	1.22 1.17	9.62 8.78	3.67 3.19	0.352 0.292	0.006 0.005	0.000 0.000	0.000 0.000
4	0.035 0.042	0.893 1.01	5.89 6.39	9.63 10.00	0.172 0.171	10.00 9.49	5.08 4.60	0.555 0.478	0.009 0.007	0.000 0.000
5	0.005 0.006	0.166 0.206	1.93 2.30	7.93 9.05	8.47 9.25	0.032 0.034	10.00 10.00	6.56 6.27	0.792 0.720	0.010 0.009
6	0.001 0.001	0.026 0.030	0.453 0.506	3.34 3.58	9.72 10.00	7.08 6.98	0.476 0.449	10.00 9.03	8.27 7.13	1.08 0.886
7	0.000 0.000	0.003 0.004	0.075 0.084	0.858 0.930	4.57 4.76	10.00 10.00	5.07 4.86	1.15 1.06	9.00 7.91	9.19 7.72
8	0.000 0.000	0.000 0.000	0.010 0.012	0.171 0.192	1.43 1.55	5.83 6.07	10.00 10.00	3.52 3.38	1.91 1.76	8.32 7.34
9	0.000 0.000	0.000 0.000	0.001 0.002	0.029 0.033	0.345 0.388	2.21 2.40	7.22 7.52	10.00 10.00	2.40 2.30	2.75 2.54

*Quantum/sec †Energy/sec

G. RELATIVE VIBRATIONAL TRANSITION PROBABILITY OF $A^2\Sigma - X^2\Sigma$ BAND SYSTEM OF AℓO

The relative vibrational transition probabilities of the $A^2\Sigma - X^2\Sigma$ band system of AℓO can be obtained from the measurement of the relative intensity of the bands and the calculated Franck-Condon factors and r-centroids. The inconsistencies in the intensity measurements of previous workers have been discussed in the preceeding quarterly report. The blue-green system of AℓO is excited by focusing the radiation from a pulse ruby laser on a pure aluminum rod (maximum impurity 50 parts per million). The experimental arrangement is shown in Figure 7. The intensities of the bands have been determined by the method of photographic photometry employing a standard lamp (GE quartz-iodine-tungsten filament lamp, Model 6.6 A/T40/1CL-200W) and a stepped wedge filter. The intensity profile of $\Delta_v = -1$ sequence obtained in this way is shown in Figure 8 which shows that the background radiation is absent. It is apparent from Figure 8 that the overlapping of the successive bands is quite large. In order to accurately determine the amount of overlapping the theoretical band profiles are being computed. The theoretical band profiles will be applied to obtain relative intensities of the bands and hence the relative vibrational transition probabilities.

H. THE MORPHOLOGY OF INTERMEDIATE OPTICALLY THICK CHEMICAL RELEASE CLOUDS - J. Pressman and H. K. Brown

In this study the image of a chemical release cloud under uniform illumination is calculated for intermediate opacities from 1 to 10 for varying angles of seeing, where there is a definite volume effect in scattering. The approach is a direct one in which the basic radioactive

Figure 7

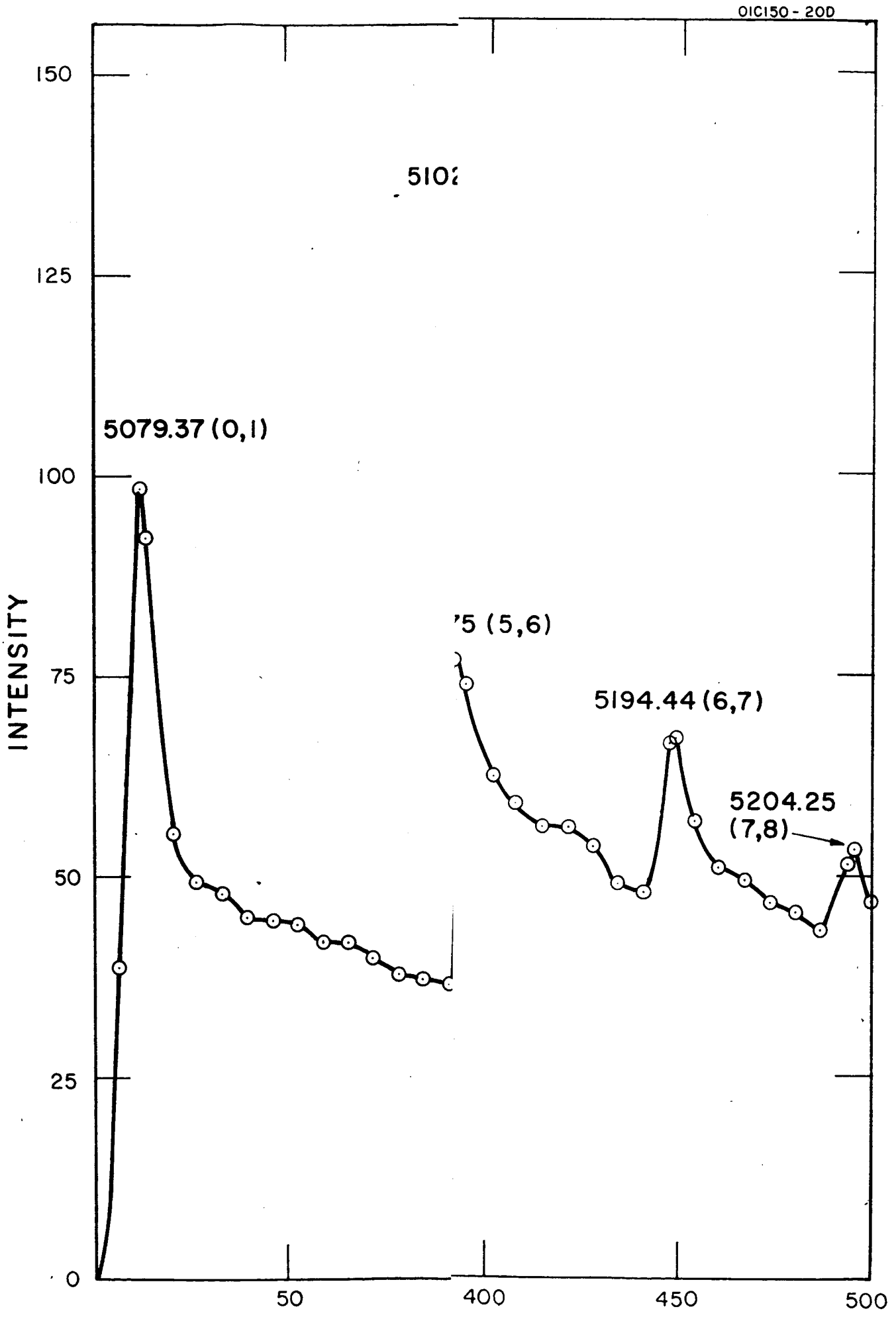
01C150 - 20D
150
125
100
75
50
25
0
INTENSITY
5102
5079.37 (0,1)
'5 (5,6)
5194.44 (6,7)
5204.25
(7,8)
50
400
450
500

transfer problem is reduced to a geometrical one of the intersection of three spheres. A simple graphical technique is described for obtaining the image, extensive tables are presented for various cases, and sample impages are drawn. A comparison is made with a rocket release experiment.

I. THE DISPERSION OF PARTICULATE MATTER IN THE UPPER ATMOSPHERE FOR DIFFERENT INITIAL VELOCITY DISTRIBUTION AND DRAG LAWS - J. Pressman and H. K. Brown

The purpose of this study is to compute the rate of growth of particulate matter in the upper atmosphere for a variety of cases. A canister is assumed to be at rest or moving, the initial velocity distribution is assumed a centrifugally determined on or a Maxwellian one from a presumed explosive burst. The drag forces are assumed to be zero, proportional to velocity, and proportional to the velocity squared. Analytical expressions are determined for all these cases.

APPENDIX A

The Chemiluminescent Reactions of Atomic Oxygen with COS and H_2S

by

A. Sharma, J. P. Padur, and P. Warneck
GCA Corporation, Bedford, Massachusetts 01730

ABSTRACT

The chemiluminescence intensity in the reactions O + COS and O + H_2S was studied in a flow system as a function of reaction time and reactant concentrations. In the initial stage of the reactions, the intensity increases linearly with time, the slope being proportional to the concentration of COS or H_2S and to the square of atomic oxygen concentration. A kinetic analysis shows that these results are consistent with the notion that the reaction responsible for the emission in both cases is

$$(3) \qquad O + SO \rightarrow SO_2 + h\nu \ .$$

From the relative intensities, it is concluded that the rate of SO formation in the H_2S reaction is 1.85 times greater than that in the COS reaction. The rate constant for reaction (3) was determined as $k_3 = 5.7 \times 10^{15}$ cc/molecule sec from comparison measurements using the air afterglow reaction as a standard. The consumption of SO radicals by reaction (3) in the later stages of the reaction is discussed, and it is concluded that another SO loss reaction must be operative in addition to reaction (3).

INTRODUCTION

Mass spectrometric investigations by Liuti, Dondes and Harteck[1] and in this laboratory[2] have shown that the first step in the reaction of oxygen atoms with carbonyl sulfide is the formation of SO radicals

$$(1) \qquad O + COS \rightarrow CO + SO \ .$$

The rate constant for this process has been determined.[2] The reaction of oxygen atoms with hydrogen sulfide has also been found[1] to yield SO radicals via

$$(2) \qquad O + H_2S \rightarrow H_2 + SO,$$

although there is probably a second operative reaction path leading to OH and SH radicals as additional products.

The chemiluminescence associated with these reactions has also been investigated.[3-7] A comparative study[3] has shown that the emission spectra from the reactions of oxygen atoms with carbonyl sulfide, hydrogen sulfide and carbon disulfide, and the SO_2 afterglow spectrum are nearly identical, featuring similar intensity distributions. These observations suggest that the emitter and the process leading to the formation of the emitter are the same in all four cases of chemiluminescence. Evidence is mounting that the reaction responsible for the emissions is

$$(3) \qquad O + SO \rightarrow SO_2^{**} + h\nu \ ,$$

as was originally suggested by Gaydon.[4] Hermann, et al.,[5] observed that

the short wavelength cut-off of the SO_2 afterglow near 2400 Å coincides with the onset of the dissociation continuum in the SO_2 absorption spectrum. Halstead and Thrush[6] found that the SO_2 afterglow intensity is directly proportional to the product of oxygen atom and SO radical concentrations. More recently, Rolfes, Reeves and Harteck[7] studied the light emission from the reaction of O-atoms with COS at low total pressures, and compared it with the $O + NO_2$ reaction resulting in the air-afterglow emission involving radiative combination of atomic oxygen with nitric oxide. Their results indicate that the two reactions are analogous and that reaction (3) proceeds via a simple two-body combination mechanism.

The present work set out to derive additional evidence for the occurrence of reaction (3) by studying the time dependence of the chemiluminescent intensity in the reactions of atomic oxygen with COS and H_2S for various initial reactant concentrations. From such experiments, the rate coefficients associated with reactions (2) and (3) could be determined. In addition, intensity profiles were obtained for the later stage of the reaction of oxygen atoms with COS to explore the possibility of other SO loss reactions besides reaction (3).

EXPERIMENTAL

The conventional fast flow system employed a cylindrical reactor of 1.9 cm internal diameter. Atomic oxygen was produced by microwave discharge. Either a 99:1 argon-oxygen mixture or pure oxygen was discharged. The second reactant entered the reactor via an inlet provided with several radially oriented holes. The inlet could be moved along the reactor axis by means of a friction drive. Observations were made downstream of the mixing point using a 1P28 photomultiplier tube connected to a Victoreen microameter. The chemiluminescent emission was viewed through a quartz window mounted on the side of the reactor. A collimating slit system was interposed so that a spatial resolution of about 0.7 mm was obtained. The corresponding time resolution was 0.7 milliseconds for linear flow rates around 10 m/sec.

Capillary flowmeters were used to measure volume flow rates of the individual gaseous components: argon, oxygen, carbonyl sulfide, and hydrogen sulfide. The concentrations of these constituents at the mixing point were determined from the fraction of the total flow rate and the prevailing total pressure measured with a McLeod gauge. The total pressure was held at 800 microns unless stated otherwise. Atomic oxygen concentrations were determined by gas titration, using the procedure described by Harteck, et al.[8] This is a two-step method. Oxygen atoms are first titrated with NO_2 to determine the maximum intensity corresponding to the

titration half-point. The NO_2 is then replaced by NO to determine the NO flow corresponding to the same intensity value. The accuracy of this method is not as good as the direct titration with NO_2, but the complications due to the 2 $NO_2 \rightleftharpoons N_2O_4$ equilibrium in measuring NO_2 flow rates are avoided.

RESULTS AND DISCUSSION

Dependence of Intensity on Time and Concentration

To investigate the time dependence of the chemiluminescence intensity, the photomultiplier currents were recorded as a function of the reactant inlet position, and the reaction time was calculated from the distance between inlet position and observation point, and the prevailing linear flow rate of the gas mixture in the reactor. Corrections concerning the origin of the time scale were required due to the insufficient spectral resolution and, in part, due to back diffusion of the admixed reactant. The introduction of both COS and H_2S gave emission intensities which increased with time and which extrapolated to zero at the origin. The observed increase of intensity with time was linear so long as the reaction times were reasonably short, and the employed concentrations were moderate. Figure 1 demonstrates this observation for the reaction of oxygen atoms with COS in a plot of intensities versus time for three initial COS concentrations. Only the highest COS concentration produces a non-linear intensity-time dependence at reaction times greater than 8 milliseconds.

The linearity of intensity with time in the vicinity of the mixing point permits the use of the initial slope of the intensity-time profile as a measure of the reaction rate. The variation of the initial slope with oxygen atom concentration for the reactions with either COS or H_2S is shown in Figure 2 using a logarithmic plot presentation. The concen-

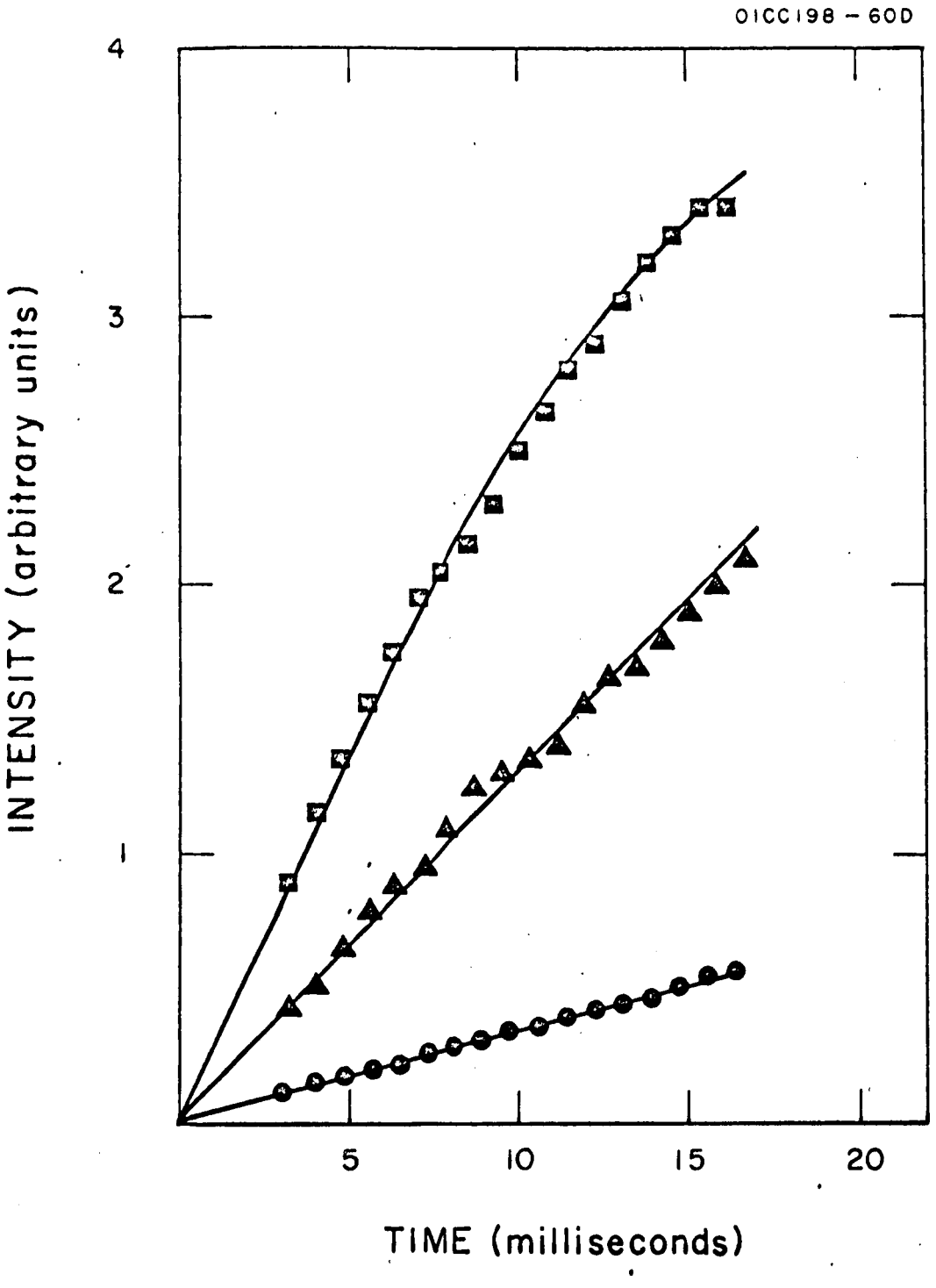

Figure 1. Chemiluminescence intensity vs reaction time in system O + COS for three initial COS pressures: 7.6 microns (●); 20.6 microns (▲); 35 microns (■); the average O-atomic pressure was 9.5 microns.

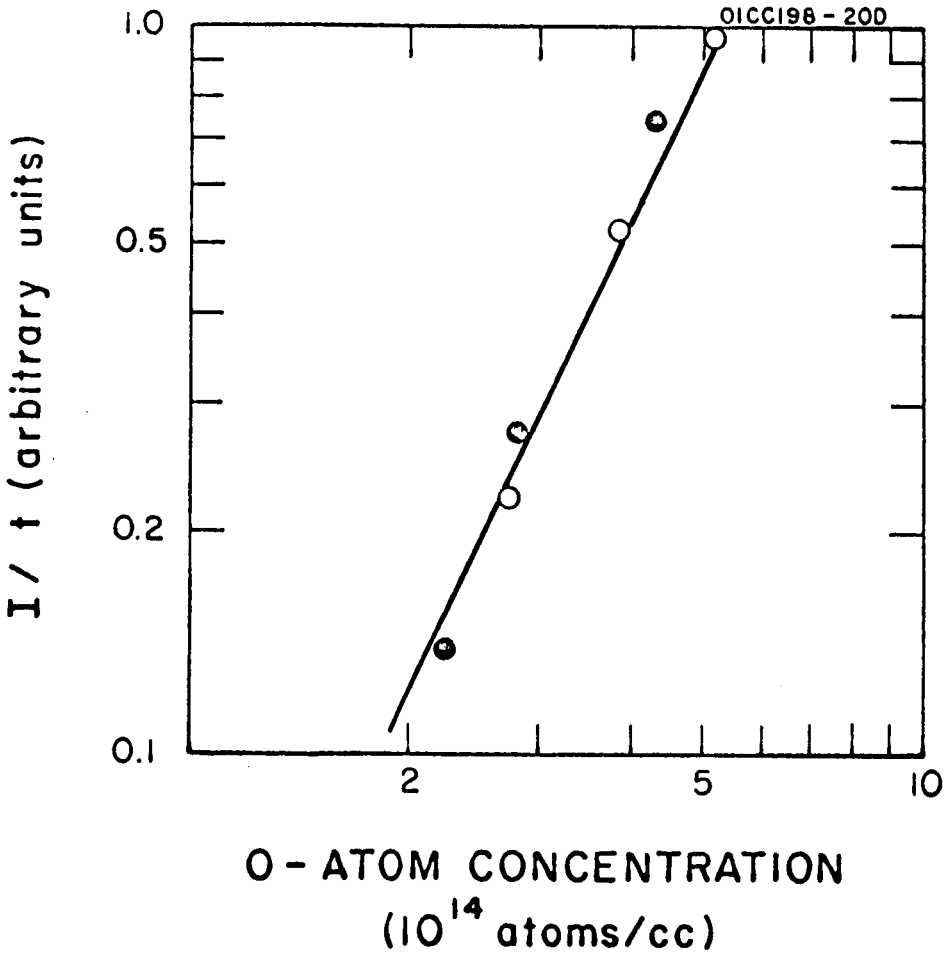

Figure 2. Initial slope of intensity-time profile as a function of O-atom concentration for the systems O + COS (●) and O + H_2O (○).

trations of COS and H_2S, respectively, were held constant in these experiments. The intensities for the H_2S reaction, actually, were by about a factor of two brighter than those shown in Figure 2, but these data points were adjusted to fall onto the same line as the COS data, so that the equivalence of the dependence on oxygen atom concentration in both cases is more clearly demonstrated. The slope of the straight line in Figure 2 is S = 2.08, indicating that the chemiluminescence intensity is proportional to the square of the oxygen atom concentration.

Figure 3 shows, in a similar fashion, the variation of the initial slope of the intensity time profile with COS concentration and H_2S concentration, respectively. Data from several runs performed on different days were used in this plot and corrected for the observed oxygen atom concentration making use of the $(O)^2$ law. Here again, the data indicate a brighter chemiluminescence for the H_2S reaction when compared with the emission from the reaction with COS. However, both plots yield straight lines with nearly identical slopes. The averaged value for the two slopes, S = 1.1, indicates a first order concentration dependence for carbonyl sulfide and hydrogen sulfide.

In addition to these experiments in which the total pressure was 800 microns, a set of experiments was carried out for the O + COS reaction at a total pressure of only 330 microns. It was established that, at the lower pressure, the intensity dependence on reaction time and initial reactant concentrations was the same as that at 800 microns, but the

overall intensity was found to be smaller. Although this result appears to indicate a pressure dependence of reaction (3), it has not been possible to verify this point in a positive manner, because the flow rate could not be adequately controlled in the present apparatus. If correct, this result would contradict the observation by Rolfes, Reeves and Harteck[7] at lower pressures that reaction (3) does not require a third body. Halstead and Thrush[6] did not provide independent information on this point. In view of our own experimental uncertainty and because the data by Rolfes et al.[7] favor a two-body process for reaction (3), their position is adopted here. In any case, most of the conclusions reached in this discussion will not be altered should it be shown in the future that reaction (3) is pressure dependent. However, it is apparent that this point requires further examination.

The results summarized in Figures 1-3 can be interpreted in terms of reactions (1) through (3), if it is taken into account that for sufficiently short reaction times the consumption of the initial reactants is still negligible. With this condition, the SO concentration is a linear function of reaction time, at least in the initial stage of the reaction where the destruction of SO radicals by reaction (3) or other follow-up reactions is not yet significant. For the reaction of atomic oxygen with carbonyl sulfide, the initial rate of SO radical production is,

$$\frac{\Delta(SO)}{\Delta t} = k_1 [O][COS],$$

and the increase of intensity ΔI produced by reaction (3) in the time interval Δt is correspondingly,

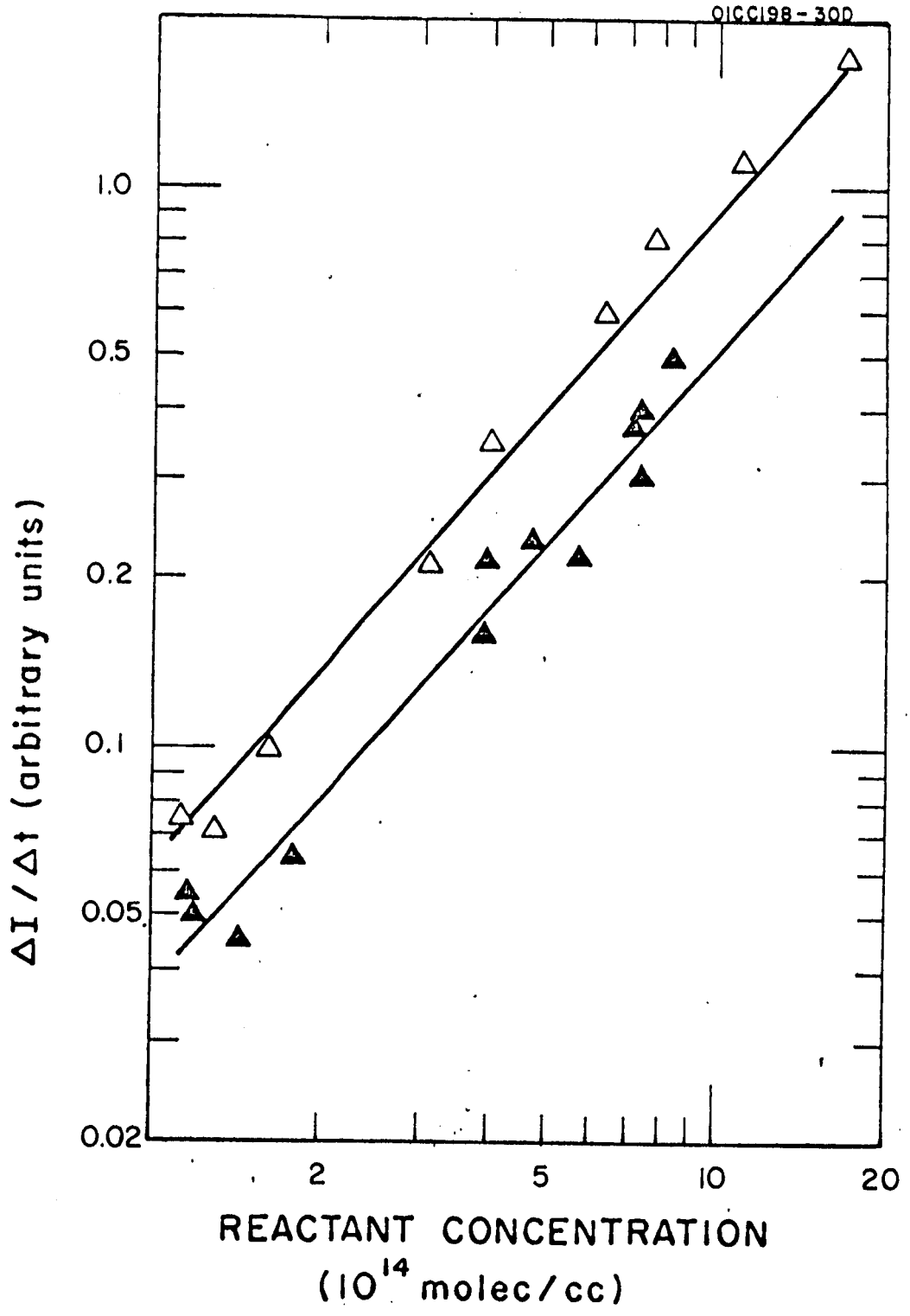

Figure 3. Initial slope of intensity-time profile as a function of COS (▲) and H_2S (△) concentrations.

$$(A)\quad \frac{\Delta I_1}{\Delta t} = k_3\,[O]\,\frac{\Delta[SO]}{\Delta t} = k_3\,k_1\,[O]^2\,[COS].$$

The right-hand side of this equation represents the initial slope of the intensity-time profile. A similar expression is derived also for the reaction of oxygen atoms with hydrogen sulfide:

$$(B)\quad \frac{\Delta I_2}{\Delta t} = k_3\,[O]\,\frac{\Delta[SO]}{\Delta t} = k_3\,k_2\,[O]^2\,[H_2S].$$

Equations (A) and (B) predict a linear relationship with initial COS or H_2S concentration, and a quadratic one for the atomic oxygen concentration. This is in agreement with the relationship found in the present experiments.

Alternatively, the present results can be used to demonstrate that the chemiluminescence intensity is proportional to the product of the concentrations of atomic oxygen and SO radicals, as required if reaction (3) is the predominant light emitting process. These results, therefore, are in good agreement with the data reported by Halstead and Thrush,[6] and by Rolfes et al.[7] It is also significant that the analysis of the present data refers to the very early stage in the reactions, because a variety of mechanisms can be suggested which lead to the observed concentration dependence, but feature different chemiluminescent reactions. However, such mechanisms would require the build-up of an intermediate concentration (such as SO), so that initially, the chemiluminescence intensity could not be a linear function of time. The observed concentration dependences and linearity with time taken together constitute strong evidence in favor of assigning reaction (3) as the principal chemiluminescent reaction.

Determination of the Rate Constants k_2 and k_3

With the identification of reaction (3) as the principal light emitting process occurring in both the O + COS and the O + H_2S reactions, it becomes possible to determine the involved rate constants by appropriate comparison experiments.

It has already been noted that the reaction of atomic oxygen with H_2S produces a brighter chemiluminescence than the reaction with COS under similar conditions. This fact can now be explained by the difference of the associated rate constants. As equations (A) and (B) show, the ratio of the initial slopes obtained for the intensity-time profiles in the two reactions is given by

$$(C) \quad \frac{\Delta I_2/\Delta t}{\Delta I_1/\Delta t} = \frac{k_2}{k_1} \frac{[H_2S]}{[COS]} \frac{[O]_2^2}{[O]_1^2} ,$$

where $[O]_1$ and $[O]_2$ refer to the initial oxygen atom concentrations prevailing in the COS and H_2S experiment, respectively. According to equation (C), the ratio of the rate constants, k_2/k_1, can be obtained directly from Figure 2, where the data are corrected for the varying initial oxygen atom concentrations. Since the logarithmic plot in Figure 2 yields parallel lines, k_2/k_1 is represented simply by the ratio of the $\Delta I/\Delta t$ values for identical COS and H_2S concentrations. The averaged ratio of rate constants obtained from these data is $k_2/k_1 = 1.85$.

In the region where the dependence of intensity on reaction time is still linear, the right-hand side of equation (C) also represents the ratios of intensities at any time t. An experiment was performed in which the chemiluminescence intensity in the vicinity of the mixing point was

recorded as a function of the COS and H_2S flow rates. The results shown in Figure 4 are appropriately corrected for the difference of oxygen atom concentration in the two cases. Since for small reactant flows the reactant concentrations are proportional to the measured flow rates, the observed linear increase of intensities for moderate flow rates again verifies the first order concentration dependence discussed above. The ratio of the slopes in Figure 4 is

$$\frac{\Delta I_2/\Delta[H_2S]}{\Delta I_1/\Delta[COS]} = \frac{k_2}{k_1} = 1.85,$$

in excellent agreement with the average value found above. Applying the previously determined value for the rate constant of the O + COS reaction, $k_1 = 0.91 \times 10^{-14}$ cc/molecule sec^2, one obtains the absolute value $k_2 = 1.70 \times 10^{-14}$ cc/molecule sec. It must be emphasized that this rate constant refers only to that portion of the O + H_2S reaction which leads to the formation of the SO radicals. The overall reaction probably includes the formation of other products so that it is faster. However, the present results indicate that these other products do not participate in the chemiluminescence mechanism.

The rate constant associated with the reaction

$$(3) \qquad O + SO \rightarrow SO_2 + h\nu$$

was determined by comparing the light emission from the O + COS reaction with that produced in the air-afterglow reaction

$$(4) \qquad O + NO \rightarrow NO_2 + h\nu.$$

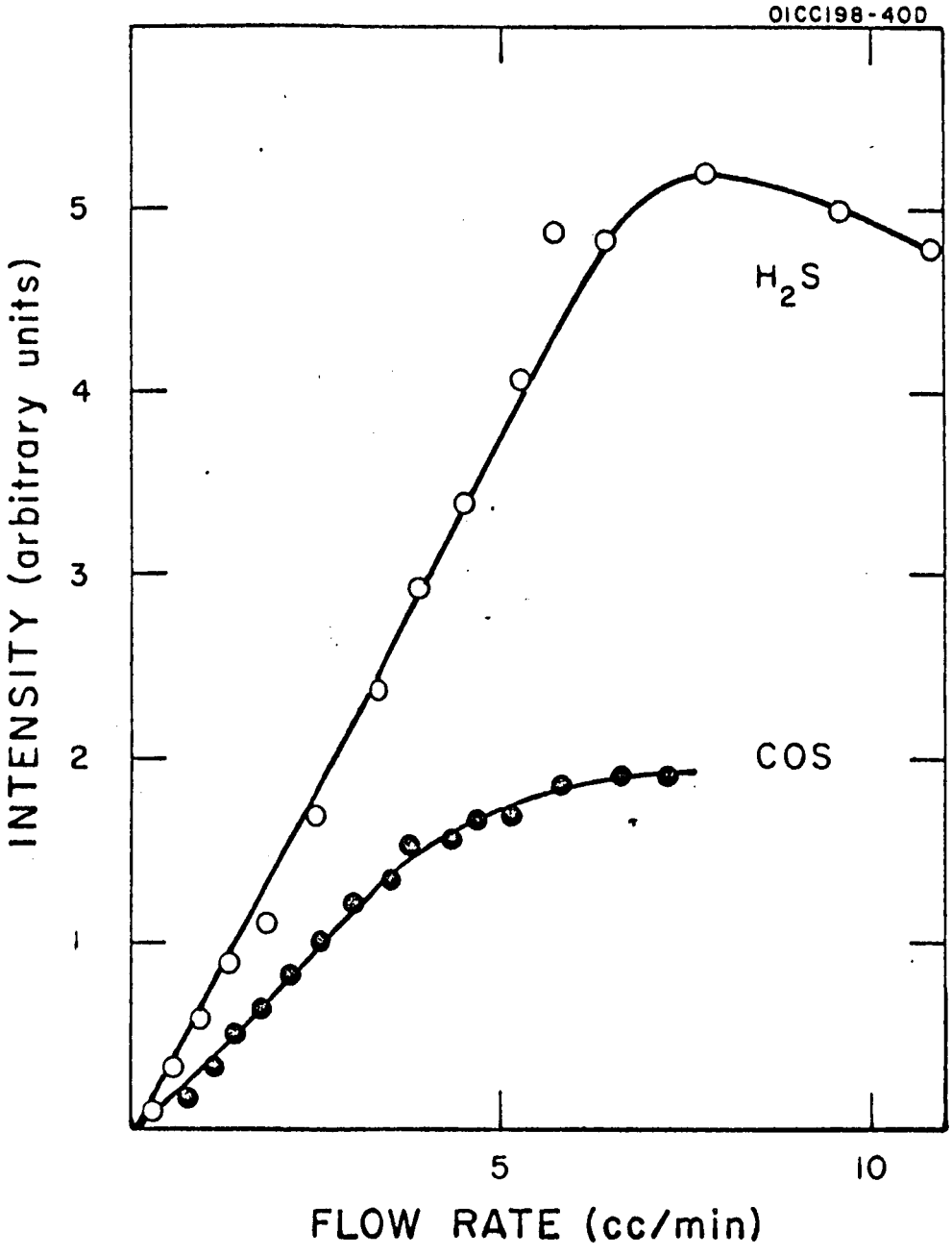

Figure 4. Intensity vs flow rate of COS (●) and H_2S (0) at constant O-atom concentration.

The relative spectral intensity distribution for reaction (3) was previously determined in this laboratory.[3] The emission lies mainly in the violet and ultraviolet portion of the spectrum. Fontijn, Meyer, and Schiff[9] have determined the spectral intensity distribution for reaction (4) and have shown that it is centered in the red and near infrared. Both emissions overlap in the 3800 to 5200Å wavelength region. An interference filter was, therefore, employed in the comparison experiment to limit the radiation seen by the photomultiplier to the region of overlap. The filter featured a transmission maximum near 4100Å and a bandwidth of 75Å. The fraction of radiation registered by the photomultiplier-filter combination compared to the total integrated emission from each reaction was determined from the known spectral response of the phototube, the transmission characteristics of the filter and the relative spectral intensity distributions for both reactions. The evaluation of the comparison experiment requires only the ratio of the two fractions, which was found to be $f_4/f_3 = 0.029$, where the subscripts refer to reactions (4) and (3), respectively.

The introduction of nitric oxide to the gas flow containing oxygen atoms results in an emission intensity which is time-independent, whereas it has been shown above that the introduction of carbonyl sulfide produces an intensity which increases linearly with time. In the first case, the intensity is given by

$$I_4 = k_4 [O] [NO] ,$$

and in the second case by equation (A). With the provision that the oxygen atom concentration remains constant, the combination of both equations yields

$$k_3 = \frac{k_4 [NO] \Delta I_1/\Delta t}{k_1 [O] [COS] I_4} ,$$

or when the total intensities I_1 and I_4 are replaced by the equivalent photomultiplier currents i_1 and i_4,

$$k_3 = \frac{f_4 k_4 [NO] \Delta i_1/\Delta t}{f_3 k_1 [O] [COS] i_4} \cdot \qquad (D)$$

The following individual rate constants were employed in the evaluation of equation (D): $k_1 = 0.91 \times 10^{-14}$ cc/molecule sec, given by Sullivan and Warneck;[2] and $k_4 = 6.4 \times 10^{-17}$ cc/molecule sec, determined by Fontijn, Meyer, and Schiff.[9]

Figure 5 shows the results of the comparison experiments. The photomultiplier currents registered upon admixture of either NO or COS to a discharged argon-oxygen mixture are plotted as a function of reaction time. From the slope of the current-time profile for the O-COS reaction, one obtains $\Delta i_1/\Delta t = 330 \times 10^{-7}$ A/sec, whereas $i_4 = 0.085 \times 10^{-7}$A. The prevalent concentrations of nitric oxide, carbonyl sulfide, and atomic oxygen are given in the legend. With these data, equation (D) yields the rate constant associated with reaction (3): $k_3 = 5.7 \times 10^{-15}$ cc/molecule sec. This value is about eight times greater than the rate constant estimate given previously by Rolfes, Reeves, and Harteck,[7] but the discrepancy is reduced by the following circumstances. First, these authors used for k_4 the earlier value[10] $k_4 = 3 \times 10^{-17}$ cc/molecule sec. Also, owing to the many experimental quantities that enter into Equation (D), the present method of determining k_3, although straightforward, is affected by a large experimental error. The derived value can be in error by as much as a factor of two in view of the uncertainties within which k_1 and k_4 are known. In addition, it must be considered that Rolfes et al.[7] worked at total pressures around 10 microns, whereas in the present experiments,

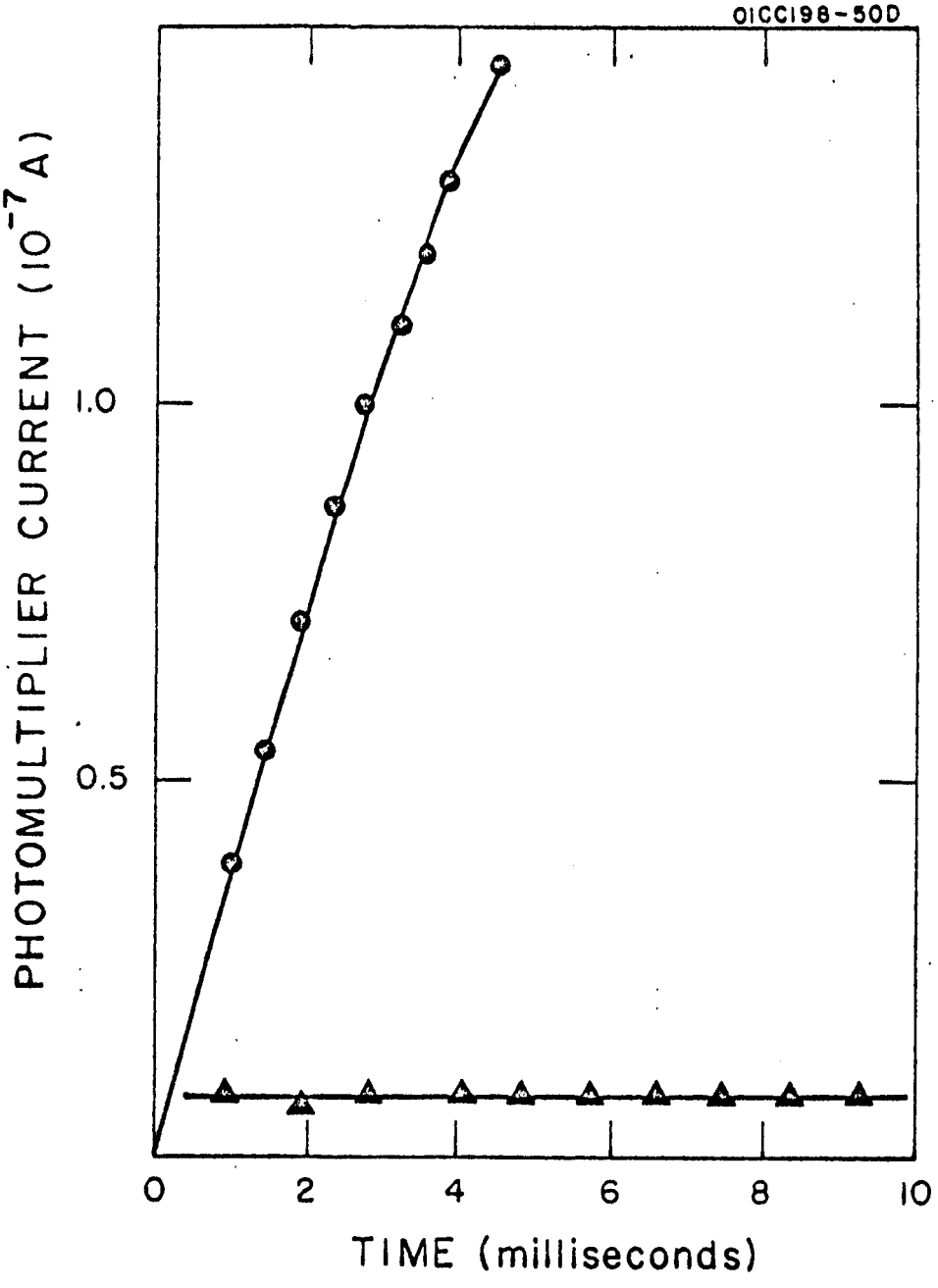

Figure 5. Intensity-time profile for O + COS (●) and O + NO (▲). Concentrations in molecules/cc are $[COS]_o = 4.2 \times 10^{14}$; $[NO]_o = 5 \times 10^{14}$; and $[O]_o = 1.65 \times 10^{14}$.

the pressure was 800 microns. The two values for k_3, therefore, are in sufficient agreement to suggest that reaction (3) is pressure independent. The rate constant value is found to be about 100 times greater than that of reaction (4), despite the indication that both reactions are of the same type. Most significant is the result that reaction (3) is almost as rapid as the precursor reaction (1). As a consequence, reaction (3) is effective in determining the course of the O + COS and O + H_2S reactions in their later stages.

SO Radical Consumption

While in the initial stage of the reactions under discussion the chemiluminescence intensity is characterized predominantly by the production of SO radicals, it is evident from the ratio of the rate constants $k_3/k_1 = 0.63$ that, in the later stages of the reactions, the consumption of SO radicals by reaction (3) cannot be ignored. The importance of SO radical losses due to secondary reactions was recognized previously, but reaction (3) had not been considered fast enough to provide a significant SO reaction channel. Instead, the reaction

$$(5) \qquad SO + SO \rightarrow SO_2 + S$$

had been suggested both by Sullivan and Warneck[2] to explain their mass spectrometer results, and by Rolfes et al.[7] to account for the deposition of sulfur in their reaction vessel. From the k_3 value found in the present work, it appears, however, that the mass spectrometer results could be equally well be explained by reaction (3) in place of reaction (5). While, of course, the present experiments could not provide detailed information on the individual reactions prevailing in the later stages of the O + COS

and O + H_2S reactions, it was nevertheless, of interest to investigate the possibility that reaction (3) constitutes the major SO loss reaction. For this purpose, the intensity profiles observed in the reaction of atomic oxygen with COS were compared with profiles calculated on the assumption that the predominant mechanism consists only of reactions (1) and (3). The results of this experiment are shown in Figure 6. Calculated intensities are plotted in the form $[SO][O]/[O]_o^2$ versus the reaction parameter $\tau = k_1[O]_o t$ for several initial reactant concentration ratios $y_o = [COS]/[O]_o$. The experimental data points were obtained with pure oxygen instead of the argon-oxygen mixtures, so that a higher initial oxygen atom concentration could be realized. A common scaling factor was applied to the experimental intensity data to facilitate the comparison.

Figure 6 clearly indicates that except in the initial stage of the reaction, the agreement between calculated and experimental intensity profiles is very poor. Not only are the observed intensities lower than the calculated ones, but the maxima also occur sooner. In addition, it appears that the observed maximum intensities do not follow the calculated trend indicated by the dashed line in Figure 6, but are lower for $y > 2$. These results lead to the conclusions that, despite its comparatively fast rate, reaction (3) alone is insufficient to explain the observed intensity profiles and that an additional reaction involving the consumption of SO radicals must be included in the overall mechanism. The reaction possibilities requiring consideration were discussed previously,[2,7], and arguments were given which favor reaction (5).

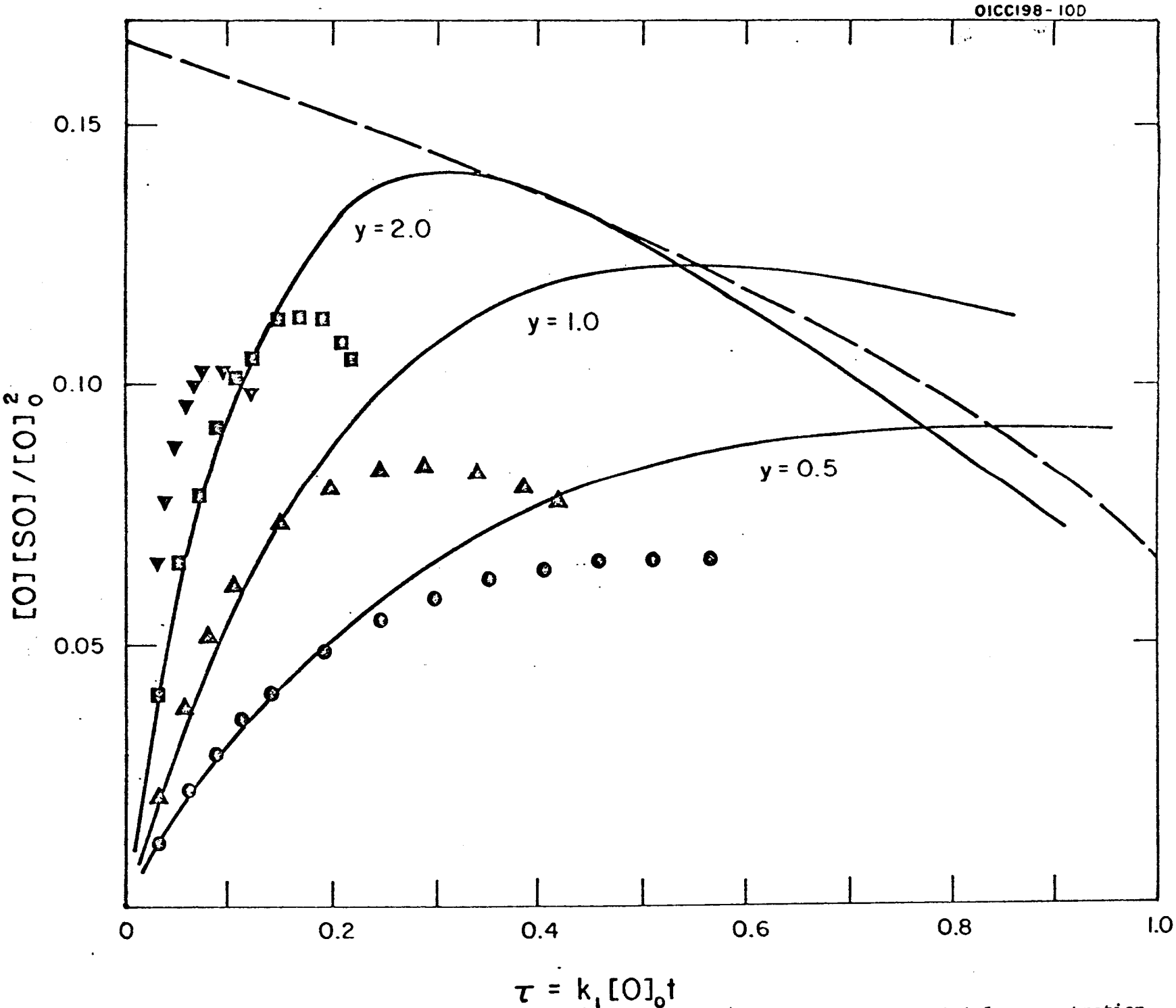

Figure 6. Intensity-time profile for the system O + COS for different initial concentration ratios $\varphi = [COS]_o/(O)_o$. Experimental data: 0.57 (●); 0.93 (▲); 1.9 (■); 3.0(▼). Calculated values shown by solid lines. The dashed line indicates loci of maxima.

CONCLUSIONS

The behavior of chemiluminescence intensity with reaction time and reactant concentrations in the initial stage of the reactions (1) O + COS and (2) O + H_2S has been found to support the suggestion that the reaction responsible for the chemiluminescence is the radiative combination of atomic oxygen with SO radicals: reaction (3). Comparative intensity measurements enabled the determination of the rate constants associated with reactions (2) and (3). The combination reaction (3) was found to be almost as fast as reactions (1) and (2), so that it causes an appreciable consumption of SO radicals in the later stages of the reactions. Nevertheless, an additional SO loss reaction is required to explain the intensity profiles observed in the later reaction stages.

REFERENCES

1. G. Liuti, S. Dondes and P. Harteck, presented at the Fall Meeting of the American Chemical Society, New York (1963).
2. J. O. Sullivan and P. Warneck, Ber. Bunsenges. 69, 7 (1965).
3. A. Sharma, J. P. Padur and P. Warneck, J. Chem. Phys. 43, 2155 (1965).
4. A. G. Gaydon "The Spectroscopy of Flames" Chapman and Hall, Ltd, London (1957).
5. L. Hermann, J. Akrich and M. Grenat, J. Quant. Spectry. Radiative Transfer 2, 215 (1962).
6. C. J. Halstead, B. A. Thrush, Nature 204, 992 (1964).
7. T. R. Rolfes, R. R. Reeves and P. Harteck, J. Phys. Chem. 69, 849 (1965).
8. P. Harteck, R. R. Reeves and G. G. Manella, J. Chem. Phys. 32, 632 (1960).
9. A. Fontijn, C. B. Meyer and H. I. Schiff, J. Chem. Phys. 40, 64 (1964).
10. A. Fontijn and H. I. Schiff, in "Chemical Reactions in the Lower and Upper Atmosphere," Interscience Publ. Inc., New York (1961) p. 239.

APPENDIX B

A Spectroscopic Study of the Chemiluminescent Reaction of Germanium Tetrahydride with Atomic Oxygen*

by

A. Sharma and J. P. Padur

GCA Corporation, Bedford, Massachusetts 01730

ABSTRACT

The spectrum of the glow produced during the gas phase reaction of germanium tetrahydride with atomic oxygen is studied in the region from 2450 to 5100 Å. About one hundred bands are measured between 2350 and 4000 Å. Almost all bands on the short wavelength side of the spectrum belong to the D-X band system of GeO. Several new bands of the D-X system are observed together with a number of unidentified bands. The present study indicates the possibility of a new band system of GeO in the region 3000 and 5000 Å.

*This work was supported by the National Aeronautics and Space Administration.

1. Introduction

The spectroscopic studies of the chemiluminous reactions of atomic oxygen with several substances have been previously undertaken by several workers and summarized by Gaydon (1957). Recently, Kaufman (1961) has reviewed the kinetics of the atomic oxygen reactions with various compounds. However, no information regarding the chemiluminescent reaction of atomic oxygen with germanium compounds is available. We have found that the reaction of germanium tetrahydride with atomic oxygen is accompanied by a strong blue chemiluminescence. On the other hand, we did not observe any visible chemiluminescence during the reaction of atomic oxygen with germanium tetrachloride.

The examination of the spectra of the chemiluminescence produced during the reaction of germanium tetrahydride and atomic oxygen reveals a large number of bands in the region from 2450Å to 5100Å. Most of the bands on the short wavelength side of the spectrum belong to the D-X system of GeO. In addition to the bands of the D-X system of GeO observed by previous investigators, we have observed a number of new bands belonging to the above system. A number of unidentified bands are also observed, which presumably indicate the presence of a new band system of the GeO molecule on the longer wavelength side of the D-X system of GeO. In this paper, we shall present the results of the spectroscopic study of the chemiluminescent reaction of germanium tetrahydride and atomic oxygen.

2. Experimental Procedure

A conventional fast flow system was used for the present study, which consists of a 2 cm i.d. pyrex tube equipped with quartz windows and

inlets for introducing atomic oxygen and other reactants. The atomic oxygen was produced by a microwave discharge through about 100:1 mixture of argon and oxygen. The dissociation of molecular oxygen provides about one percent of atomic oxygen in the presence of very little molecular oxygen. The flow tube dimensions and the pumping speed were such that the linear flow velocity of gases were of the order of 1000 cm/sec. The depletion of atomic oxygen due to recombination between the discharge and the reaction tube was only a few percent of the initial atomic oxygen concentration produced by the microwave discharge. The germanium tetrahydride or germanium tetrachloride (from Alfa Inorganics, specified minimum purity of 99 percent) was introduced into the reaction tube through a flow meter and a needle valve. A blue glow was observed during the reaction of germanium tetrahydride and atomic oxygen. However, no visible chemiluminescence was observed when germanium tetrachloride was introduced in the reaction tube together with the atomic oxygen.

The spectrum of the chemiluminescence produced during the reaction of germanium tetrahydride and atomic oxygen was studied with a grating monochromator, Hilger's small quartz spectrograph and a Jarrel-Ash 1.5m grating spectrograph. The initial spectrum was recorded with a Perkin-Elmer (Model 99) monochromator equipped with a 600 line/mm grating blazed at 5000Å and an E.M.I. 9558Q photomultiplier tube. In order to find the true relative intensity of the observed spectrum, the spectral response of the recording system was obtained from the observed spectrum of a standard light source (GE quartz iodine tungsten filament lamp, Model 6.6A/T4Q/1CL-200W). The absolute irradiance of the lamp was obtained from Stair et al. (1963). The initial recorded spectrum of the

chemiluminescence produced during the reaction of germanium tetrahydride and atomic oxygen was corrected for the spectral response of the recording system and the corrected profile of the recorded spectrum is shown in Figure 1. It can be seen from the corrected spectrum (Figure 1) that its intensity is strongest in the wavelength region around 3100Å. Since the sensitivity of the recording system drops considerably at wavelengths shorter than 3000Å, the spectrum of the chemiluminescence was photographed with a Hilger's small quartz spectrograph and is shown in Plate 1. The spectrum photographed with this spectrograph shows the presence of a large number of bands between the wavelength of 2500Å and 5000Å.

The dispersion and resolution of the small quartz spectrograph was not sufficient for the definite identification of the observed bands. Therefore, a spectrum was photographed with a 1.5m Jarrel-Ash grating spectrograph with a grating blazed at 3000Å and reciprocal dispersion of about 11Å/mm. The exposure time required to obtain a good spectrum on 103 a-F film was about 2 hours. A wide slit of about 2 mm width was used because of the low intensity of the chemiluminescence and small light gathering power of the grating spectrograph. This has necessarily resulted in some loss of resolution. An enlargement of the photographed spectrum is shown in Plate 2.

3. Experimental Results

The spectrum recorded with the 1.5m grating spectrograph was used for the measurement of the wavelength of the band heads which are given in the first column of Tables I and II. The second column of Tables I and II shows the visually estimated intensity of the bands.

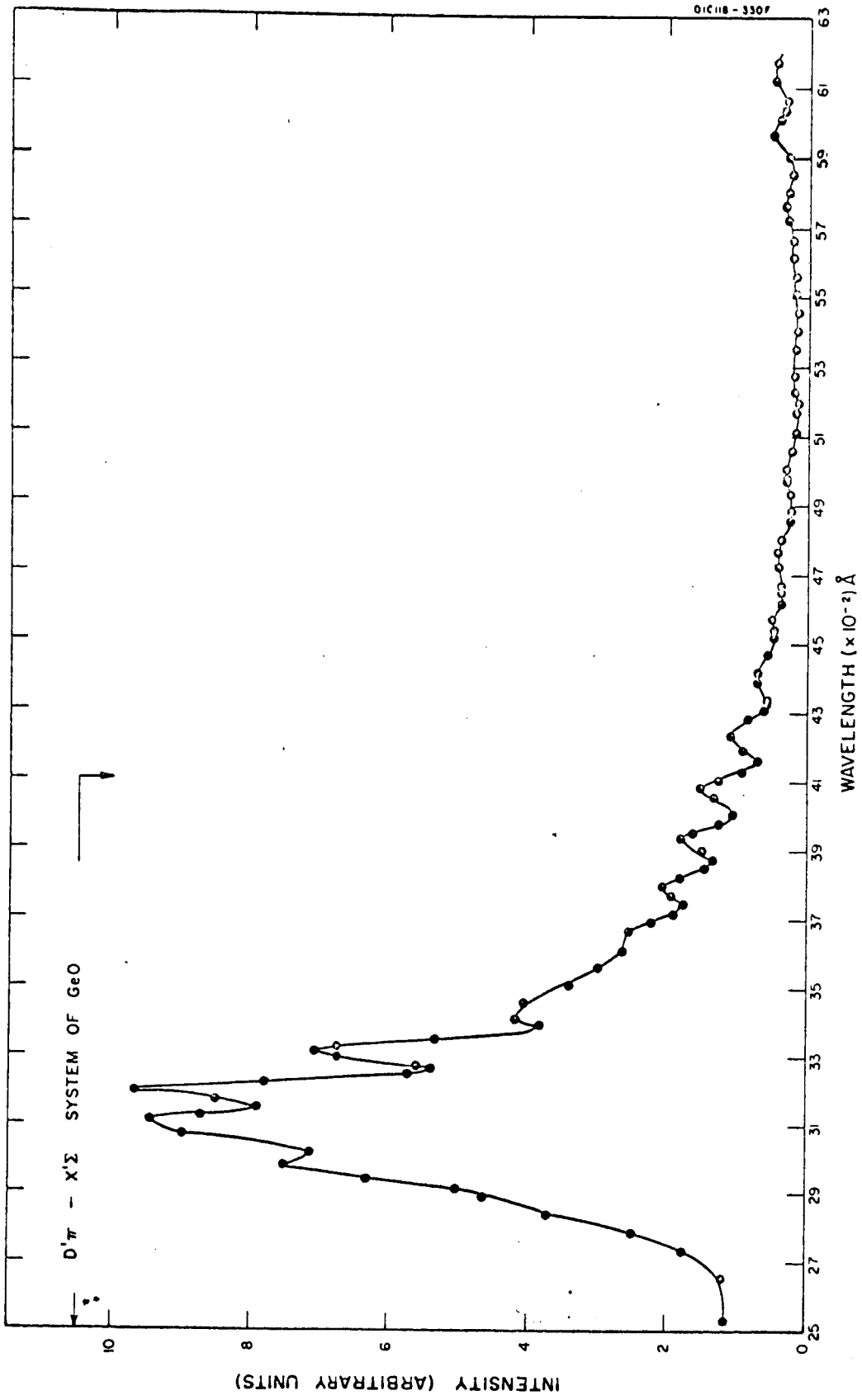

Figure 1. The corrected spectrum of the chemiluminescence produced during the reaction of germanium tetrahydride with atomic oxygen.

THE SPECTRUM OF CHEMILUMINESCENCE PRODUCED DURING THE REACTION OF GERMANE WITH ATOMIC OXYGEN.

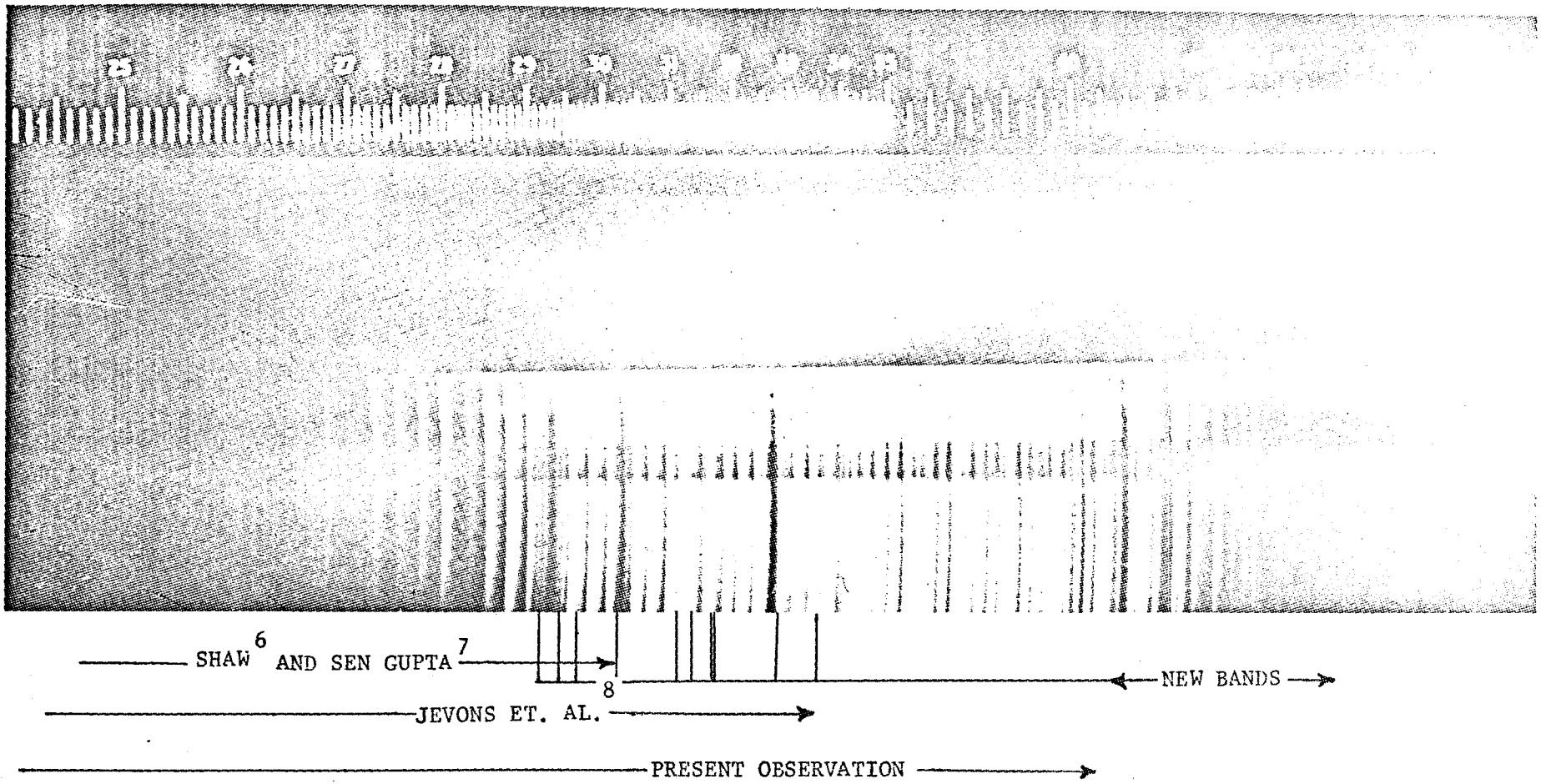

Plate 1 - The spectrum of the chemiluminescence produced during the reaction of germanium tetrahydride with atomic oxygen photographed with a Hilger's small quartz spectrograph.

THE SPECTRUM OF CHEMILUMINESCENCE PRODUCED DURING
THE REACTION OF GERMANE WITH ATOMIC OXYGEN

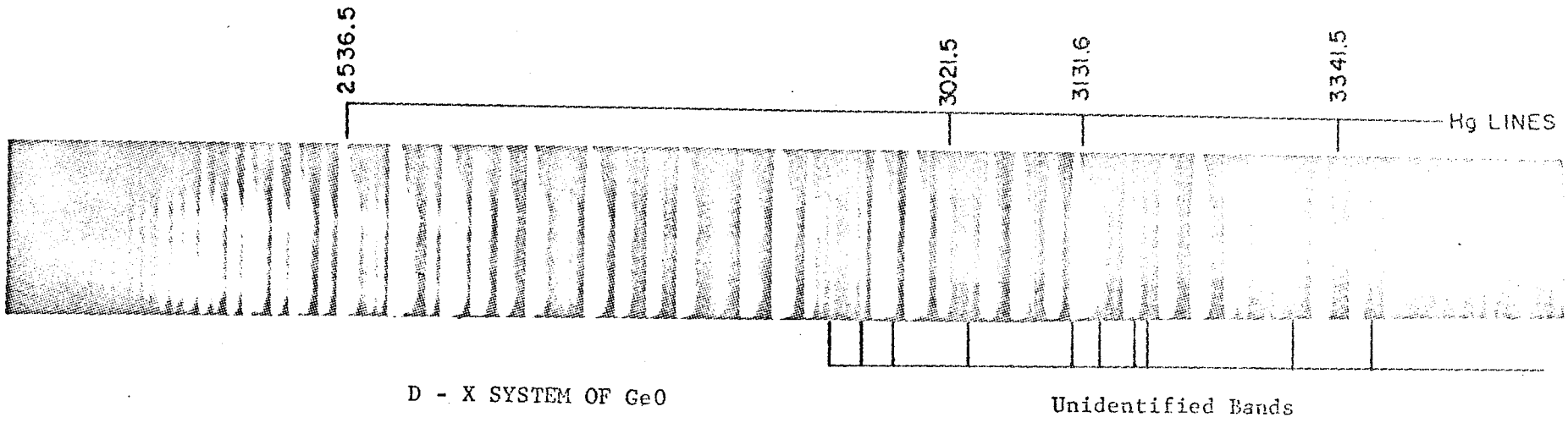

Plate 2 - The spectrum of the chemiluminescence produced during the reaction of germanium tetrahydride with atomic oxygen photographed with a Jarrel-Ash 1.5 m grating spectrograph.

TABLE I

THE IDENTIFICATION OF THE BANDS OF D-X SYSTEM OF GeO

Measured λ Å	Intensity Visual Estimate	λ (v′, v′′) (Jevons et al,1937)	Identification λ Calculated (v′, v′′)
2364.7*	1		2365.85 (11,2)
2373.6*	1		2375.4 (9, 1)
2386.1*	2		2385.67 (7, 0)
2397.1*	2		2398.3 (10,2)
2406.8*	2		2408.29 (8, 1)
2418.9*	6		2419.85 (6, 0)
2429.4*	1		2431.33 (9, 2)
2441.40	10	2441.9 (7, 1)	2442.61 (7, 1)
2454.0	12	2454.8 (5, 0)	2454.80 (10,3), 2455.52 (5, 0)
2465.1*	4		2465.81 (8, 2)
2477.3	5	2477.8 (6, 1)	2478.45 (6, 1)
2491.5	18	2492.2 (4, 0)	2489.43 (9, 3), 2492.80 (4, 0)
2501.9*	2		2501.80 (7, 2)
2514.8	10	2514.88 (5, 1)	2513.50 (10,4), 2515.89 (5, 1)
2430.0	30	2531.10 (3, 0)	2531.76 (3, 0)
2562.4*	1		2563.35 (7, 3)
2571.0	30	2571.83 (2, 0)	2572.52 (2, 0)
2587.6*	2		2587.76 (8, 4)
2602.8*	12		2602.85 (6, 3)
2613.5	30	2514.13 (1, 0)	2612.62 (9, 5), 2615.20 (1, 0)
2621.90	15	2619.5 (4, 2)	2619.36 (4, 2)
2627.8*	6		2627.4 (7, 4)
2638.0	12	2639.17 (2, 1)	2637.9 (10,6), 2638.85 (2, 1)
2644.9*	12		2644.17 (5, 3)
2652.2*	1		2652.46 (8, 5)
2658.5	20	2659.42 (0, 0)	2659.90 (0, 0)
2661.1	20	2662.33 (3, 2)	2662.93 (3, 0)
2682.2	30	2682.98 (1, 1)	2683.78 (1, 1)
2713.4	4	2707.4 (2, 2)	2712.40 (5, 4)
2720.4*	2		2719.85 (8, 6)
2730.17	20	2730.02 (0, 1)	2730.90 (0, 1)
2754.6*	15		2755.4 (1, 2)
2780.1	15	2779.71 (2, 3)	2780.55 (2, 3)
2804.2	20	2804.17 (0, 2)	2805.09 (0, 2), 2805.73 (3, 4)
2837.4*	15		2836.25 (7, 7)
2845.9*	4		2844.3 (10, 9)
2856.2	15	2855.42 (2, 4)	2855.87 (2, 4), 2857.89 (5, 6)
2881.6	30	2881.75 (0, 3)	2881.95 (3, 5), 2882.71 (0, 3)
2893.8*	5		2890.93 (9, 9)
2907.5	16	2908.1 (1, 4)	2908.57 (1, 6), 2908.80 (4, 6)

TABLE I (Continued)

Measured λ Å	Intensity Visual Estimate	λ (v', v'') (Jevons et al, 1937)	Identification λ Calculated (v', v'')
2919.3*	2		2919.0 (10, 10)
2961.8	20	2963.04 (0, 4)	2961.68 (3, 6), 2963.99 (0, 4)
2969.6*	5		2968.13 (9,10)
2988.9	30	2989.89 (1, 5)	2988.96 (4, 7), 2990.56 (1, 5)
3016.5*	10		3016.73 (5, 8), 3017.61 (2, 6)
3048.8	5	3048.76 (0, 5)	3047.8 (9,11), 3048.76 (0, 5)
3075.5	25	3075.7 (1, 6)	3073.81 (7,10), 3073.18 (4, 8)
			3076.51 (1, 6)
3104.2	16	3103.1 (2, 7)	3104.31 (2, 7), 3103.4 (8, 11)
3132.4	4	3131.6 (3, 8)	3132.62 (3, 8)
3134.3*	4		3133.1 (9, 12)
3139.0*	1		3138.58 (0, 6)
3158.3*	2		3158.6 (7, 11)
3166.1	12	3165.9 (1, 7)	3166.67 (1, 7)
3196.2	12	3194.3 (2, 8)	3195.26 (2, 8)
3221.0	30	3222.9 (3, 9)	3221.3 (9,13), 3224.36 (3, 9)
			3220.8 (6, 11)
3248.7*	8		3251.0 (7,12), 3252.6 (10, 14),
			3253.98 (4, 10)
3262.2*	6		3261.37 (1, 8)
3291.0	6	3289.7 (2, 9)	3290.76 (2, 9)
3312.4*	1		3313.6 (9,14), 3314.8 (6, 12)
3320.8	15	3319.4 (3, 10)	3320.69 (3, 10)
3325.3*	20		3331.21 (0, 8)
3352.3*	15		3349.2 (4, 11)
3380.2*	6		3378.0 (8,14), 3382.0 (5, 12)
3412.5*	1		3410.4 (9,15), 3413.7 (6, 13)
3422.0*	4		3421.0 (3, 11)
3436.9*	6		3435.15 (0, 9)
3454.3*	3		3453.3 (4, 12)
3463.4*	8		3465.72 (1, 10)
3484.7*	1		3485.2 (5, 13)
3491.8*	8		3494.6 (2, 11)
3519.2*	6		3517.6 (6, 14)
3592.8*	1		3593.5 (5, 14)
3610.5*	2		3608.2 (2, 12)
3638.6*	3		3640.8 (3, 13)
3794.4*	1		3793.3 (4, 15)
3812.7*	2		3815.8 (1, 13)

TABLE II

THE UNIDENTIFIED BANDS

Measured λ Å	Intensity
2928.2	1
2944.5	2
2952.1	4
2978.0	6
3003.4	3
3040.2	1
3053.4	16
3090.9	1
3122.5	12
3148.0	1
3175.4	8
3185.6	1
3299.6	1
3304.9	1
3370.7	1
3473.1	0
3549.1	2
3558.7	3
3581.2	2
3669.7	2
3682.0	1
3700.0	2
3732.8	2
3776.7	2
3826.0	2
3860.0	1

The spectrum of the chemiluminescence produced during the reaction of germanium tetrahydride and atomic oxygen is extensive and consists of about one hundred bands between 2350Å and 4000Å. It may be noted from Plate 2 that most of the observed bands are degraded to the longer wavelength. However, due to the wide slit, the degradation of some of the bands is uncertain. Previous workers (Pearse and Gaydon, 1963) have observed red-degraded bands of the D-X system of GeO in a region between 2342Å and 3319Å. It was found that all the thirty bands belonging to the D-X system of GeO observed by Jevons et al. (1937) can be identified in the present spectrum. The wavelength of the bands measured by Jevons et al. (1937) are given in the third column of Table I. Because of the similar appearance of the remaining bands, in the same region, it was suspected that some of the remaining bands may also belong to the D-X system of the GeO molecule. Therefore, the wavelengths of the bands belonging to the D-X system of GeO with v' up to 10 and v'' up to 15 were calculated from the following expression given by Jevons et al.

$$\nu = 37762.4 + (651.3u' - 4.2u'^2) - (985.7'' - 4.3u''^2)$$

where $u = v + 1/2$. With the help of the calculated wavelength of the band heads, a number of remaining bands are identified and are indicated by asterisks in Table I. The calculated wavelengths of the identified bands belonging to the D-X system of GeO with the vibrational quantum numbers involved in the transition are given in the fourth column of Table I.

A number of additional bands which cannot be identified definitely with the bands of the D-X system of GeO are collected in Table II. The three strongest unidentified bands are at 3053.4Å, 3122.5Å and 3175.4Å,

which are probably the bands belonging to the $^2\Sigma \rightarrow ^2\pi$ system of OH. However, the above identification is not conclusive due to the presence of the other bands of the D-X system of GeO in the same region.

4. Discussion

The unique combination of ω'_e and ω''_e ($3\omega'_e \simeq 2\omega''_e$) has resulted in a narrow grouping of several bands which together with the low resolution further complicate the unique identification of some bands. For example, the 3,5 band at 2881.95Å, 0,3 band at 2882.71Å and 6,7 band at 2884.69Å lie very close to each other and, therefore, are not resolved. A number of such cases are shown in Table I. However, it may be concluded that almost all bands on the short wavelength side of the spectrum belongs to the D-X system of GeO, which was first studied by Shaw (1937) and SenGupta (1937) in emission from a carbon arc containing germanium compounds. Shaw (1937) observed the bands from 2441Å to 2989Å and SenGupta extended their observations from 2342Å to 3292Å. However, Jevons et al. (1937) recognized the fact that to obtain greater contrast between band head and overlying structure of neighboring bands, a source giving a lower temperature distribution would appear to be necessary. Consequently, they used an uncondensed discharge through a flowing mixture of $GeCl_4$ and oxygen and were able to extend the D-X system of GeO to the 3319Å. However, in addition to the GeO bands, they observed GeI lines, GeCl bands and a continuum. This is due to the non-selective excitation of spectra in electric discharges. The presence of additional different features in the spectra of electrical discharges renders the observation of the desired spectrum difficult. On the other hand, the excitation of spectra by chemiluminescent reaction is very

selective and is comparatively free from the presence of other spectral features. Therefore, we have been able to extend the D-X system of GeO to 3800Å and also have been able to observe a number of new bands of the same system (marked by asterisks in Table I) which have not been reported by the previous workers.

In addition to the bands belonging to the D-X system of GeO, there are several unidentified bands and are given in Table II. Most of these bands lie between 3000Å and 3800Å. A comparison of the spectra taken with the two spectrographs show that a number of bands between 4000Å and 5000Å observed in the spectrum (Plate 1) photographed with a Hilger's small quartz spectrograph are not observed in the spectrum photographed with the Jarrel-Ash 1.5m grating spectrograph. This is understandable because the grating is blazed for 3000Å and, therefore, the efficiency of the grating in the region between 4000Å and 5000Å is low. Moreover, the spectral sensitivity of the 103-a-F emulsion is also low in this region. However, the observation of a number of unidentified bands on the long wavelength side of the D-X system of GeO indicates a strong possibility of a new band system of GeO in the region between 3000Å and 5000Å.

The possibility of a new band system of GeO on the longer wavelength side of the D-X system is indicated from the comparison of the observed band systems belonging to the diatomic oxides of the elements of the IV-a group of the periodic table (CO, SiO, GeO, SnO and PbO). The energy level diagrams of these molecules and the observed transitions are shown in Figure 2. The higher energy levels and the corresponding transitions of CO are not shown. Barrow, et al. (1954) have remarked that the

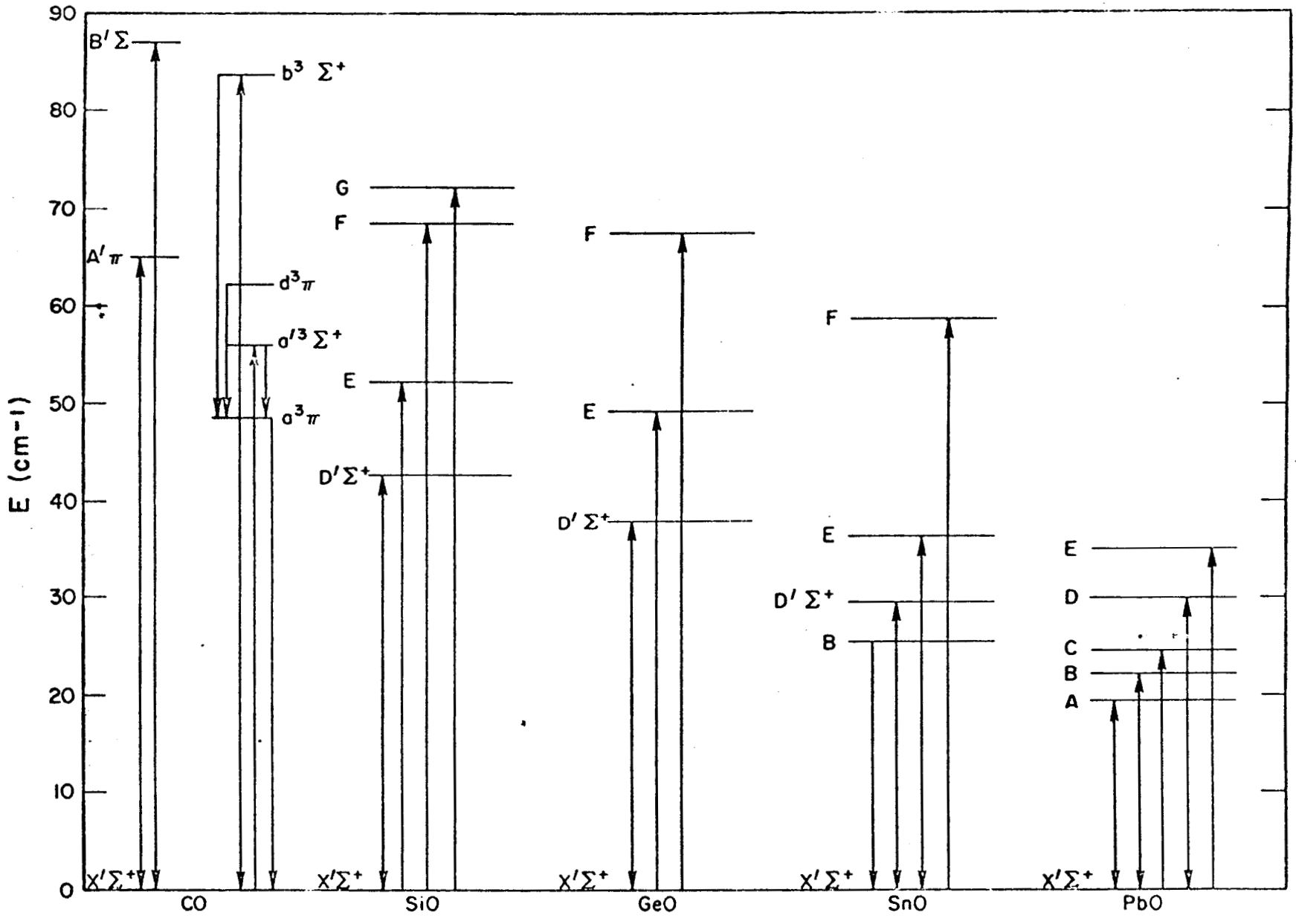

Figure 2. The energy level diagram and the observed transitions of the diatomic oxides of the elements of IV-a group. Higher energy levels and corresponding transitions of CO are not shown.

band system corresponding to the B-X transition of SnO have not been observed in the case of SiO or GeO. This may be due to the spin forbidden nature of the transition in the light molecules. Since the GeO molecule is intermediate between the lightest and heaviest molecule of this group, a weak band system on the longer wavelength side of the D-X (analogous to the B-X systems of the PbO and SnO molecules) may be expected, because the corresponding state of the GeO molecule may partly approach the Hund's case C.

It is, therefore, concluded that the study of the chemiluminous reactions of atomic oxygen can give more spectroscopic information than available from conventional spectroscopic sources. The spectrum of the chemiluminescence produced during the reaction of germanium tetrahydride and atomic oxygen should be investigated for identifying a new band system in a region between 3000Å and 5000Å.

It has been mentioned earlier that no visible chemiluminescence was observed during the reaction between germanium tetrachloride and atomic oxygen. This observation may be compared with the similar observations of the reactions of carbon compounds with atomic oxygen. The reactions of hydrocarbons with atomic oxygen generally produce chemiluminescence, but no visible chemiluminescence was reported during the reaction of carbon tetrachloride with atomic oxygen (Ung et al., 1962). The above observations indicate a similarity in the atomic oxygen reactions of the hydride and chloride of carbon and germanium which belong to the same group of the periodic table.

REFERENCES

Barrow, R. F. and Rowlinson, H. C., Proc. Roy. Soc. 224A, 374-88 (1954).

Gaydon, A. G., Spectroscopy of Flames, John Wiley and Sons, Inc., New York (1957).

Jevons, W., Bashford, L. A. and Briscoe, H. V. A., Proc. Phys. Soc. 49, 543-53 (1937).

Kaufman, F., Progress in Reaction Kinetics, Part I, Edited by Porter, Pergamon Press, N. Y. (1961).

Pearse, R. W. B. and Gaydon, A. G., The Identification of Molecular Spectra, John Wiley and Sons, Inc., N. Y. (1963).

SenGupta, A. K., Z. Phys. 105, 487 (1937).

Shaw, R. W., Phys. Rev. 43, 1043 (1933); 51, 12-4 (1937).

Stair, R., Schneider, W. E. and Jackson, J. K., Appl. Optics 2, 1151-4 (1963).

Ung, A. Y. M. and Schiff, H. I., Can. J. Chem. 40, 486-94 (1962).

APPENDIX C

The True Potential Energy Curves of $X^2\Sigma$ and $A^2\Sigma$ States of the AℓO Molecule*

by

A. Sharma
GCA Corporation, Bedford, Massachusetts 01730

The $A^2\Sigma - X^2\Sigma$ band system for AℓO is of considerable astrophysical and geophysical importance. For example, the relative intensity of the bands belonging to the $A^2\Sigma - X^2\Sigma$ system of AℓO observed[1-3] during the rocket release of aluminum compounds in the upper atmosphere at twilight have been used to obtain information regarding upper atmospheric temperatures. The interpretation of such experiments require information concerning relative vibrational transition probabilities and Franck-Condon factors. The Franck-Condon factors for the above band system have been calculated by Nicholls[4] and Tawde et al.[5] after assuming that the $A^2\Sigma$ and $X^2\Sigma$ states of AℓO follows the Morse curve. Zare et al.[6] have shown that, in certain cases, the Franck-Condon factors are quite sensitive to the shape of the potential energy curves. Therefore, the true potential curves of the $A^2\Sigma$ and $X^2\Sigma$ states of AℓO are calculated and compared with the Morse potential.

A test for finding whether a potential energy curve of a diatomic molecule can be represented by a Morse function has been given by

*This work was supported by the National Aeronautics and Space Administration.

Pekeris,[7] who has shown that the following relation between the spectroscopic constants holds for a Morse curve:

$$\alpha_e = \frac{6\sqrt{\omega e x e B e^3}}{\omega e} - \frac{6 B e^2}{\omega e} \quad . \tag{1}$$

The deviation of the value of α_e calculated by Means of Eq. (1) from the observed value can then serve as an indication of the deviation of the Morse function from the true potential function of the respective state. Table 1 shows the comparison of the calculated and observed value of α_e. The spectroscopic constants (cm^{-1}) involved in the calculation have been taken from Tyte and Nicholls.[8] It can be concluded from Table 1 that the $X^2\Sigma$ state of AℓO is approximately represented by the Morse function, but the $A^2\Sigma$ state is expected to show larger deviation.

In view of the above finding, the true potential energy curve of the $A^2\Sigma$ and $X^2\Sigma$ states of AℓO are calculated by the Rydberg-Klein-Rees method described by Zare.[9] The potential is constructed from the observed vibration and rotational term values rather than by an analytical form. The computer program described by Zare[10] was used for the IBM-1094 Computer. The spectroscopic data required for the computation were taken from Tyte and Nicholls.[8] They have calculated the G(v) values from the bandhead measurements of Shimouchi,[11] who has measured the bandheads with an accuracy of ± 0.1 Å to ± 0.3 Å. Since we found that the difference between the G(v) values calculated from the bandhead and those calculated from the band origin lies within the accuracy of the

TABLE 1

State	ω_e	$\omega_e x_e$	Be	α_e observed	α_e calculated
$X^2\Sigma$	979.23	6.97	0.64136	5.80×10^{-3}	5.78×10^{-3}
$A^2\Sigma$	870.05	3.52	0.60408	4.47×10^{-3}	3.55×10^{-3}

measurements of the bandheads, the G(v) values given by Tyte and Nicholls[8] were used. The results are given in Tables 2 and 3. The calculated potential energy curves are compared with the Morse curves in Figures 1 and 2, which shows that the agreements between the true potential and Morse potential is reasonable for the $X^2\Sigma$ state - particularly for vibrational levels $v \lesssim 6$. However, the deviation of the true potential for $A^2\Sigma$ state from the corresponding Morse potential is appreciable for even lower vibrational levels.

TABLE 2

Potential Energy Curve for $A^2\Sigma$ State of AℓO

(J = 0 Rotational State)

(v + 1/2)	U(r) cm^{-1}	r_+ Å	r_- Å
0	0	1.6668	
0.5	434.1	1.7325	1.6080
1.5	1295.3	1.7850	1.5685
2.5	2149.6	1.8235	1.5430
3.5	2996.6	1.8563	1.5233
4.5	3836.0	1.8860	1.5070
5.5	4668.1	1.9135	1.4929
6.5	5492.1	1.9394	1.4804
7.5	6309.1	1.9642	1.4693
8.5	7118.2	1.9880	1.4592
9.5	7921.0	2.0111	1.4499
10.5	8715.3	2.0337	1.4413
11.5	9505.3	2.0552	1.4337

TABLE 3

Potential Energy Curve for $X^2\Sigma$ State of AlO

(J = 0 Rotational State)

(v + 1/2)	U(r) cm^{-1}	r_+ Å	r_- Å
0	0	1.6176	
0.5	487.9	1.6808	1.5633
1.5	1452.1	1.7309	1.5261
2.5	2401.4	1.7688	1.5026
3.5	3336.1	1.8014	1.4845
4.5	4257.8	1.8311	1.4696
5.5	5165.1	1.8589	1.4567
6.5	6058.1	1.8854	1.4452
7.5	6936.6	1.9110	1.4349
8.5	7801.1	1.9355	1.4257
9.5	8660.4	1.9593	1.4175
10.5	9487.3	1.9850	1.4084
11.5	10310.0	2.0065	1.4022

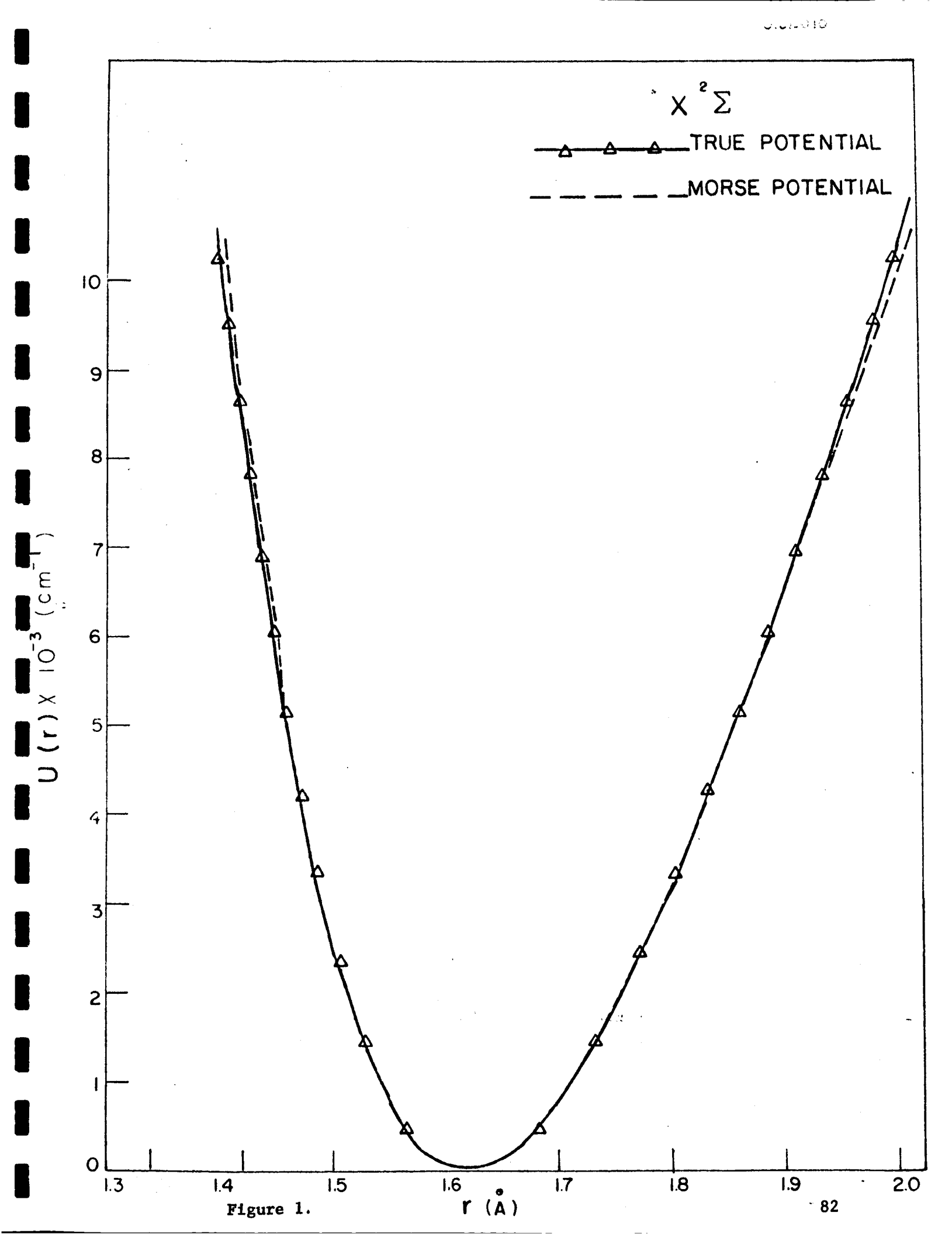
$X\,^2\Sigma$
TRUE POTENTIAL
MORSE POTENTIAL
U (r) X 10^{-3} (cm^{-1})
0
1
2
3
4
5
6
7
8
9
10
1.3
1.4
1.5
1.6
1.7
1.8
1.9
2.0
r (Å)

Figure 1.

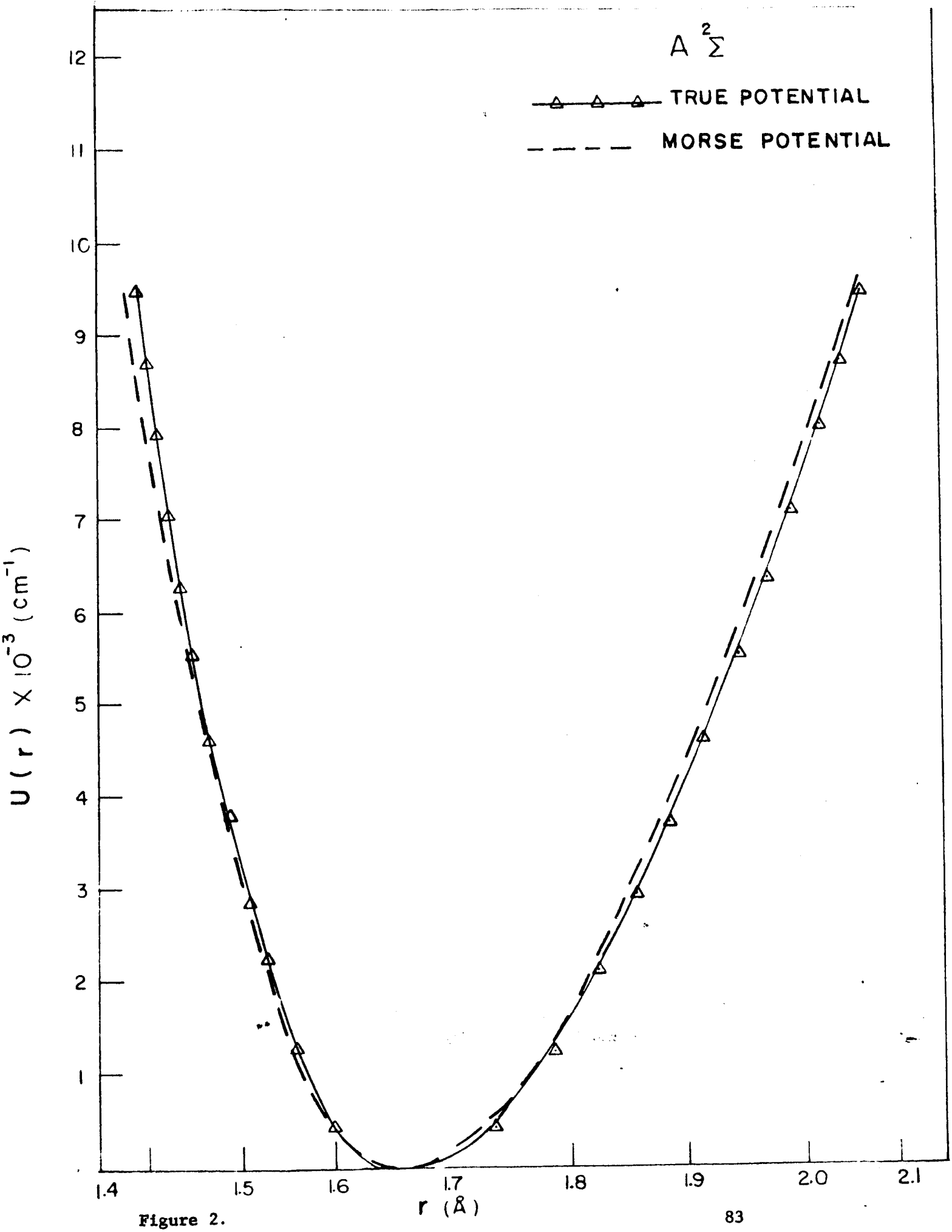
A ²Σ
TRUE POTENTIAL
MORSE POTENTIAL
U (r) X 10⁻³ (cm⁻¹)
r (Å)
12
11
10
9
8
7
6
5
4
3
2
1
1.4
1.5
1.6
1.7
1.8
1.9
2.0
2.1

Figure 2.

REFERENCES

1. B. Authier, Ann. Geophysique 20, 353 (1964).
2. O Harrang, Planet. Space Sci. 12, 567 (1964).
3. B. Authier, J. E. Blamont and G. Carpenter, Ann. Geophysique 20, 342 (1964).
4. R. W. Nicholls, J. Res. Natl. Bur. Stand. 66A, 227 (1962).
5. N. R. Tawde and V. M. Korwar, Proc. Phys. Soc. Lond. 80, 794 (1962).
6. R. N. Zare, E. O. Larson and R. A. Berg, J. Mol. Spectrosc. 15, 117 (1965).
7. C. L. Pekeris, Phys. Rev. 45, 98 (1934).
8. D. C. Tyte and R. W. Nicholls, Identification Atlas of Molecular Spectra; I: The $A\ell\Pi - A^2\Sigma - X^2\Sigma$ Blue Green System. Research Report of Molecular Excitation Group, Department of Physics, University of Western Ontario, London, CANADA, 1964.
9. R. N. Zare, J. Chem. Phys. 40, 1934 (1964).
10. R. N. Zare, University of California Radiation Laboratory Report UCRL-10925, 1963.
11. M. Shimouchi, Science of Light 7, 101 (1958).

APPENDIX D

Studies of Ion-Neutral Reactions by a Photoionization Mass Spectrometer Technique*

by

Peter Warneck
GCA Corporation, Bedford, Massachusetts 01730

(Received 9 May 1966)

ABSTRACT

The use of a photoionization mass spectrometer for ion-molecule reaction studies is described. Ion source pressures up to 200 microns are employed, measured directly with a McLeod gauge. A method is described for determining ion residence time in the ion source at constant repeller field, using a pulsed light source. Drift velocities, diffusion coefficients, and ion temperatures are given for N_2^+ ions in air as derived from an analysis of ion pulse shapes. Reaction studies are reported for nitrogen ions in air and nitrogen, and for hydrogen ions in hydrogen. The associated rate constants are derived.

*Supported by the National Aeronautics and Space Administration under contracts NASW-1341 and NAS5-9161.

INTRODUCTION

The significance of ion-neutral reactions in fields as diverse as gas discharge phenomena, mass spectrometry, radiation chemistry, upper atmosphere physics, and flame ionization has stimulated a surge of investigations concerned with ion reaction kinetics. The subject has been extensively reviewed.[1-6] A large number of studies employed mass spectrometers equipped with high pressure ($> 10^{-4}$ torr) electron impact ion sources, but for these investigations, it is unfortunate that electron impact generally results in a host of ions of different types due to ion fragmentation. Unless the electron energies used are close to the ionization threshold, the subsequent reaction kinetics can be sufficiently complex to prevent an unambiguous assignment of reaction paths and individual rate constants.

In the present work, this difficulty is overcome by the use of a photoionization source. The general features of photoionization mass spectrometers are well described in the literature[7-11] and the advantages of photoionization over the more common electron impact ionization have been pointed out. Giese,[6] and Tanaka and co-workers[12] have discussed the photoionization technique also with respect to ion-molecule reaction studies. The outstanding feature is the ease with which ionizing energies can be selected using a monochromator of only moderate resolving power, so that by operating at photon energies near the threshold of a selected ionization process, the degree of fragmentation can be controlled. With

exception of the recent work of Koyano et al.[12] and the ion-molecule reaction experiment reported by Cook and Samson,[13] the principal objective of photoionization mass spectroscopy formerly has been the study of primary processes at pressures sufficiently low to exclude the occurrence of secondary reactions. The present work, by contrast, involves pressures up to 200 microns, and in this pressure domain, the effects of ion-neutral reactions are well displayed.

Aside from interest in the fundamental behavior of ions in high pressure ion sources, the emphasis in the present work lies on the determination of phenomenological rate constants. The corresponding basic experimental requirements may be briefly reviewed. The rate constant k associated with reaction

$$N^+ + A \rightarrow M^+ + B$$

is defined by the rate equation

$$-\frac{dN^+}{dt} = \frac{dM^+}{dt} = k\, N^+ A \qquad (1)$$

or by the equivalent integrated expression valid for the case when the neutral reactant concentration remains essentially constant

$$k = \frac{1}{A\tau} \log N_o^+/N^+ = \frac{1}{A\tau} \log N_o^+/(N_o^+ + M_o^+ - M^+). \qquad (2)$$

Here, the symbols N^+, M^+, and A stand for the concentrations of the respective species, N_o^+ is the initial concentration of the parent ion, and τ is the average residence time of the parent ion N^+ in the source. Clearly,

the experimental parameters to be measured for a determination of k include the partial pressure of A, the ratio of ion currents N_o^+/N^+ or N_o^+/M^+, and the residence time τ. Of these, the measurement of τ if most problematic and deserves comment.

At sufficiently low pressures in the source, the ions moving in the extraction field are accelerated freely without impeding collisional encounters, so that the residence time can be calculated from Newton's equation of motion, privided the electric field strength and the flight distance are known. This has been the basis for most rate constant determinations in the past. Little uncertainty usually exists concerning the flight distance, but the fields, as calculated from the applied potentials, can be distorted by contact potentials, surface charges, or field penetration into the source. The experimental determination of actual fields in the source is difficult and apparently has not been attempted. As the pressure in the source is increased, ions suffer collisions on their way to the extraction orifice and the discrepancies between real and calculated residence times becomes more serious. However, at sufficiently high ion source pressure, the motion of ions in the repeller field is drift, and the residence time becomes, in principal, calculable again. Nevertheless, current knowledge about drift velocities in many cases cannot be extrapolated toward the conditions existing in the ion source, so that there is a real need for a method to determine experimentally the parent ion residence times, regardless of the environmental conditions in the source.

In view of the importance of residence time determinations, a considerable effort was devoted to this task in the present study. Residence times were obtained from delay time measurements made possible by the use of a pulsed light source. Delay time data also provided information on drift velocities, diffusion coefficients, and ion temperatures for N_2^+ in air. The present method is applied to ions moving in a time independent repeller field. This method is quite different from that developed by Talrose and Frankevich,[14] who let the ions react in an essentially field-free region and then sampled them by means of a pulsed extraction field; and that by Hand and von Weyssenhoff,[18] who employed a time-of-flight mass spectrometer.

EXPERIMENTAL

Apparatus

Only the principle features will be given here since a more detailed description has appeared elsewhere.[19] Briefly, the following components are involved: a 1/2-m Seya vacuum uv monochromator operated in conjunction with a Weissler-type repetitively pulsed nitrogen spark light source, a stainless steel ion source located at the monochromator exit, a sodium salicylate-coated photomultiplier detector for relative intensity measurements, a 180-degree magnetic analyzer with wedge-shaped air gap, and a 20-stage electron multiplier ion detector followed by a vibrating reed electrometer and strip chart recorder. Differential pumping is employed to achieve ion source pressures up to 200 microns while simultaneously keeping the analyzer pressure in the 10^{-6} torr range.

A cylindrical ion source is used with ion extraction occurring in axial direction through a 0.7 mm diameter orifice. An appropriately biased repeller plate provides the necessary extraction field. Photoions are formed along the plane of the light beam perpendicular to the cylinder axis. The center of ion formation is located 3 mm away from the extraction orifice. With the optical entrance slit to the source in focal position and with the slit bars adjusted to a width of 0.25 mm, the average width of the light beam inside the source is 0.6 mm. The resulting spectral resolution is approximately 5 Å. Subsequent optical slits are wide enough so that the release of photoelectrons from light striking the walls is avoided. Photoelectrons produced at the confining slit are prevented from from entering the source by means of a small auxiliary field.

The gas pressure in the ion source is measured directly with a McLeod gauge through the hollow stem of the repeller. Gases enter the source through the circular gap between the repeller plate and the surrounding walls, and they leave the source mainly through the light beam exit slit. Flow and pressure are adjusted by leak valves. Research quality cylinder gases are employed, with traces of moisture being removed by a trap cooled with liquid nitrogen or Dry Ice. A cold trap was used also in conjunction with the McLeod gauge. Errors in the pressure determination cause by the mercury vapor stream effect[20] were not corrected for since they were generally smaller than the involved reading errors.

Determination of Residence Times

The spark light source was operated with a repetition rate of 120 pulses/sec. The average individual pulse duration was about half a microsecond which, in comparison to most ion source residence times, was sufficiently short to justify the notion of essentially instantaneous ion deposition. A notable exception were residence times for hydrogen ions, which were of the same magnitude as the pulse duration.

Ion source residence times were determined from measurements of the total time delay between the formation of ions in the source and their arrival at the mass spectrometer collector. A calibrated Textronix oscilloscope triggered by the photomultiplier signal was used for this purpose. A reproducibility of ± 0.2 microsecond was achieved in these measurements. The total delay time thus obtained is a composite of the residence time of ions in the source and the ion flight time in the mass spectrometer. However, the residence time strongly varies with the repeller field, whereas the ion flight time is nearly independent of the repeller field within certain limits. An extrapolation toward infinite repeller fields, corresponding to negligible residence times, thus provides the ion flight time in the spectrometer which can then be applied to derive the residence time for any chosen repeller potential setting. Figure 1 illustrates this extrapolation. The measured variation of delay time with repeller voltage for a given ion source pressure is plotted versus the inverse repeller voltage. The ion flight time is determined from the intercept of the curve with the ordinate. Figure 2, which gives results for

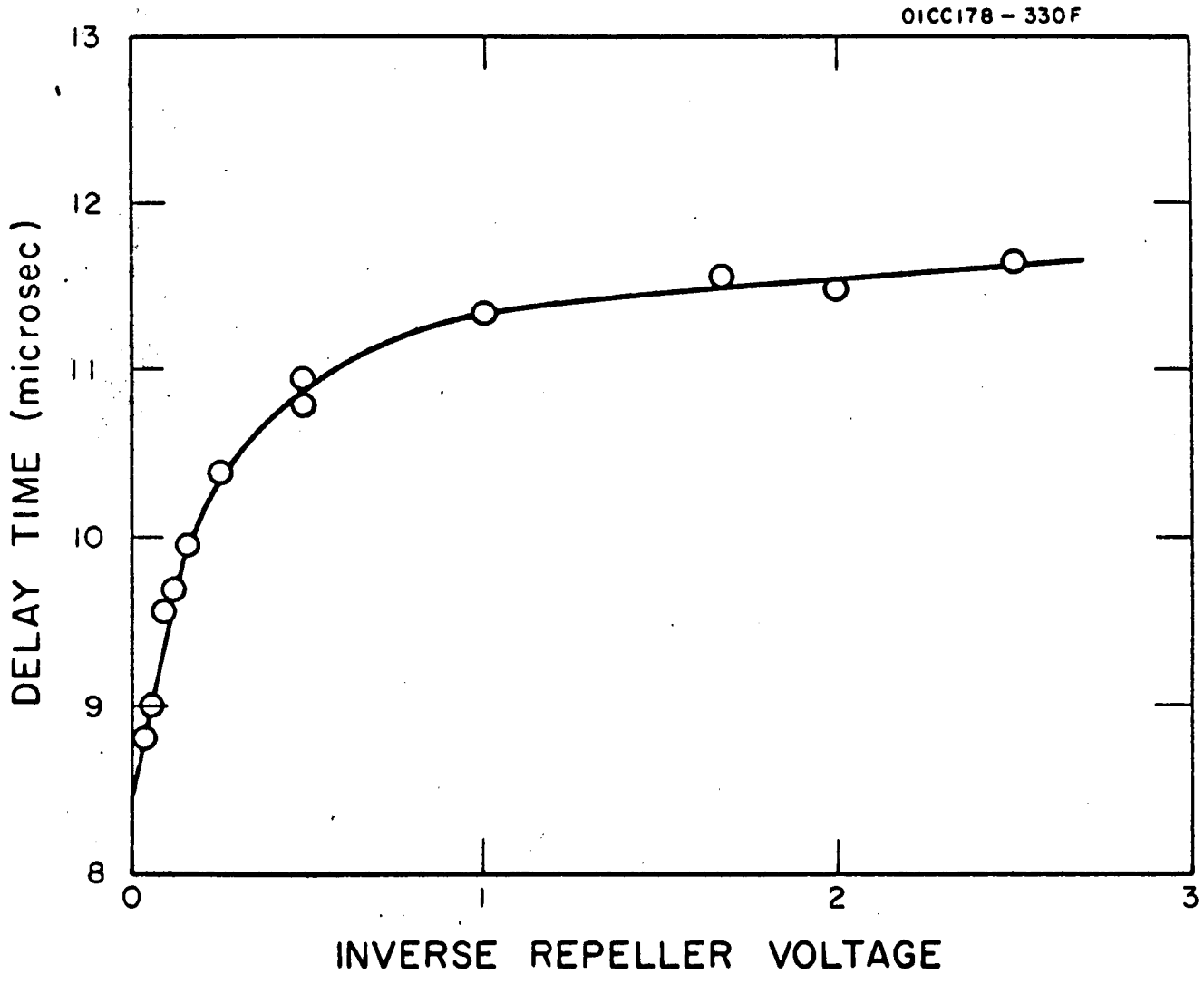

Figure 1. Variation of ion pulse delay time with inverse repeller voltage ($volt^{-1}$). Free flight time is derived from the intercept on the ordinate.

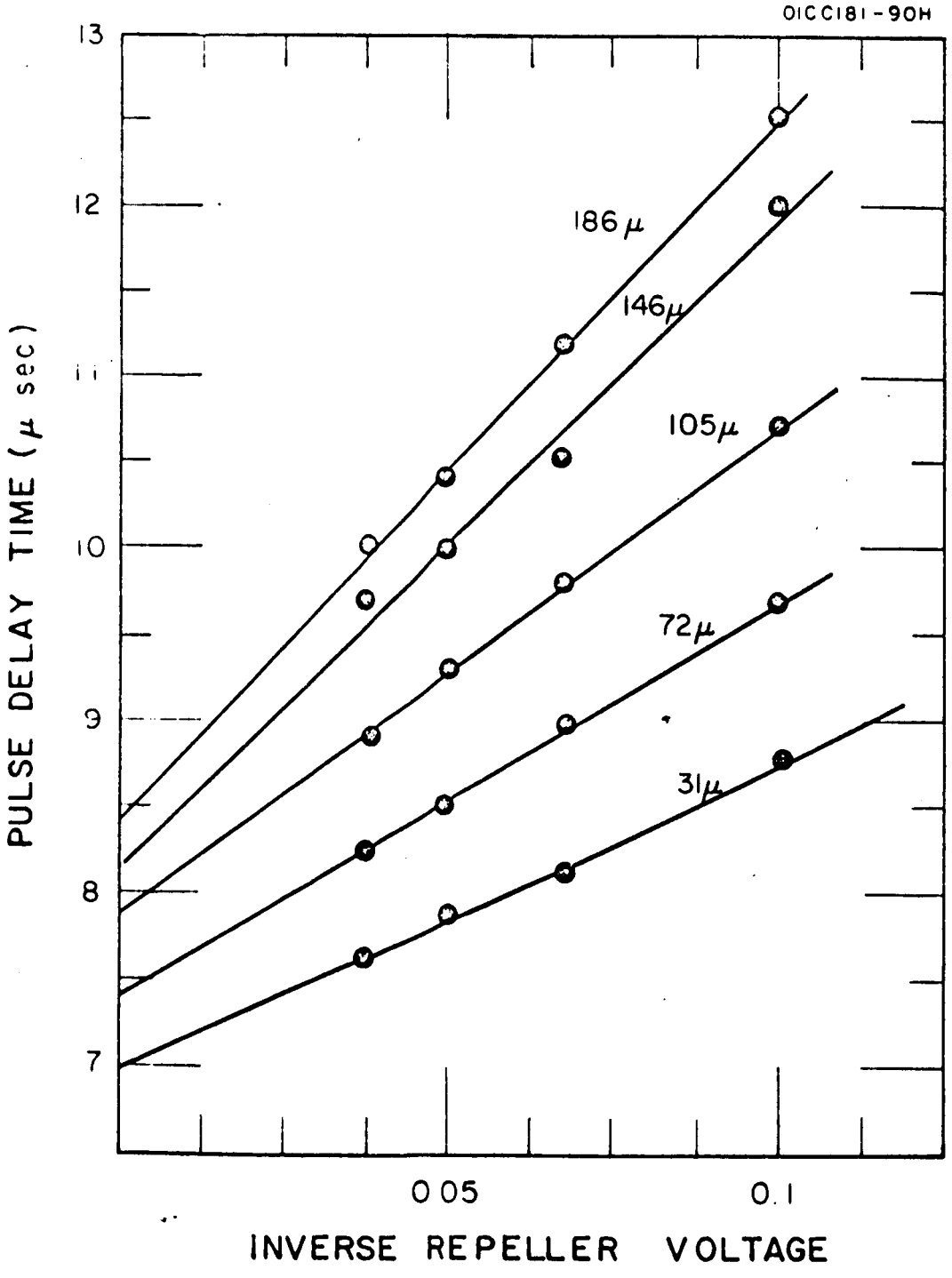

Figure 2. Variation of ion pulse delay times with inverse repeller voltage for various pressures in the source, demonstrating linearity of extrapolation for repeller voltages 10 to 30 volts.

nitrogen ions in air at various pressures, demonstrates that the extrapolation is essentially linear in the vicinity of the ordinate. This linearity has been found to hold for all ions and pressure regions investigated so far. In view of the square root relationship between residence time and repeller potential at low pressures, the possibility of plotting delay time data versus the square root of the inverse repeller voltage was also tested. Linearity of extrapolation was again observed, as expected, but the extrapolation toward the intercept on the ordinate were somewhat longer and, hence, less certain. A comparison of ion flight times derived from both types of plots gave almost identical results.

The ion flight times obtained by these procedures still require a correction, since the assumption that the ion flight time remains unaffected by a change in the repeller potential is valid only for sufficiently small repeller fields. The validity of this assumption breaks down when the ion velocity resulting from acceleration in the repeller field becomes significant in comparison to that acquired in the accelerating region outside the ion source. The effect to be expected can be calculated from the applied acceleration potential (750 volts) and the approximately known geometry of the ion orbit, resulting in a correction factor 0.94 for ion flight times determined from both types of plots discussed above. It was also established by these calculations that the repeller potentials actually applied in the experiments (0-30 volts) were well within the range of repeller potentials for which extrapolations are valid.

For the interpretation of residence time measurements, it is also necessary to discuss the behavior of ion pulse shapes displayed by the oxcilloscope. Figure 3 shows the observed and expected pulse shapes for two density distributions perpendicular to the plane of ion formation in the ion source. The rectangular shape on the left corresponds to the initial ion distribution produced by the light beam. The associated idealized pulse shape was observed whenever pressures were sufficiently low and repeller voltages sufficiently high so that residence times were short. For long residence times, as they were observed at pressures above 50 microns and with low repeller voltage settings, the pulses developed long feet and their shape corresponded better to the Gaussian distribution shown in Figure 3 on the right. At high pressures, when the ions traveling toward the source exit suffer many collisions, the broadening of the initially rectangular ion distribution is interpreted as being due to diffusion. At low pressures, when ionic motion is not hampered by collisions, the change in the ion density profile must be produced by the influence of the thermal distribution of initial ion velocities. The influence of charge repulsion is negligible for the ion densities encountered in these experiments.

From Figure 3, it is apparent that the center of the ion distribution is represented by the half-rise point of the charge buildup at the detector. Accordingly, the average residence times should be determined from the half-rise time of the ion pulse observed on the oscilloscope. Unfortunately, the measurement of half-rise times was not always found convenient because of the presence of jitter and statistical noise particularly for low

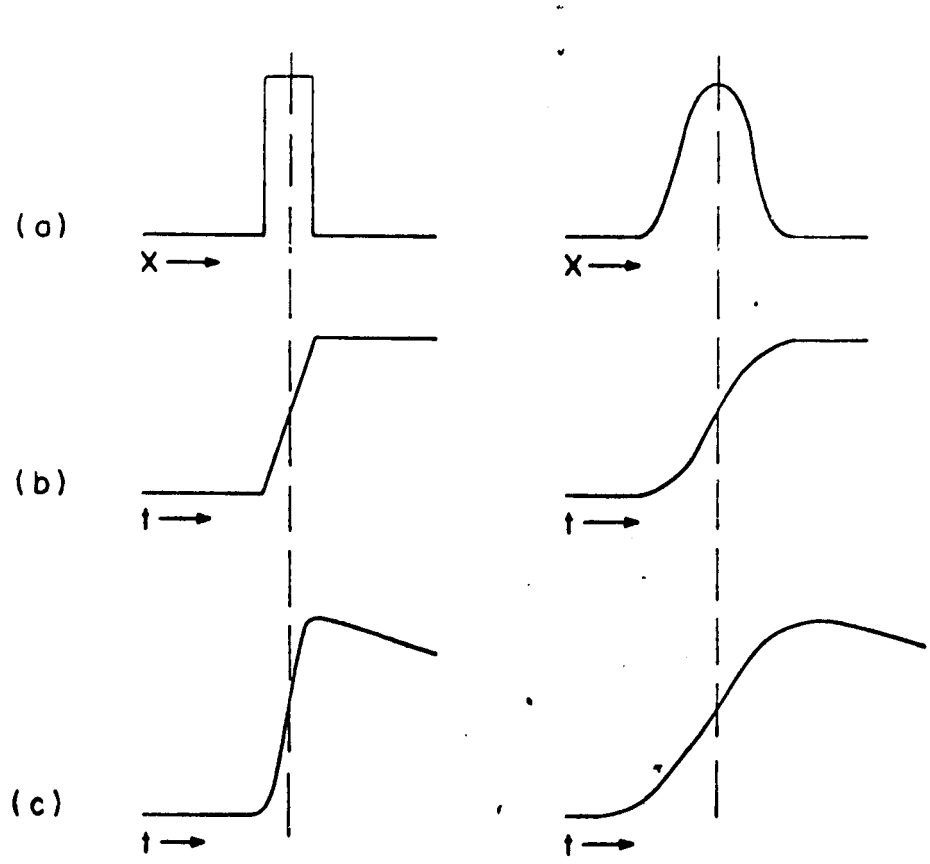

Figure 3. Spectral ion distributions in the source (a) and associated pulse shapes at the collector: idealized (b); observed (c). Two cases are shown; a rectangular distribution on the left, a Gaussian one on the right.

ion currents. An additional uncertainty is introduced by the finite time constant of the RC element connecting the mass spectrometer collector to the oscilloscope, so that the pulse height against which the half rise point is to be measured is lowered.

These difficulties are avoided when the pulse onset is used for time delay measurements. However, the use of first arrival times provides only a lower limit to the delay and residence time, and the derivation of average residence times consequently requires a correction to take into account the broadening of the ion distribution. Appropriate correction formulae are derived in the appendix. In the high pressure domain, where pulse broadening is caused by ion diffusion, the average residence time τ_o can be expressed by

$$\tau_o = \tau/(1 - 1.28 \sqrt{2D\tau/d}) \ . \qquad (3)$$

Here, τ is the lower limit residence time derived from the first arrival of the ion pulse, D is the diffusion coefficient of ions under consideration, and d is the distance from the origin of these ions to the ion source exit. A similar formula is applicable at low pressures where the pulse broadening is due to initial thermal velocities of the ions:

$$\tau_o^2 = \tau^2/(1 - 1.28\, \tau \sqrt{\frac{kT}{m}}/d) \ , \qquad (4)$$

with k being the Boltzmann constant, T the gas temperature, and m the mass of the ionic species under consideration.

RESULTS AND DISCUSSION

Performance of Apparatus

It is commonly assumed in ion-molecule reaction studies that ion current ratios measured at the mass spectrometer detector are equivalent to the ratios of ion fluxes generated in the source. Several fundamental effects, however, can invalidate the assumption of equal collection efficiencies for all ions. The factors discussed here include pressure, ion-electron conversion at the multiplier detector, and the variation of ion collection from the source for ions with different kinetic energy.

The use of high pressures in a mass spectrometer ion source generally leads to ion current-pressure relationships which are nonlinear, even in the absence of ion-molecule interactions. Such nonlinearities were observed to occur in the present experiments, mainly at pressures exceeding 100 microns. Predominantly, the cause is non-uniform absorption of ionizing radiation in the source. This effect has been discussed previously.[19] If absorption cross sections are available for the wavelength region of interest, appropriate corrections can be applied. It appears, however, that several other effects can also contribute to the observed nonlinearity of ion current with pressure. The following possibilities were explored: (a) dependence on light intensity, (b) variation with repeller potential, and (c) broadening of mass peaks. These studies were made with oxygen in the ion source as no ion-molecule reactions were observed to occur for O_2^+ ions in O_2 up to 200 microns pressure.

(a) To study the influence of light intensity but keep the other parameters constant, it was necessary to adjust intensities by variation of the monochromator entrance slit setting. Since this procedure affects the resolution, the 685 Å group of nitrogen lines were used for the measurements. This group consists of an unresolved triplet well isolated from other lines in the vicinity. Accordingly, any effects caused by a change of the effective absorption cross section are minimized. At 685 Å, the energy is still insufficient to produce dissociative ionization of O_2 so that only O_2^+ ions are present. Photomultiplier currents were used as a measure of the light intensity. The results are shown in Figure 4, where the observed ion currents divided by the photomultiplier currents are plotted as a function of ion source pressure. A lowering of the normalized ion currents is apparent at pressures above 100 microns when a high light intensity is used. The reason for the intensity dependence is not entirely clear, but it may be noted that with the use of pulsed light sources as in the present experiments, transient ion densities of the order of 10^8 ions/cc can be reached so that space charge effects might become significant. The study of ion-molecule reactions obviously requires operation at lower light intensities where this effect is negligible.

(b) Variation of the repeller potential causes a variation of the ion intensity at any ion source pressure owing to a change in the ion collection efficiency. When adjusting for this effect, it was found that a variation of the repeller potential had no influence upon the ion intensity as a function of pressure for the investigated range of repeller potentials, 1 to 10 volts, corresponding to field strength of approximately 1.6 to 16 volts/cm.

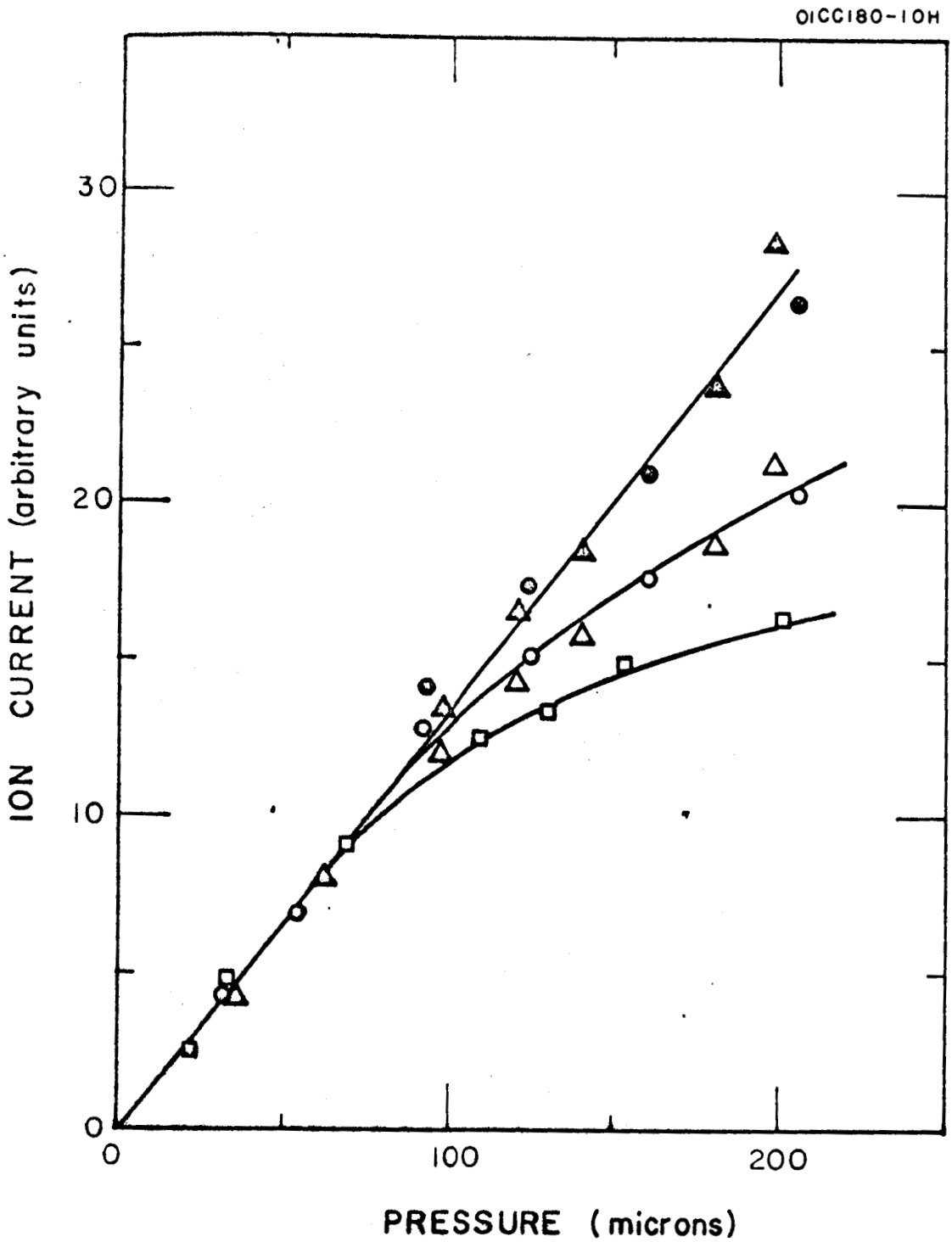

Figure 4. O_2^+ ion current in oxygen normalized with respect to incident light intensity as measured by photomultiplier, Δ-1.6 x 10^{-7} A; O-11.1 x 10^{-7} A; □ - 32.5 x 10^{-7} A. Filled symbols represent absorption corrected data obtained with the assumption that the effective ionization region extends through the entire width of the source. This procedure tends to maximize the correction. For the sake of clarity, the absorption correction of the high intensity data was omitted.

(c) Since ion currents customarily are measured at the maximum rather than by the area underneath a mass peak, it was of interest to investigate the equivalence of both procedures. This test was again performed with ionizing light at 685 Å. The data shown in Figure 5 are normalized with respect to each other to facilitate comparison. Up to 120 microns, the data are equivalent but at higher pressures, the use of peak heights gives lower relative values. At these pressures, the mass peaks develop tails in the direction of lower energies, indicating an increase in the energy spread of the ions which undoubtedly is caused by energy losses during ion-neutral collisions in the accelerating region outside the ion source. Other effects produced by collisions include a broadening of the ion beam before it enters the spectrometer and loss of beam intensity due to self scattering. The last two processes, however, have little influence upon the ion current in the present experimental arrangement because of the large solid angle of acceptance associated with the employed magnetic analyzer.

For the study of ion-molecule reactions, it as also important to establish the signal conversion efficiency of the electron multiplier detector for ions of different mass (and type), since ion discrimination would affect the observable reactant-product ratios. Owing to the small ion currents available in the present experiment, this effect could not be evaluated directly. However, at sufficiently low source pressure, ion production is proportional to the product $\gamma\sigma p$, where γ is the photoionization yield, σ the absorption cross section at the employed wavelength, and p is the gas pressure in the source. Hence, it should be possible to estimate the

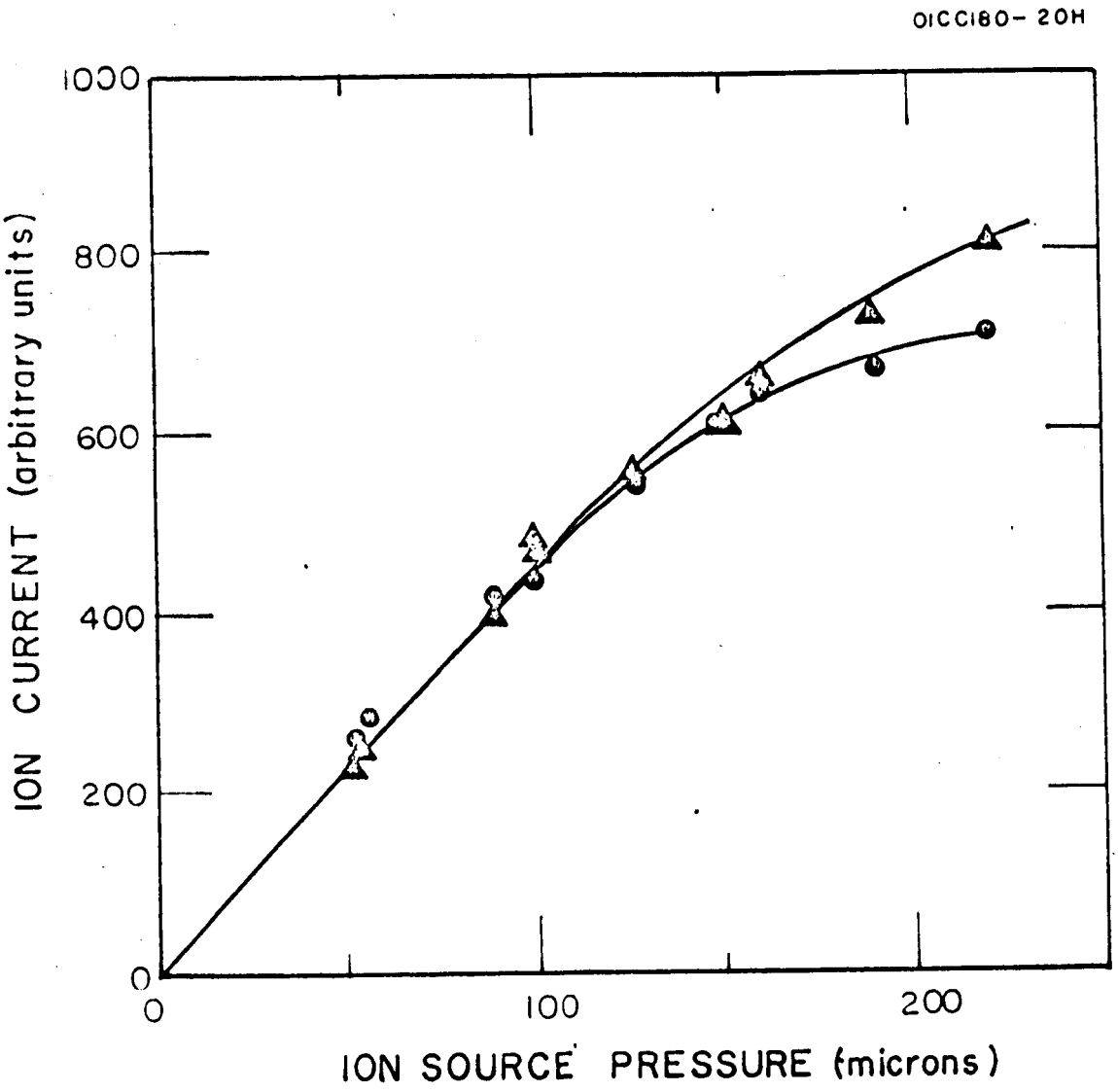

Figure 5. O_2^+ ion intensity in oxygen derived from the height of the mass peak (●) and the area underneath it (▲).

relative multiplier conversion efficiencies from a comparison of ion currents observed for various gases and corrected for the pertinent values of $\gamma\sigma p$, provided the ion collection from the source is independent of the nature of the ions. Appropriate experiments with 685 Å radiation employed argon, nitrogen, oxygen, carbon monoxide, carbon dioxide, hydrogen, and methane as sample gases. Photoionization yields and absorption cross sections for the first five gases were taken from the tables given by Samson and Cairns,[21] those for hydrogen and methane from the data by Cook and Metzger.[22,23] Although the results for relative multiplier conversion efficiencies showed considerable scatter due to the accumulation of various errors, they displayed no trends within the investigated m/e region indicating that mass discrimination, if present, is a small effect. Although this result is at variance with the findings of Inghram and Hayden,[24] it is consistent with our previous data obtained with 584 A helium resonance radiation.[19] It is noteworthy that, in both cases, the response of the detector for methane ions was persistently higher relative to that for the other sample gases, if the fragmentation yield for CH_3 and CH_2 ions[25] was taken into account.

While these results appear to justify the assumption of equal collection efficiencies for all ions present in the source, there is evidence that the collection efficiency decreases for ions which have acquired excess kinetic energy during a reaction. The balance between reactant consumption and product evolution was briefly studied for the dissociative charge transfer porcesses involving helium ions and nitrogen or oxygen. These reactions were discussed by Ferguson et al.[26] and by Moran and Friedman.[27] The details of this experiment will not be reported here, but

it is significant that the reaction of helium ions with nitrogen gave product ion intensities in perfect balance with helium ion losses, whereas in the reaction with oxygen when studied at low pressures, only 20 percent of the consumed helium ions could be recovered as O^+ ions. No other products were discernible. As the gas pressure was increased so that O^+ product ions underwent collisions on their path to the extraction orifice, the product-reactant loss ratio was improved. Moran and Friedman[27] have shown that the reaction of helium ions with oxygen results in oxygen ions having excess kinetic energies. On the other hand, the reaction with nitrogen is essentially thermoneutral so that the resulting products are in the thermal kinetic energy range. The present results, therefore, lead to the conclusion that the employed ion source geometry and low electric field disfavor the collection of ions endowed with excess kinetic energies. The influence of this factor is greatest at low pressures, but it is subdued when ion-neutral collisions are sufficient to moderate the energy excess.

Residence Times

Figure 6 gives the variation of residence times with pressure for nitrogen ions in air with a repeller potential of 1 volt. Of the two sets of data shown, the upper one was obtained from the half-rise time of the ion pulse and represents the true average residence times, whereas the lower refers to the earliest arrival times of the ion pulse. The observed decrease of residence times with decreasing pressure is expected. Extrapolation toward low pressures gives a limiting value which is in reasonable agreement with the residence time calculated from the equation for collision-free acceleration of the ions (3.3 μ sec). From the data shown in Figure 6, drift velocities of nitrogen ions in air, their diffusion coefficients, and the associated ionic temperatures can be deduced.

Drift velocities were obtained from the relation $v = d/\tau_o$ and are shown in Figure 7 in a logarithmic plot versus the relative field strength E/p. The observed slope of nearly $1/2$ indicates a root relationship. Also shown by the solid and broken lines are results reported by Martin et al.[28] and by Dahlquist[29] for N_2^+ ions in nitrogen. Good agreement is obtained even though the present results refer to air. Nevertheless, our data are considered only moderately accurate because of the difficulties involved in defining the true electric field. At E/p values greater than 45, the data are even less acceptable since the pressures become too low to justify the model of drift.

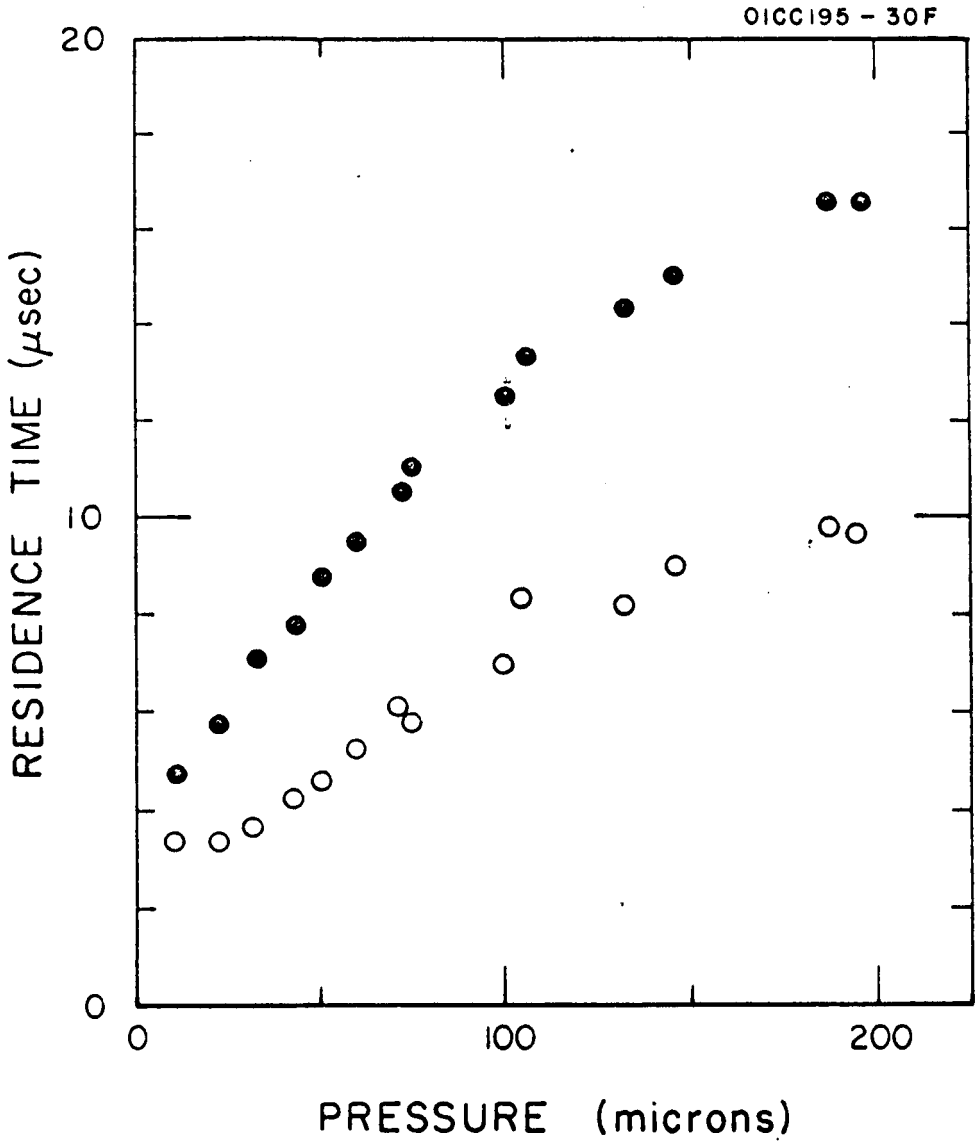

Figure 6. N_2^+ ion residence times in air as a function of pressure, derived from first arrival time (O) and half-rise time (●) of ion pulse at the collector.

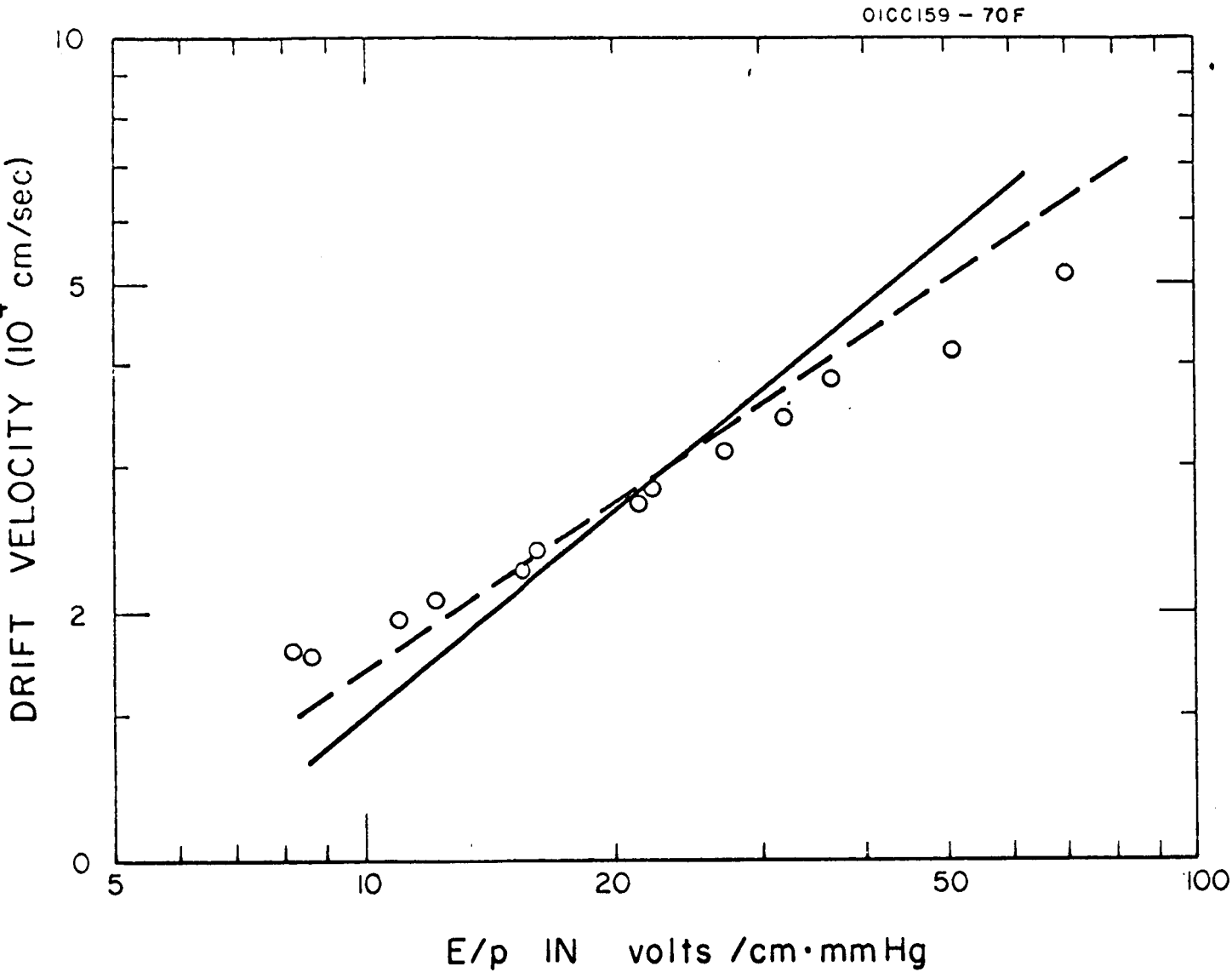

Figure 7. Drift velocities of N_2^+ ions in air as deduced from residence times in the source. Circles indicate present data, the solid line data by Martin et al., the broken line data by Dahlquist.

Diffusion coefficients were calculated from τ and τ_o with the aid of Equation (3). The results are shown in Figure 8 as a function of reciprocal pressure. The observed linear relationship confirms the interpretation that the broadening of the ion density profile in the ion source is due to diffusion. The here derived diffusion coefficients have the expected gas kinetic values. The linear relationship with 1/p breaks down for pressures less than 40 microns, which is also the limit to which meaningful drift velocities could be determined. At lower pressures, the number of collisions an ion encounters on its way to the sampling orifice evidently is insufficient to sustain the mechanisms of diffusion and drift. In this pressure region, the motion of ions changes from drift to free acceleration.

The independent determination of diffusion coefficients in these experiments permits also the derivation of ion temperatures from the relationship $T_i = eD/k\mu$. Here, e is the charge of the ion, k the Boltzmann constant, and $\mu = v/E$ the ionic mobility. Temperatures derived in this way are plotted versus E/p in Figure 9. The large scatter of data is due mainly to the variation in the diffusion coefficients. The solid line shown was obtained with the use of least square averaged diffusion coefficients. It is interesting to note the approximate linearity with E/p. The relationship $T_i = T_{gas} + a\ E/p$ for nitrogen ions in nitrogen was originally proposed by Varney.[30] The slope in Figure 9 is a = 11, which is in excellent agreement with that deduced by Varney (a = 12.5) from drift velocity measurements at different temperatures. However, since

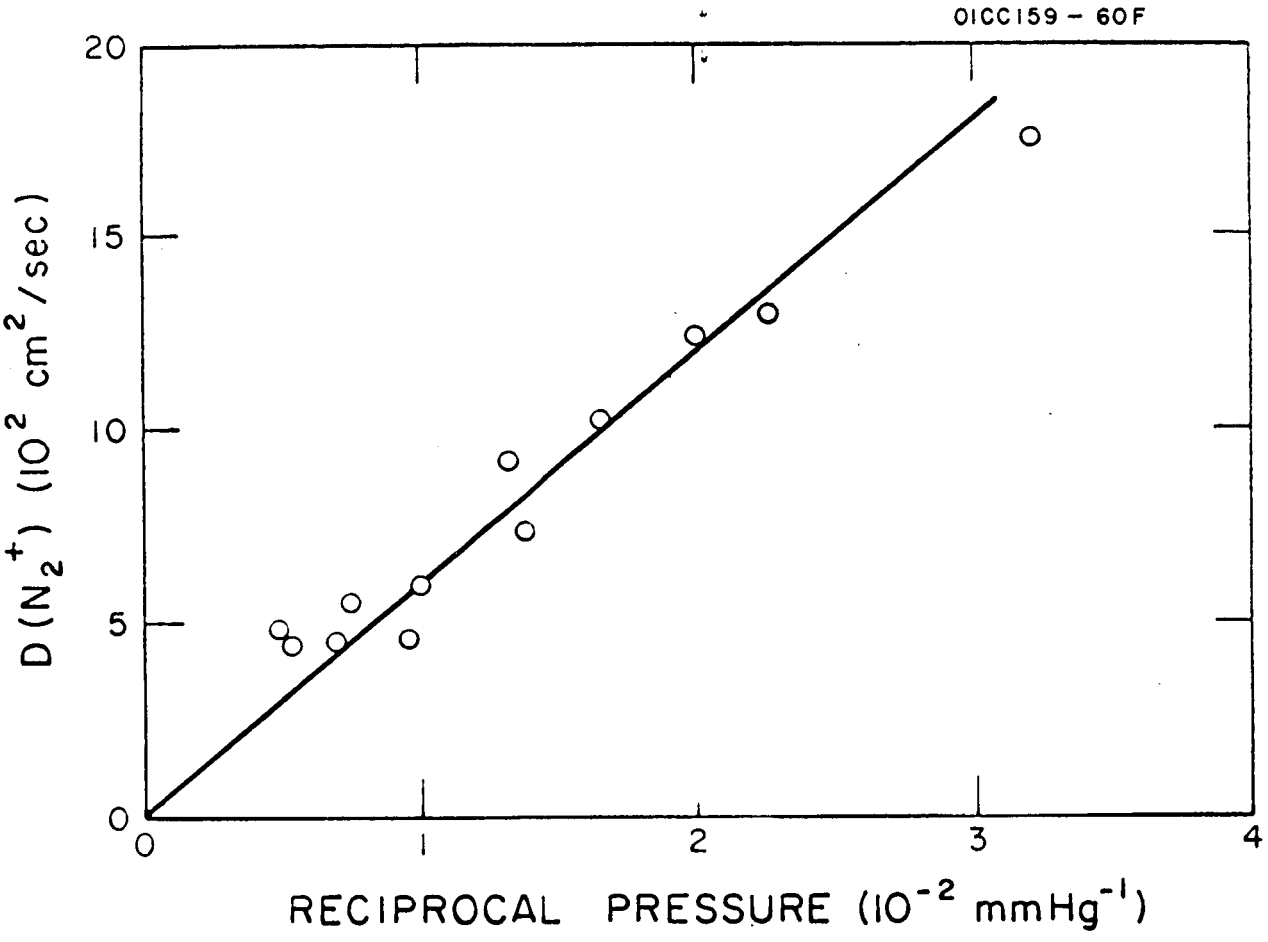

Figure 8. Diffusion coefficients of N_2^+ ions in air as derived from the broadening of the ion profile in the source.

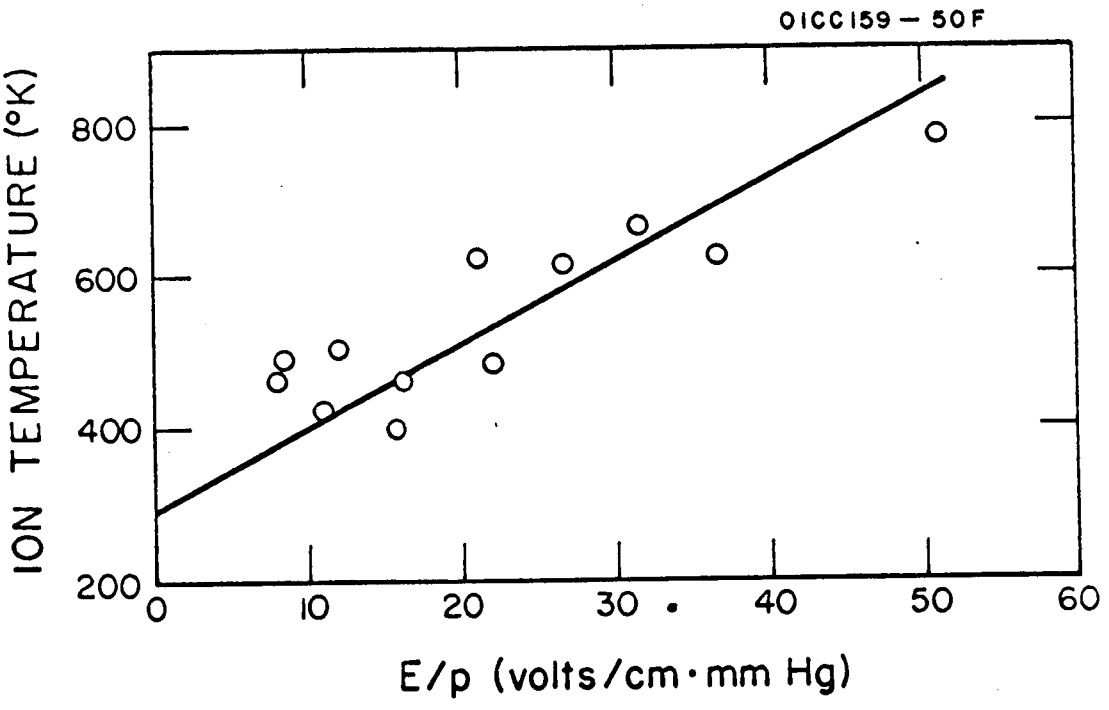

Figure 9. N_2^+ ion temperature in air versus relative filed strength E/P.

Varney derived the temperature scale from considerations of the equilibrium between N_4^+ and N_2^+ ions, his data really refer to the temperature of the N_4^+ ion, although he assumed them applicable also to N_2^+ ions. As a consequence, the obtained agreement may be coincidental. At present, it is not known whether the observed (approximate) linearity of T_i with E/p has general applicability, but from the derivation of the ion temperature, it is clear that it should depend on the detailed behavior of ion mobility.

Ion Molecule Reaction Rates

Rate constants are reported here for the reaction of nitrogen ions with oxygen and nitrogen, and for the proton transfer reaction in hydrogen. More specifically, these reactions read

$$(1)\quad N_2^+ + O_2 \rightarrow O_2^+ + N_2$$

$$(2)\quad N_2^+ + O_2 \rightarrow NO^+ + NO$$

$$(3)\quad N_2^+ + N_2 \rightarrow N_4^+$$

$$(4)\quad H_2^+ + H_2 \rightarrow H_3^+ + H$$

The above reactions were studied with radiation centered at 764 Å wavelength. Owing to the limited wavelength resolution, the employed radiation contained several component lines, the three strongest being NIV 765.1, NIII 764.4, and OV 760.4 Å. The associated energy spread is 0.1 eV. The available photon energy lies 0.64 eV above the threshold for N_2^+ formation and 0.75 eV above that for H_2^+ formation. Although this is insufficient for the production of ions in electronically excited states, it includes the excitation of vibrational or rotational levels. Specifically, for H_2^+, the occurrence of vibrational excitation has been demonstrated by Doolittle and Schoen[31] in this wavelength region.

Reactions (1) and (2) were studied with air introduced to the system at source pressures up to 200 microns. Reaction (1) proceeded rapidly while Reaction (2) was negligible under all conditions. Figure 10 shows the N_2^+ and O_2^+ ion currents observed as a function of pressure for a repeller voltage setting of 0.5 volt. Occurrence of Reaction (1) is evidenced by the rise of O_2^+ current at the expense of the N_2^+ current. Also shown in Figure 10 is the sum of both current which, in this case, exhibits an almost linear

pressure dependence. The deviations from linearity are attributable to the increase of light absorption in the source. The limiting ratio of the ion currents at low pressures, $R = i(N_2^+)/i(O_2^+)$, was determined by expansion of Figure 10 as R = 7.1. The ratio expected from the known absorption and photoionization coefficients,[21] taking into account only the three strongest lines contributing to the radiation, weighed according to their intensity, is R = 8.5. The agreement is reasonable if it is considered that the wavelength setting may have favored either one of the outer lines of this group.

Rate constants determined from the data shown in Figure 10 are given in Table I. The initial ion currents, $i(N_2^+)_o$ and $i(O_2^+)_o$, were deduced from the sum of the observed ion current multiplied by the ratio R measured at low pressures. N_2^+ residence times were determined from first arrival times of the ion pulse at the detector, and the correction according to Equation (3) was applied. The residence times thus found were somewhat smaller than those shown in Figure 6 despite the smaller repeller potential employed. However, these measurements were made early in this work, when a larger extraction orifice was used so that field penetration probably raised the field strength actually existing in the source. The data shown in Table 2 were obtained under conditions more nearly resembling those pertaining to Figure 6. The diameter of the extraction hole in this second series of runs was 0.7 mm (as used throughout in later experiments), and the repeller potential was approximately 1.5 volts. The rate constants obtained from both series of runs are in excellent agreement with each other indicating that the employed method of residence time determination yields correct results independently of

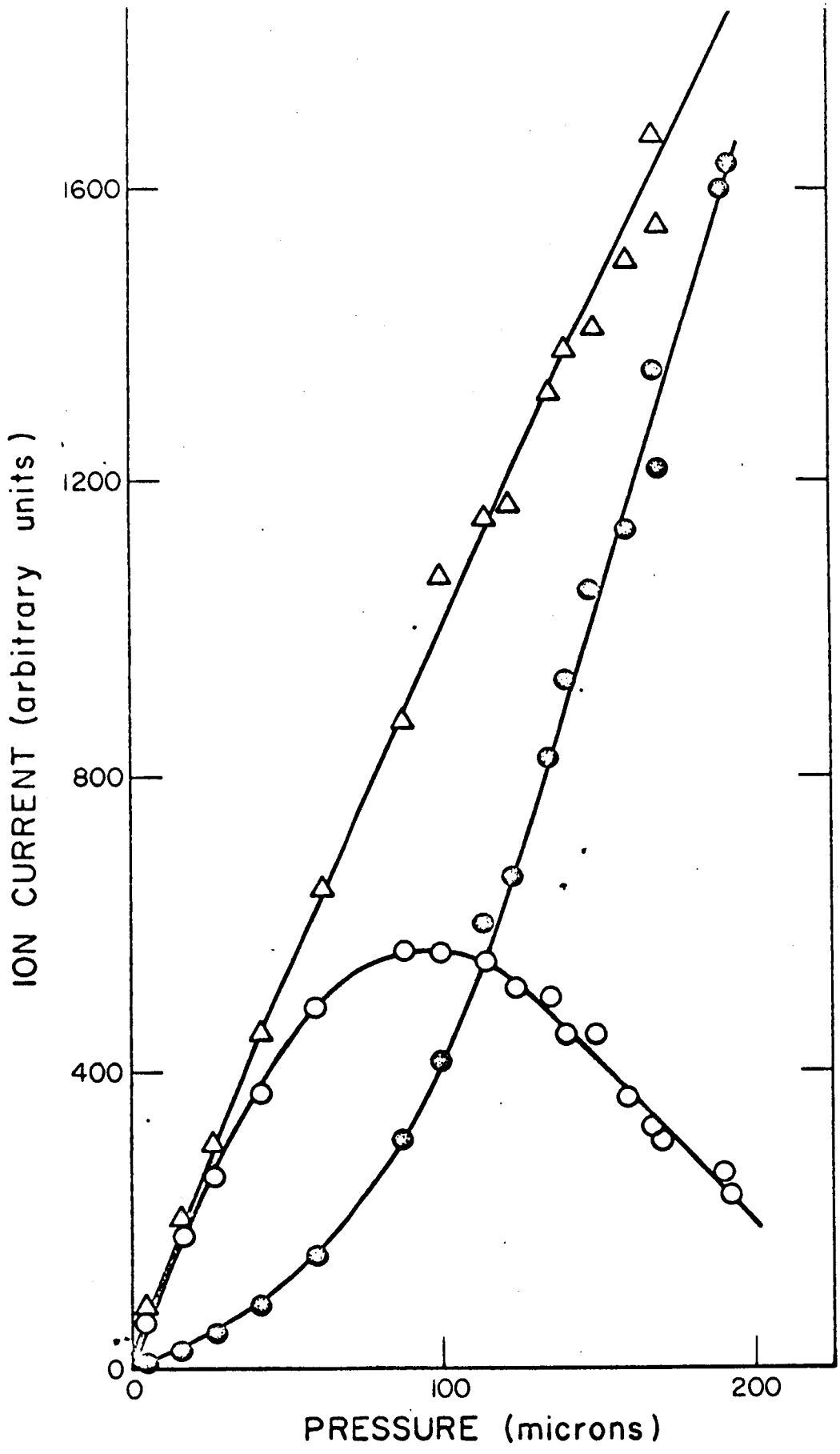

Figure 10. Variation of ion intensities in air with pressure: O O Nitrogen ions; ● Oxygen ions; △ sum of both.

TABLE I. Rate constants for the reaction $N_2^+ + O_2$.

P microns	(N_2^+)	(O_2^+)	$(N_2^+)_o$	$(O_2^+)_o$	τ μ sec	$\log \frac{(N_2^+)_o}{(N_2^+)_o - \Delta(O_2^+)}$	$k \times 10^{10}$ cc/molecule sec
	(arbitrary units)						
41	370	81	396	55	2.6	0.031	1.01
60	490	156	566	80	3.8	0.063	0.96
87	565	310	766	108	5.6	0.134	0.96
100	560	415	854	120	6.8	0.184	0.94
114	550	600	1007	142	7.6	0.263	1.06
123	508	662	1025	144	8.4	0.305	1.22
135	498	830	1162	163	9.6	0.370	0.99
140	450	930	1208	170	10.0	0.431	1.07
149	452	956	1232	173	10.4	0.439	0.99
160	367	1135	1315	185	11.2	0.554	1.07
168	320	1355	1465	207	11.6	0.665	1.19
170	302	1215	1355	191	11.8	0.612	1.06
190	260	1600	1629	239	12.8	0.783	1.12
192	236	1638	1640	231	12.9	0.868	1.22

average $k_1 = 1.06 \times 10^{-10}$ cc/molecule sec

TABLE II. Rate constants for the reaction $N_2^+ + O_2$.

P microns	(N_2^+)	(O_2^+)	$(N_2^+)_o$	$(O_2^+)_o$	τ μ sec	$\log \frac{(N_2^+)_o}{(N_2^+)_o - \Delta(O_2^+)}$	$k \times 10^{10}$ cc/molecule sec
		(arbitrary units)					
30	480	100	500	70	3.1	0.028	1.07
44	535	144	582	84	3.7	0.048	1.04
66	580	260	735	104	5.3	0.104	1.03
85	530	380	796	112	6.2	0.178	1.18
102	530	485	888	125	7.1	0.226	1.09
128	435	700	994	140	8.4	0.360	1.16
136	410	720	989	139	8.7	0.385	1.14
140	410	765	1030	145	9.0	0.400	1.11
160	335	990	1180	166	9.8	0.521	1.16
176	290	1130	1345	190	10.5	0.521	0.99
196	240	1360	1400	197	11.3	0.771	1.22
200	250	1340	1390	196	11.4	0.752	1.15

average $k_1 = 1.11 \times 10^{-10}$ cc/molecule sec

repeller potential settings and the resulting fields. Significantly, the individual rate constants exhibit no trends as the pressure is varied, although according to Figure 9 the ionic temperature decreases as the pressure is increased. This shows that at least in the 300 to 700°K region, the rate constant for Reaction (1) is temperature independent. The value averaged from the data shown in Tables I and II is $k_1 = 1.1 \times 10^{-10}$ cc/molecule sec, in approximate agreement with the previous estimate of 2×10^{-10} cc/molecule sec by Fite et al.,[32] and in excellent agreement with the value $k_1 = 1.0 \times 10^{-10}$ recently established by Ferguson and collaborators.[33] Their experimental results were obtained under entirely different experimental conditions, i. e., with a steady flow technique involving several torr of helium as a buffer gas. The close agreement of results thus adds confidence in the present experimental technique.

Reaction (2) has not been observed in these experiments and only an upper limit to its rate constant can be given. Even at pressures exceeding 200 microns, no nitric oxide ions could be detected. However, in this pressure region, the O_2 peak generated by Reaction (1) developed a tail, a portion of which covered the m/e = 30 region of the mass spectrum. From the current ratio of the background to that of the mass number 32 peak, the upper limit rate constant for Reaction (2) was found to be 3×10^{-4} that of Reaction (1) or $k_2 \leq 3 \times 10^{14}$ cc/molecule sec. This is an order of magnitude smaller than the upper limit value derived by Galli et al.[34] In this particular case, the photoionization mass spectrometer is used with advantage, since as Talrose[35] has demonstrated, the commonly employed electron impact ion sources generate NO from nitrogen oxidation at the hot filament.

Reaction (3) was studied in nitrogen at source pressures from 90 to 200 microns. At lower pressures, N_4^+ ions could still be discerned, but usable data were difficult to obtain because of excessive noise. Water vapor was a noticeable impurity despite the application of a liquid nitrogen cooled trap. Apparently, the formation of H_2O^+ ions occurs by a very fast charge transfer reaction involving nitrogen ions. The intensities of the m/e = 18 peak were, therefore, added to the sum of N_2^+ and N_4^+ ion currents to determine the initial N_2^+ currents required for the determination of rate constants, although this correction amounted to only a few percent. Table III shows the data including residence times and rate constants computed from Equation (3). The magnitude of the derived rate constants is in reasonable agreement with that reported by Fite et al.[32] ($k_3 = 5 \times 10^{-13}$ cc/molecule sec), but the present data are in disagreement in that they exhibit a trend with pressure. Seemingly, Reaction (3) is not a bimolecular process as predicted by Fite et al. A plot versus pressure in Figure 11 shows that the pressure dependence of the rate constants derived for the bimolecular process is linear and that an extrapolation toward zero pressure goes through the origin of the plot. This is clear evidence that Reaction (3) involves a third body and should properly be written

$$(3a) \quad N_2^+ + 2N_2 \rightarrow N_4^+ + N_2 \ .$$

In view of the attachment nature of this reaction, the participation of a third body is required to stabilize the resultant N_4^+ ion. However, at sufficiently high pressures, the reaction can become effectively bimolecular if the lifetime of the N_4^+ complex is longer than the mean free flight time of the ions between collisions so that stabilization is always effective.

TABLE III. Rate constants for the reaction $N_2^+ + N_2$.

P microns	(N_2^+) (arbitrary units)	(N_4^+)	N_o	$(N_4^+)/N_o$	τ μ sec	$k_3 \times 10^{13}$ cc/molecule sec	$k_{3a} \times 10^{29}$ $cc^2/molecule^2 sec$
94	1330	11	1365	.0082	10.0	2.61	8.42
98	1290	12	1302	.0092	10.5	2.71	8.38
115	1420	20	1440	.0139	11.8	3.10	8.18
120	1400	27	1460	.0185	12.2	3.84	9.30
130	1470	30	1500	.0200	13.0	3.60	8.40
142	1510	40	1550	.0258	13.8	4.00	8.55
154	1560	51	1611	.0317	14.6	4.27	8.40
165	1510	64	1616	.0406	15.4	4.73	8.70
177	1560	81	1691	.0492	16.0	5.27	9.02
185	1540	96	1686	.0588	16.6	5.62	9.20
194	1510	108	1666	.0668	18.7	5.45	8.50
195	1515	111	1686	.00617	17.2	5.75	8.85

N_o = sum of ion intensities at m/e = 28, 56, and 18.

average $k_{3a} = 8.5 \times 10^{-29}$ $cc^2/molecule^2 sec$

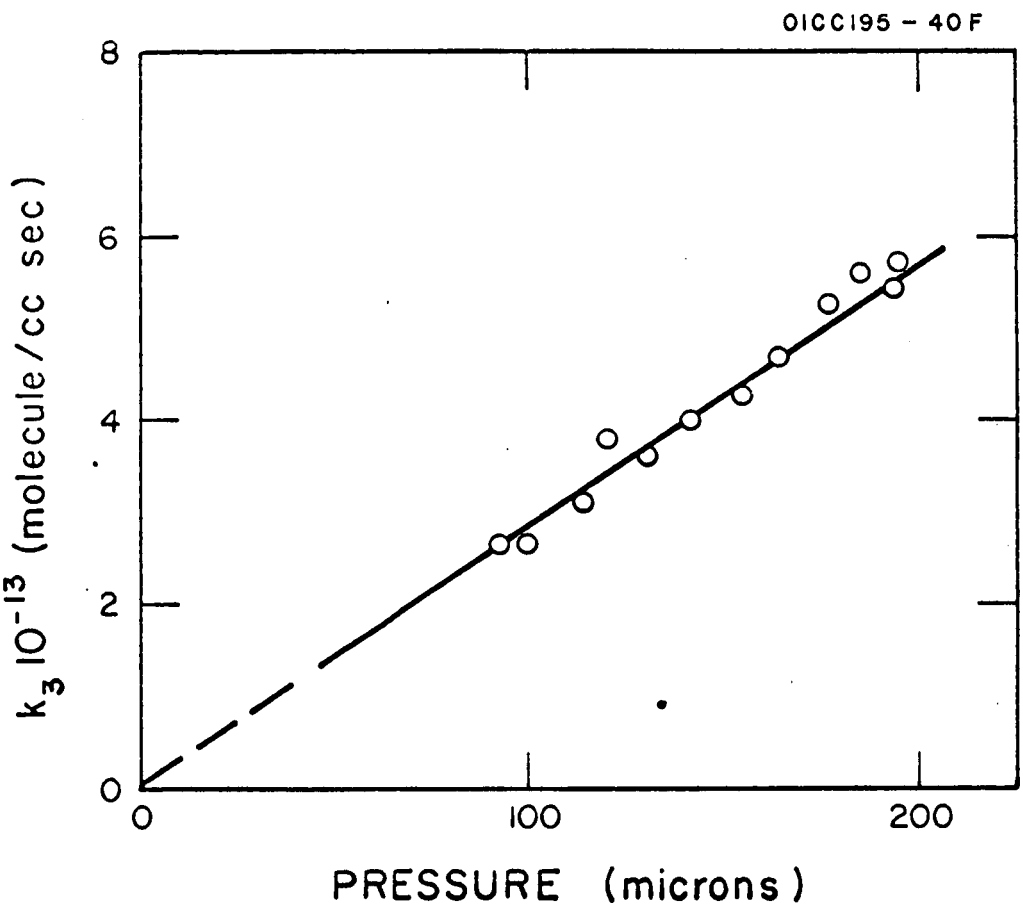

Figure 11. Variation of rate constant k_3 with pressure.

In the pressure range used here, this case evidently does not apply. The rate constants associated with Reaction (3a) are obtained from the bimolecular rate constants k_3 divided by the corresponding number density of nitrogen. An averaged rate constant $k_{3a} = 8.5 \times 10^{-29}$ cc^2/molecule^2 sec is derived from the data shown in Table III.

It should not be overlooked that N_4^+ ions can also dissociate upon collisions. In fact, Varney[30] has successfully interpreted drift velocity data in nitrogen on the basis that N_2^+ and N_4^+ ions are in thermal equilibrium. It remained, therefore, to check upon this possibility under the present experimental conditions. With the use of the equilibrium constant and the temperature scale for N_4^+ ions given by Varney, the degree of dissociation of N_4^+ ions was found inappreciable. Further, an attempt to fit the present data into a thermal equilibrium scheme failed both qualitatively and quantitatively. The conclusion is that the ion residence time in the source is insufficient for equilibrium conditions to develop. On the other hand, this is precisely the situation which enables the determination of the rate constant associated with Reaction (3a).

Reaction (4) was studied mainly to provide an additional check on the applicability of the present techniques. With hydrogen admitted to the source, the H_2^+ and H_3^+ ion intensities observed varied with pressure as shown in Figure 12. The repeller potential in this case was one volt, resulting in a field of approximately 1.5 volt/cm. The pressure dependence resembles that found by Saporoschenko,[36] who used an ion pathlength of 0.5 cm and 4 volt repeller potential. The $H_2^+ - H_3^+$ conversion is essentially

complete at 50 microns pressure. The mode of ionic motion in this pressure domain is predominantly collision-free acceleration. Indeed, residence times derived from first arrival measurements of the ion pulse were found to be pressure independent. Accordingly, Equation (4) has to be applied to correct for the pulse broadening due to the initial thermal velocities of the produced ions. As has been pointed out, residence time for hydrogen ions is of the same magnitude as the duration of the light pulse. However, first arrival time measurements should still give essentially correct residence time. The average residence time thus deduced is 1.1 μ sec, in close agreement with the value calculated from the assumed electric field. The average rate constant derived from the data shown in Figure 12 is $k_4 = 1.85 \times 10^{-9}$ cc/molecule sec, in good agreement with the experimental value of 2×10^{-9} cc/molecule sec given by Reuben and Friedman[37] for low repeller fields, and with the value calculated from theory.[38, 39] The agreement with Saporoschenko's data is less satisfactory, but his measurements were made at higher fields and correspondingly smaller residence times. His results are more in accord with Giese and Maier's[40] data, which approach the theoretical value as the ion velocities are lowered toward the thermal range.

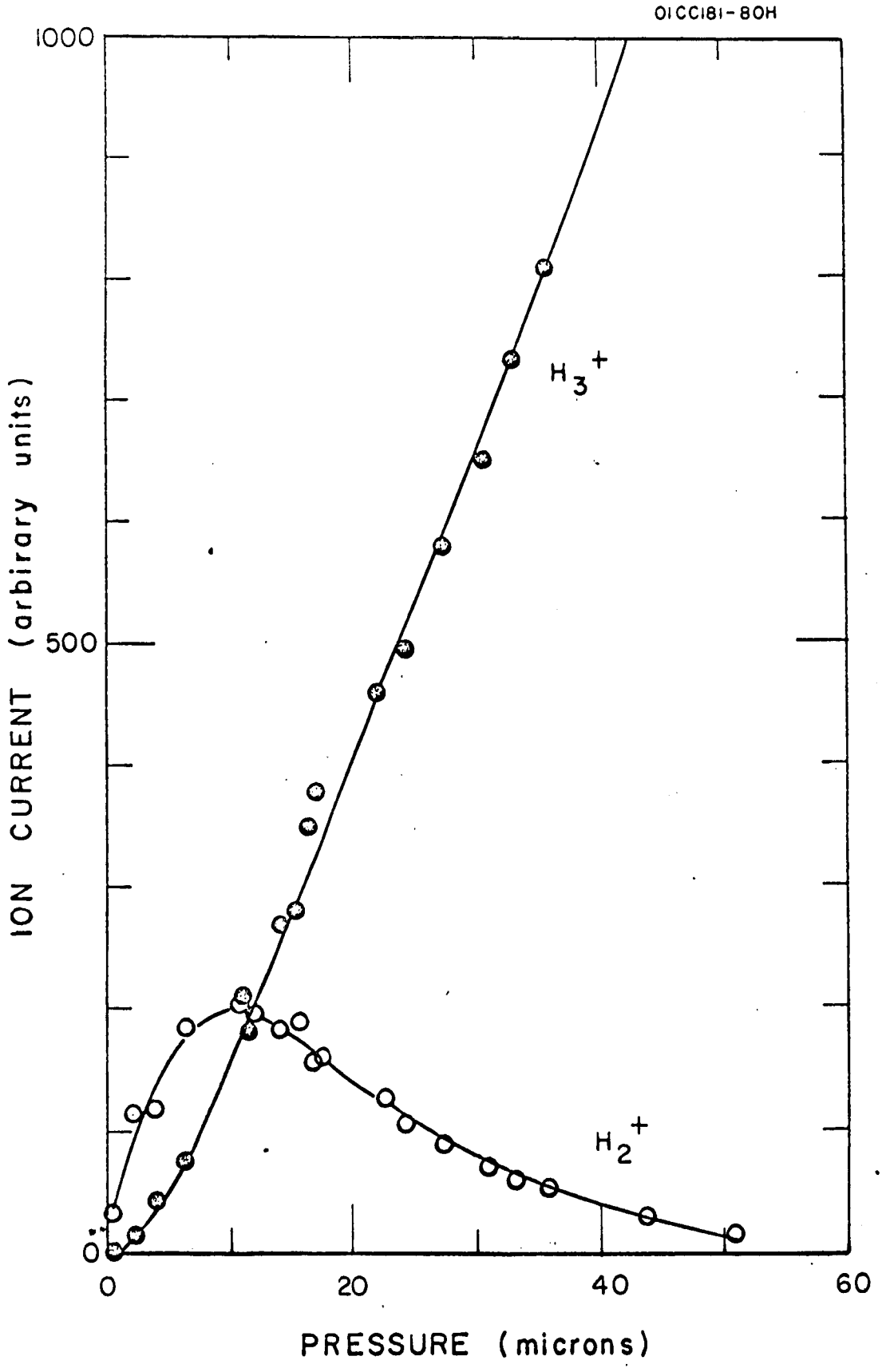

Figure 12. Variation of ion intensities in hydrogen as a function of pressure.

CONCLUSIONS

The present investigation differs from previous mass spectrometer investigations of ion-molecule reactions in two respects: (a) photoionization replaces the more commonly employed electron impact mode of ion formation and (b) a new technique is employed for the determination of ion residence times in the source in the presence of a constant repeller field. The ensuing advantages are: first, the state of the primary ions is reasonably well defined by the choice of ionizing wavelength and second , residence times can be obtained without a detailed knowledge of the electric field configuration in the ion source. This is particularly valuable at higher pressures where residence times are not calculable from Newton's formula. The interpretation of ion pulse shapes in terms of ion density distribution enables the determination of ion diffusion coefficients from the broadening of the density profile, and ultimately the derivation of approximate ion temperatures. It is an important finding that at pressures above 50 microns, where the basic motion of ions is drift in the electric field the ionic temperatures are in the thermal range provided only moderate fields are applied. Finally, rate constants for several reactions involving nitrogen and hydrogen ions are given and compared with existing data where available. Satisfactory agreement is obtained in all cases, indicating that the methods applied here are useful in extending rate constant determination toward higher pressures .

APPENDIX

To evaluate the effect of diffusion on a group of ions moving in the source under the influence of a field, consider the following idealized physical situation. It is assumed that ions are deposited by a delta source release at the instant $t = 0$ in the plane $x = 0$, and that a one dimensional Gaussian ion concentration profile develops due to diffusive motion perpendicular to the plane of origin:

$$n(x, t) = N_o (4\pi Dt)^{-1/2} \exp(-x^2/4Dt) .$$

Here, x is the distance from the center of the profile, N_o is the total number of ions generated per unit area in the plane of origin, and D is the diffusion coefficient.

Superimposed upon diffusion is the motion of ions toward the sampling orifice due to the applied electric field. Since the field is also perpendicular to the plane of origin, it is convenient to express x in terms of the drift velocity v and the time t. In the pressure region where diffusion occurs, the drift velocity is constant, so that $x = d - vt$ with d being the known distance from the center of the light beam to the sampling aperture. If the average residence time $\tau_o = d/v$ is introduced, $x = d(1 - t/\tau_o)$.

Consider now the flux of ions entering the sampling aperture. The contributions of both drift and diffusion give the flux

$$Q(v, t) = vn(x, t) - D \frac{\partial n(x, t)}{\partial t} = vn(x, t) + \frac{xn(x, t)}{2t} .$$

The buildup of charge at the detector located behind the sampling aperture is given by the time integral

$$P(v,\ t) = \int_o^t Q(v,\ t)\ dt = \int_o^t n(x,\ t)\ (v + \frac{x}{2t})\ dt\ ,$$

which can be evaluated to yield

$$P(v,\ t) = 1/2\ N_o\ [1 - \text{erf}\ (x/2\sqrt{Dt})]\ .$$

The determination of the time $t = \tau$ at which ions are first detected requires the definition of a threshold. Since experience has shown that the average practical detection limit is around ten percent of the total pulse height displayed on the oscilloscope, it is reasonable to set $P(v,\ t) = 0.1\ N_o$ and evaluate the error function accordingly. This leads to

$$0.906 = x/2\sqrt{D\tau} = d(1 - \tau/\tau_o)/2\sqrt{D\tau}$$

which can be rearranged to yield

$$\tau_o = \tau/[1 - (1.28/d)\sqrt{2D\tau}]\ .$$

In the low pressure region where the motion of ions is governed by collision-free acceleration in the electric field, the broadening of the ion concentration profile is due to the thermal distribution of initial ion velocities, and

$$n(x,\ t) = \frac{N_o}{t}\left(\frac{m}{2\pi kT}\right)^{1/2} \exp\left(-\frac{m}{2kT}\frac{x^2}{t^2}\right).$$

Here, m is the mass of the ion, k the Boltzmann constant, and T the temperature. The flight velocity is no longer constant, but the acceleration a provided by the field is. Similarly as above, $x = d - at^2/2 = d(1 - t^2/\tau_o^2)$ and by the same arguments, one derives for this case

$$\tau_o = \tau^2/[1 - (1.28\tau/d)\sqrt{kT/m}] .$$

REFERENCES

1. J. B. Hasted, in Advances in Electronics and Electron Physics, Vol. XIII, p. 1, ed. L. Marton, Academic Press, New York (1960).
2. F. W. Lampe, J. L. Franklin, and F. H. Field, in Progress in Reaction Kinetics, Vol. 1, p. 69, ed. G. Porter, Pergamon Press, Oxford (1961).
3. C. E. Melton, in Mass Spectrometry of Organic Ions, ed. F. W. McLafferty, Academic Press, New York (1963).
4. D. P. Stevenson, in Mass Spectrometry, ed. C. A. McDowell, McGraw Hill, New York (1963).
5. J. F. Paulson, Ann. de Geophysique 20, 75 (1964).
6. G. F. Giese, in Advances in Chemical Physics, Vol. X Molecular Beams, p. 247, ed. J. Ross, Interscience Publ., New York (1966).
7. G. L. Weissler, J. A. R. Samson, M. Ogawa, and G. R. Cook, J. Opt. Soc. Am. 49, 338 (1959).
8. H. Hurzeler, M. G. Inghram, and J. P. Morrison, J. Chem. Phys. 27, 313 (1958); 28, 76 (1958).
9. R. I. Schoen, J. Chem. Phys. 37, 2032 (1962).
10. F. J. Comes and W. Lessman, Z. Naturforschung 19a, 65 (1964).
11. V. H. Dibeler and R. M. Reese, J. Res. Natl. Bur. Std. 68a, 409 (1964).
12. I. Koyano, I. Omura and I. Tanaka, J. Chem. Phys. 44, 3850 (1966).
13. G. Cook and J. A. R. Samson, Bull. Am. Phys. Soc. 4, 454 (1959).
14. V. L. Talrose and E. L. Frankevich, Zh. Fiz. Khim. 34, 2709 (1960).

This pulse method has also been used by others to study ion formation in reactions of excited atoms.[15-17]

15. P. M. Becker and F. W. Lampe, J. Am. Chem. Soc. 86, 5347 (1964).

16. P. M. Becker and F. W. Lampe, J. Chem. Phys. 42, 3857 (1965).

17. W. Kaul, Proc. VI Intern. Conf. Ionization Phenomena In Gases, p. 169, Paris (1963).

18. C. W. Hand and H. von Weyssenhoff, Can. J. Chem. 42, 195 (1964); 42, 2385 (1964).

19. W. Poschenrieder and P. Warneck, J. Appl. Phys. 37, 2812 (1966).

20. H. Ishii and K. Nakayama, Trans. 8th Vacuum Symposium, p. 519, ed. L. E. Preuss, Pergamon Press, New York (1961).

21. J. A. R. Samson and R. B. Cairns, J. Geophys. Res. 69, 4583 (1964); 70, 99 (1965).

22. G. R. Cook and P. H. Metzger, J. Opt. Soc. Am. 54, 968 (1964).

23. P. H. Metzger and G. R. Cook, J. Chem. Phys. 41, 642 (1964).

24. M. G. Inghram and R. J. Hayden, "Mass Spectroscopy" Nuclear Sciences Series Report No. 14, National Academy of Sciences (1954).

25. V. H. Dibeler, M. Krauss, R. M. Reese, and F. N. Harllee, J. Chem. Phys. 42, 3791 (1965).

26. E. E. Ferguson, F. C. Fehsenfeld, D. B. Dunkin, A. L. Schmeltekopf, and H. I. Schiff, Planet. Space Sci. 12, 1169 (1964).

27. T. F. Moran and L. Friedman, J. Geophys. Res. 70, 4992 (1965).

28. D. W. Martin, W. S. Barnes, G. E. Keller, D. S. Harmer, and E. W. McDaniel, Proc. VI Intern. Conf. Ionization Phenomena in Gases, p. 295, Paris (1963). E. W. McDanield, G. E. Keller, D. L. Albritton, T. M. Miller, and D. W. Martin have presented more refined results at the IVth International Conference on the Physics and Electronic and Atomic Collision, Quebec, Canada (1965). The more recent results are slightly lower than those shown in Figure 7.

29. J. A. Dahlquist, J. Chem. Phys. 39, 1203 (1963).

30. R. N. Varney, J. Chem. Phys. 31, 1314 (1959).

31. P. H. Doolittle and R. I. Schoen, Phys. Rev. Letters 14, 348 (1965).

32. W. L. Fite, J. A. Rutherford, W. R. Snow, and V. A. J. van Lint, Discussion Faraday Soc. 33, 264 (1962).

33. P. D. Goldan, A. L. Schmeltekopf, F. C. Fehsenfeld, H. I. Schiff, and E.E. Ferguson, J. Chem. Phys. 44, 4095 (1966); Planet. Space Sci. 13, 919 (196

34. A. Galli, A. Giardini-Guidoni, and G. G. Volpi, J. Chem. Phys. 39, 518 (1963).

35. V. L. Talrose, M. I. Markin, and I. K. Larin, Disc. Faraday Soc. 33, 257 (1962).

36. M. Saporoschenko, J. Chem. Phys. 42, 2760 (1965).

37. B. G. Reuben and L. Friedman, J. Chem. Phys. 37, 1636 (1962).

38. H. Eyring, J. O. Hirschfelder, and H. S. Taylor, J. Chem. Phys. 4, 479 (1936).

39. G. Gioumousis and D. P. Stevenson, J. Chem. Phys. 29, 294 (1958).

40. G. F. Giese and W. B. Maier, J. Chem. Phys. 39, 739 (1963).